4.0 RESULTS AND DISCUSSION

Dental caries is a complex, contagious illness caused by the dominant microbial action in the mouth, leading to the deterioration of the crown and root tissues over time. It is associated with specific cariogenic oral bacteria *Streptococcus mutans,* and fermentable sugary diets (Lewis, 2018). Several herbal remedies reported in the literature have proven antibacterial properties against this caries-causing microorganism. In developing nations, 80% of the population relies on natural remedies for oral hygiene due to their affordability, accessibility, and relatively low risk of adverse effects. It's essential to scientifically validate the efficacy of these herbs in combating dental caries (Refaey et al. 2024).

Medicinal plants, rich in biologically active compounds, are valuable natural sources of antibiofilm agents (Mastoor et al. 2022). These plant-derived compounds disrupt polymer matrix formation, suppress cell adhesion and attachment, interrupt extracellular matrix generation, and reduce bacteria virulence properties. In addition, they prevent bacterial biofilm formation, aggregation, and adhesion by altering surface characteristics like hydrophobicity, hydrophilicity, roughness, and texture (Atazhanova et al. 2024). Thus, the current study investigated the anti-cariogenic potential of selected plant extracts against oral pathogens. The study involved a comprehensive approach, including phytochemical analysis, antioxidant, antimicrobial, and anti-glucosyltransferase activity using *in vitro* and *silico* analysis. Additionally, a polyherbal dentifrice was optimized and formulated using the selected plant extracts and evaluated for its quality parameters, toxicity profile, and anti-cariogenic efficacy. The results and discussion of the study are presented here.

PHASE I

4.1 Screening of Plants for Anticariogenic Activity Against Oral Pathogens

4.1.1 Preliminary Phytochemicals Screening

4.1.2 Quantification of Phytoconstituents

4.1.3 Quantification of Total Antioxidants

4.1.3.1 Estimation of Total Phenolic Content

4.1.3.2 Estimation of Total Flavonoid Content

4.1.4 *In vitro* DPPH Radical Scavenging Assay

4.1.5 Antimicrobial Activities of Plant Extracts

4.1.5.1 Antimicrobial Activities of Plant Extracts on Clinical Cariogenic Isolates

4.1.5.2 Determination of the MIC and MBC/MFC

4.1.5.3 Biofilm Eradication Potential of Plant Extracts

PHASE II

4.2 *In silico* Identification of Inhibitors from Selected Plant Extracts against Glucosyltransferase-C of *S. mutans*

4.2.1 Retrieval of Active Compounds from Selected Plant Parts

4.2.2 Molecular Docking Studies

4.2.3 Molecular Dynamic Simulation

PHASE III

4.3 Preparation and Evaluation of Polyherbal Dentifrice (PHDF)

4.3.1 Design of Experiments (DOE) Modeling to Determine Synergistic Antibacterial Combinations of Plant Extracts

4.3.2 Preparation of Polyherbal Dentifrice (PHDF)

4.3.3 Evaluation Parameters for Polyherbal Dentifrice (PHDF)

4.3.3.1 Organoleptic Evaluation

4.3.3.2 Physiochemical Evaluation

4.3.3.3 Rheological Evaluation

4.3.4 Cytotoxicity Evaluation of PHDF

4.3.5 Atomic Absorption Spectrometric Analysis of PHDF

4.3.6 Cost Analysis of Polyherbal Dentifrice

PHASE IV

4.4 Anticariogenic Efficacy of Formulated PHDF

4.4.1 Determination of Inhibitory Zone Diameter, MIC, and MBC/MFC

4.4.2 Effect of PHDF on the Cell Surface Hydrophobicity of *S. mutans*

4.4.3 Effect of PHDF on Glycolytic pH Drop

4.4.4 Biofilm Eradication Potential of PHDF

4.4.5 SEM Analysis of PHDF Treated *S. mutans* Biofilms

PHASE V

4.5 Validation of Therapeutic Activity of PHDF Against Dental Caries Through Network Pharmacology Approach

4.5.1 Deciphering the Repairing Mechanism of PHDF for Dental Caries

4.5.2 Screening of Potential Targets of Active Components in PHDF

4.5.3 Analysis of Protein-Protein Interaction (PPI) Network

4.5.4 Compound Target Network Construction

4.5.5 Compounds Target Pathway Analysis

4.5.6 Gene Ontology (GO) Functional Enrichment Analysis of Biological Process, Cellular Components, and Molecular Functions

4.5.7 KEGG Pathway Enrichment Analysis

4.5.8 Validation of Key Targets-Compound Interaction using Molecular Docking

4.5.9 Effect of Potential PHDF Compounds on *S. mutans*

PHASE I

4.1 Screening of Plants for Anticariogenic Activity Against Oral Pathogens

To harness the therapeutic potential of plants, a comprehensive investigation into the presence of different phytochemicals including tannins, alkaloids, terpenoids, flavonoids, and phenolic compounds is crucial for their medicinal value. These phytochemicals are vital for plant defense mechanisms and exhibit a range of biological activities, including antimicrobial, anti-inflammatory, and antioxidant effects (Sidhu et al. 2020). The quantification of secondary metabolites provides useful information on the concentration and potency of these bioactive compounds in plant extracts, ensuring therapeutic effectiveness (Edeoga et al. 2005). Evaluation of the antioxidant activity of these plants is also essential, as oxidative stress constitutes the pathogenesis of numerous chronic diseases. Plant antioxidants can scavenge harmful free radicals, protect against cell damage, maintain health, and prevent diseases (Muscolo et al. 2024). The plant's bioactive compounds are non-nutritive chemicals, that can inhibit the growth of oral pathogens responsible for causing dental disorders (Tzimas et al. 2024). In addition, these natural substances promote oral health by eradicating biofilm formation and acid production, which

ensures the prevention of dental caries and plaque formation (Palombo, 2011). With this background, the selected plants were screened and quantified for their bioactive compounds and evaluated for their antioxidant and antimicrobial efficacies against oral pathogens. The results of phase I are reported and discussed below.

The limitations of chemical treatments and the growing challenge of antibiotic resistance have led to a high demand for novel and potent plant-based antimicrobial agents. Exploring various plants for such properties presents a promising strategy and incorporates effective bioactive compounds that eliminate oral pathogens responsible for tooth and gum diseases (Cruzeiro et al. 2022). In the present study, methanol extracts of twelve plants namely, *Achyranthes aspera* Root (AAR), *Acalypha indica* Leaf (AIL), *Azadirachta indica* Leaf (AZL), *Abrus precatorius* Leaf (APL), *Barleria cuspidata* Leaf (BCL), *Euphorbia hirta* Leaf (EHL), *Ficus benghalensis* Prop root (FBP), *Piper betle* Leaf (PBL), *Psidium guajava* Leaf (PGL), *Pongamia pinnata* Leaf (PPL), *Tridax procumbens* Leaf (TPL), and *Solanum virginianum* Fruit (SVF) were screened for the presence of diverse phytochemicals. Major secondary metabolites were quantified and further evaluated for their antioxidant properties using the DPPH assay. All twelve plant extracts were subjected to antimicrobial activity against oral clinical isolates and were subsequently screened for further validation.

4.1.1 Preliminary Phytochemical Screening

Qualitative preliminary screening of phytochemicals in methanol extracts of selected plants revealed the presence of several phytoconstituents. The study identified bioactive compounds contributing to the medicinal properties of the plants. The presence and absence of multiple phytochemicals using methanol plant extracts are depicted in **Table 4.1**.

Medicinal plants supply plenty of phytochemicals like alkaloids, flavonoids, phenols, saponins, terpenoids, and tannins, which have gained recognition for their antimicrobial efficacy. These antimicrobial agents from various plant sources, when combined, exhibit an enhanced efficacy in inhibiting the growth of diverse microorganisms (Tzimas et al. 2024). Hence, the presence of these phytoconstituents was observed by the color change, precipitation, and ring

formation upon adding chemicals to the selected twelve methanol plant extracts. The results indicated that EHL, PBL, and PGL possessed more compounds than other plant extracts, and among the twenty tested compounds, alkaloids, flavonoids, tannins, vitamin C, terpenoids, and phenolic compounds were detected in most of the plant extracts. Besides, alkaloids were abundant in AAR, tannins in AAR and PBL, terpenoids in AAR, AZL, BCL, FBP, PGL, and SVF, quinones in PBL, and saponins in PBL, PGL, and PPL. Phenols, flavonoids, and vitamin C primarily enhance antioxidant activity to balance free radicals and reduce oxidative stress (Diaz et al. 2012).

Table 4.1. Preliminary screening of phytochemicals in different plant extracts

Phytochemicals	AAR	AIL	AZL	APL	BCL	EHL	FBP	PBL	PGL	PPL	TPL	SVF
Protein & AA	-	+	-	-	-	+	-	+	+	-	-	-
Carbohydrate	++	+	+	-	-	+	+	+	+	-	+	+
Starch	-	+	-	+	+	+	-	+	-	-	++	-
Alkaloid	+++	+	+	+	+	+	+	+	+	+	++	+
Flavonoid	+	+	+	+	+	+	+	++	+++	+	+	+
Tannin	+++	++	+	+	+	++	+	+++	++	++	++	++
Phenols	+	+	+	+	+	++	+	+	+++	+	+	+
Steroid	++	+++	+	-	-	+	+	+++	-	+	+++	+
Terpenoid	+++	+	+++	-	+++	++	+++	++	+++	-	+	+++
Cardiac glycoside	-	-	+	+	+	++	+	++	++	++	+	-
Catechin	-	-	+	+	-	+	-	-	+	+	++	-
Quinones	++	-	-	-	-	+	++	+++	++	+	-	++
Anthocyanin	-	+	-	++	++	+	-	++	-	+	+++	+
Saponin	+	++	++	++	-	+	-	+++	+++	+++	-	+
Coumarins	+	+	+	-	-	+	-	+	+	+	+	+
Anthraquinone	-	-	-	-	-	-	-	+	-	-	+	-
Vitamin C	+++	+	++	+++	+++	+++	+++	+	+++	+	+++	+++
Resins	-	-	+	+	+	++	+	+	+	+	-	-
Acidic Compounds	++	+	-	-	-	++	-	++	-	-	+	-
Volatile Oils	+++	++	-	-	++	++	+++	+	-	+	+	+

+++ = Appreciable amount, ++ = Moderate amount, + = Trace amount, - = Not detected. AAR-*Achyranthes aspera* Root, AIL-*Acalypha indica* Leaf, AZL-*Azadirachta indica* Leaf, APL-*Abrus precatorius* Leaf, BCL-*Barleria cuspidat Leaf*, EHL-*Euphorbia hirta* Leaf, FBP-*Ficus benghalensis* Prop root, PBL-*Piper betle* Leaf, PGL-*Psidium guajava* Leaf, PPL-*Pongamia pinnata* Leaf, TPL-*Tridax procumbens* Leaf, SVF-*Solanum virginianum* Fruit.

These antioxidants help reduce gum inflammation, protect against carcinogens responsible for mouth cancer, neutralize acid-producing cariogenic microbes, and enhance overall gum health (Manna & Khan, 2024). Consequently, PGL mainly indicated the higher presence of phenols and flavonoids. Vitamin C was highly found in all the extracts except AIL, PBL, and PPL. The extracts of EHL

and PBL expressed the major presence of resins, acidic compounds, and volatile oils when compared to others.

In agreement with our findings, many researchers reported the existence of these compounds in *A. aspera* root extracts (Tiwari et al. 2018), *Acalypha indica* leaf methanol extracts (Kumar & Sharma, 2024), *Azadirachta indica* leaf extracts (Sharma & Patel, 2018; Ayele et al. 2022), *A. precatorius* leaf methanolic extracts (Gawade & Farooqui, 2021; Rajeshwar et al. 2015), *B. cuspidata* leaf methanolic extracts (Mehatar & Badar, 2022), *E. hirta* leaf extracts (Print et al. 2015), *F. benghalensis* prop root (Etratkhah et al. 2019) and combined leaf extracts *of P. guajava* and *P. betle* leaf extracts (Rameshwari & Priya, 2020; Basit et al. 2023), *Pongamia pinnata* (Sattar et al. 2024), and *Tridax procumbens* leaf methanolic extracts (Dhanabalan et al. 2008).

4.1.2 Quantification of Phytoconstituents

The quantified content of phytochemicals like alkaloids, tannins, terpenoids, and vitamin C in twelve plant extracts is presented in **Table 4.2.** Total alkaloid content in selected plants exhibited moderate to high levels, with significant variations among the samples (**Figure 4.1**). TPL exhibited the highest alkaloid content (52.37±0.011mg/g), followed by AIL (51.89±0.017 mg/g), EHL (51.74±0.024mg/g), PBL (49.56±0.014mg/g), and BCL (48.63±0.046mg/g). In contrast, APL, FBP, AAR, and SVF showed lower alkaloid content of 21.86±0.001, 22.17±0.021, 23.73±0.063, and 24.50±0.006mg/g, respectively.

The total tannin content of the twelve plant extracts widely varied, ranging from 11.31±0.012mg/g to 191.4±0.126mg/g (**Figure 4.2**). The highest amount of tannin was found in the PGL (191.4±0.126mg/g), followed by PPL (153.26±0.11mg/g) and AAR (111.5±0.992mg/g). Moderate amounts of tannin were detected in the PBL, SVF, AZL, and FBP with the values of 69.42±0.041mg/g, 47.55±0.066, 38.97±0.302, and 32.13±0.033mg/g, respectively. AIL, TPL, and BCL showed a lower tannin content of 11.31±0.012, 13.19±0.009, and 13.32±0.007mg/g, respectively. The total terpenoid content of the twelve plant extracts ranged from 5.041±0.002 to 19.92±0.017mg/g. The TPL exhibited the highest concentration of 19.92±0.017mg/g followed by BCL (16.61±0.012mg/g), PBL (15.62±0.010mg/g), and EHL (14.21±0.006mg/g) as shown in **Figure 4.3**.

Table 4.2. Quantification of phytoconstituents in selected plant extracts

Plant samples	Alkaloid (Atropine/g)	Tannin (TAE/g)	Terpenoid (Linalool/g)	Vitamin C (AA/g)
AAR	23.73±0.063	111.5±0.992	6.297±0.014	112.6±0.004
APL	21.86±0.001	29.66±0.024	5.789±0.007	118.5±0.064
AIL	**51.89±0.017**	11.31±0.012	13.87±0.034	189.0±0.028
AZL	34.59±0.040	38.97±0.302	7.118±0.007	173.6±0.154
BCL	48.63±0.046	13.32±0.007	**16.61±0.012**	**309.0±0.007**
EHL	**51.74±0.024**	26.70±0.022	14.21±0.006	**586.6±0.038**
FBP	22.17±0.021	32.13±0.033	5.355±0.007	142.6±0.036
PBL	**49.56±0.014**	69.42±0.041	15.62±0.010	267.8±0.043
PGL	29.05±0.024	**191.4±0.126**	6.900±0.002	117.5±0.048
PPL	31.95±0.062	153.26±0.11	6.079±0.010	103.5±0.014
TPL	**52.37±0.011**	13.19±0.009	**19.92±0.017**	**370.9±0.300**
SVF	24.50±0.006	47.55±0.066	5.041±0.002	133.9±0.037

The values represented are mean± SD. The concentration of different phytochemicals was statistically significant ($p<0.05$) among the plant species. AAR-*Achyranthes aspera* Root, AIL-*Acalypha indica* Leaf, AZL-*Azadirachta indica* Leaf, APL-*Abrus precatorius* Leaf, BCL-*Barleria cuspidata* Leaf, EHL-*Euphorbia hirta* Leaf, FBP-*Ficus benghalensis* Prop root, PBL-*Piper betle* Leaf, PGL-*Psidium guajava* Leaf, PPL-*Pongamia pinnata* Leaf, TPL-*Tridax procumbens* Leaf, SVF-*Solanum virginianum* Fruit.

The vitamin C of all the twelve plant extracts possessed a significant range, from 103.5±0.014 to 586.6±0.038mg/g, indicating a significant variation. The leaves of *E. hirta, T. procumbens, and B. cuspidata* exhibited the highest ascorbic acid concentrations of 586.6±0.038, 370.9±0.300, and 309.0±0.007mg/g, respectively, indicating their potential as rich sources of vitamin C with antioxidant properties. In contrast, PPL had the lowest ascorbic acid content of 103.5±0.014mg/g, when compared to other plant extracts (**Figure 4.4**).

In our study, the selected medicinal plants possess a diverse range of quantified secondary metabolites when compared to the earlier research. The variations in the mean total content of estimated compounds are related to several geographic and environmental factors as plant variety, soil growth conditions, climate, and processing (Ayele et al. 2022). Additionally, the difference in results can be attributed to the type of extraction solvent, time, pH, temperature, and extraction method used (Turkmen et al. 2006).

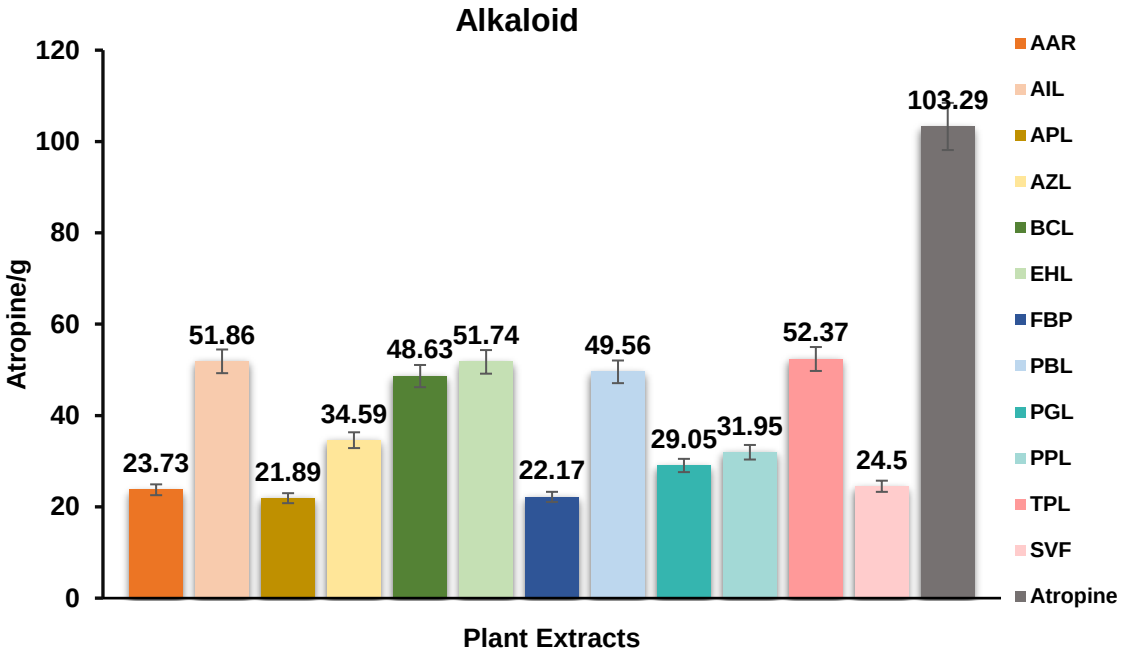

Figure 4.1. Estimation of total alkaloid content in selected plant extracts

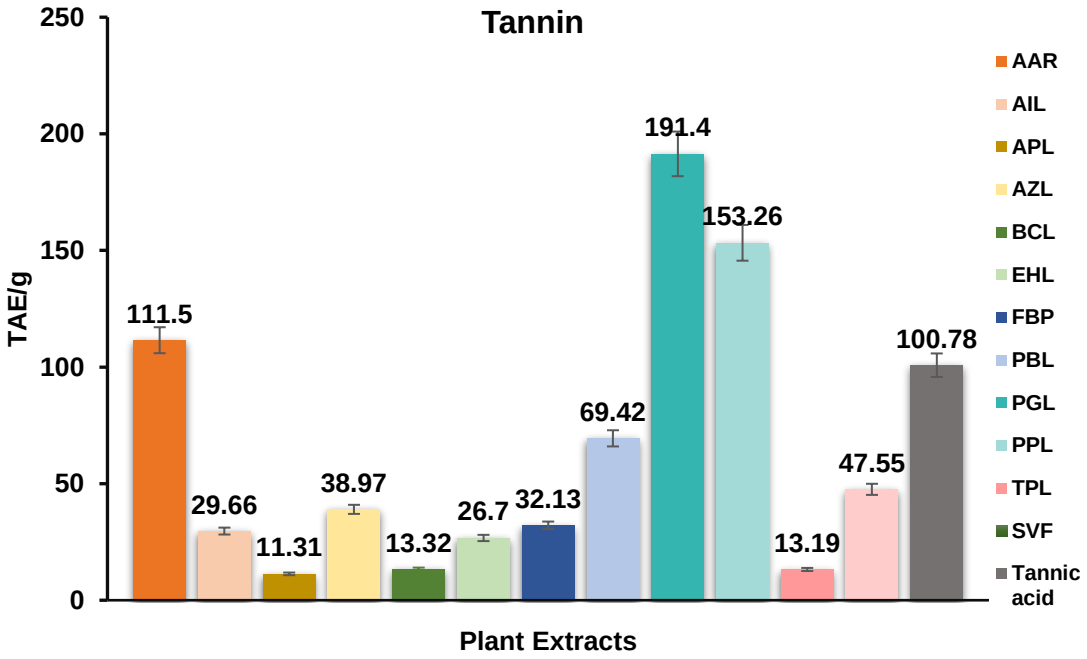

Figure 4.2. Estimation of total tannin content in selected plant extracts

AAR-*Achyranthes aspera* Root, AIL-*Acalypha indica* Leaf, AZL-*Azadirachta indica* Leaf, APL-*Abrus precatorius* Leaf, BCL-*Barleria cuspidata* Leaf, EHL-*Euphorbia hirta* Leaf, FBP-*Ficus benghalensis* Prop root, PBL-*Piper betle* Leaf, PGL-*Psidium guajava* Leaf, PPL-*Pongamia pinnata* Leaf, TPL-*Tridax procumbens* Leaf, SVF-*Solanum virginianum* Fruit.

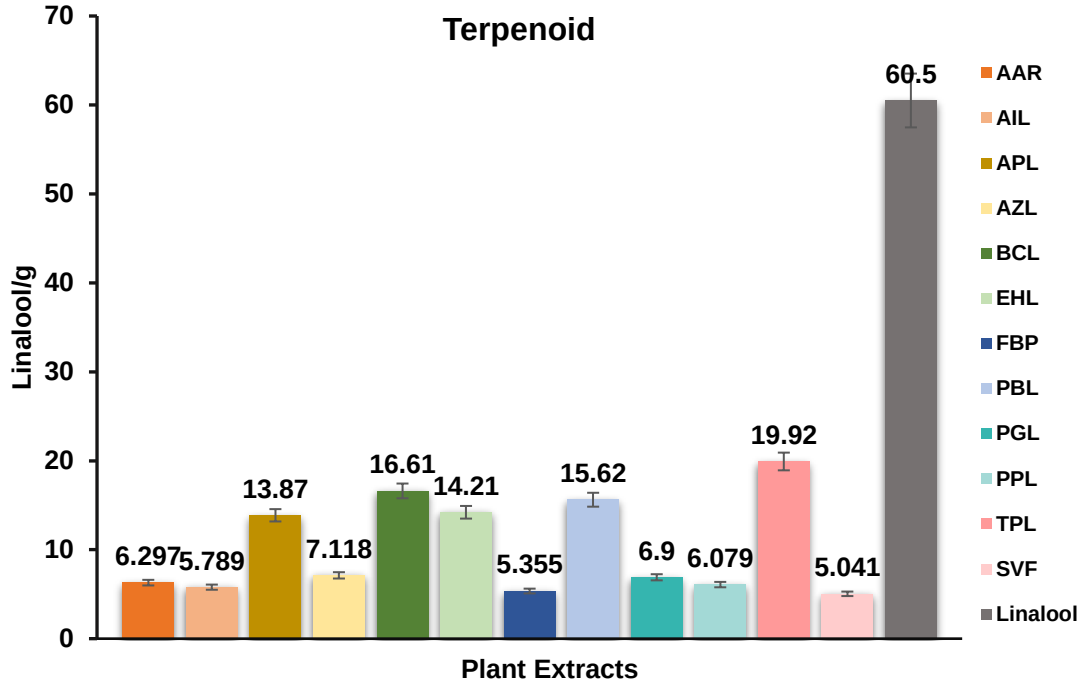

Figure 4.3. Estimation of total terpenoid content in selected plant extracts

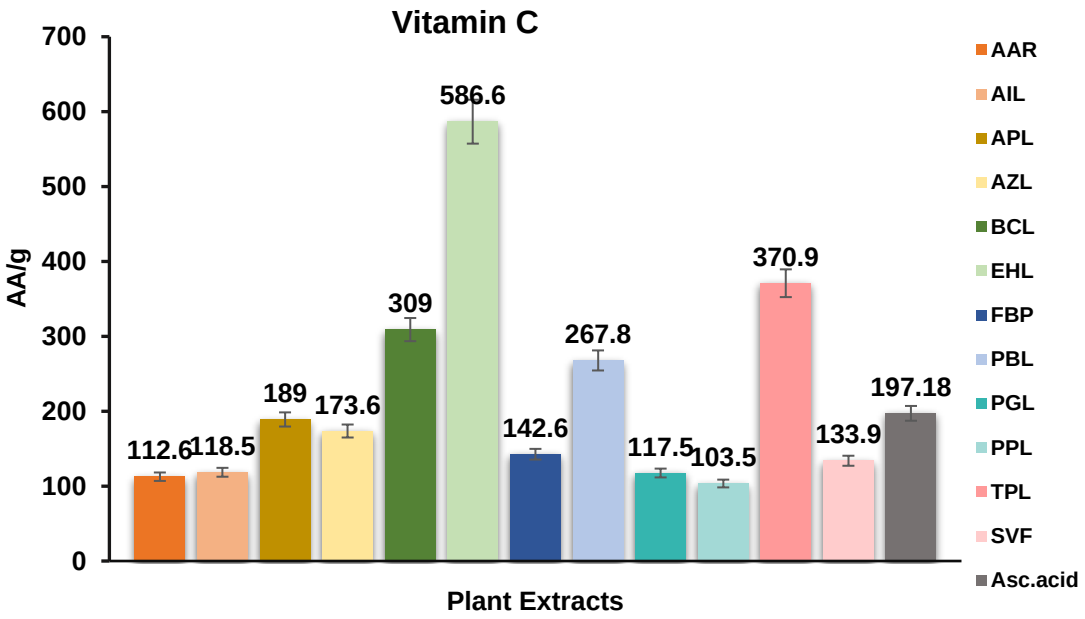

Figure 4.4. Estimation of vitamin C content in selected plant extracts

AAR-*Achyranthes aspera* Root, AIL-*Acalypha indica* Leaf, AZL-*Azadirachta indica* Leaf, APL-*Abrus precatorius* Leaf, BCL-*Barleria cuspidata* Leaf, EHL-*Euphorbia hirta* Leaf, FBP-*Ficus benghalensis* Prop root, PBL-*Piper betle* Leaf, PGL-*Psidium guajava* Leaf, PPL-*Pongamia pinnata* Leaf, TPL-*Tridax procumbens* Leaf, SVF-*Solanum virginianum* Fruit.

Similarly, several researchers have quantified various phytocompounds such as the total alkaloid and terpenoid content (10.73% and 13.135%) in *Azadiracta indica* leaf aqueous extracts (Nur Sazwi et al. 2013), a higher tannin content of 0.32mg TAE/g in ethanol leaf extracts of *Acalypha indica* (Tasmim et al. 2021), and a total alkaloid and tannin content of 13.6 mg/100g and 53.5mg TAE/g in ethanol aerial part extracts of *Acalypha indica* (Senthilkumar & Rani, 2024).

Previous studies revealed a significant amount of terpenoids of (38.59±2.70mg/g) in ethanolic *E. hirta* leaf extracts (Swarna Sudha & Padmini, 2023), tannin content of 26.1±0.80mg TAE/g in the *P. betle* leaf methanol extracts (Basit et al. 2023), ascorbic acid and alkaloid content of 0.255±0.006 mg/g, and 14.3±2.3mg/g, respectively (Bhardwaj & Naruka, 2023), tannin (0.016 TAEmg/g), and alkaloid (153.33mg) in *P. guajava* leaf extract (Santhosh & Sarojini, 2024) and alkaloid content of 10.191g/kg in methanolic leaf extract of *T. procumbens* (of alkaloids (Ikewuchi et al. 2015).

4.1.3 Quantification of Total Antioxidants

Flavonoids and other phenolic compounds are secondary metabolites containing OH groups derived from amino acids. Over, 8000 naturally occurring phenolic compounds, half of these being flavonoids have been reported for their effective biological activities, particularly as antioxidants (Tungmunnithum et al. 2018). These compounds play a crucial role in protecting the plant against ultraviolet radiation, pathogens, and parasites, and also aid in attracting pollinators and dispersing fruits. The hydroxyl groups in these extracts facilitate free radical scavenging, contributing to their antioxidant properties (Aryal et al. 2019). Hence, estimating TPC and TFC in plant extracts is crucial due to their strong antioxidant properties, which are linked to numerous health benefits and also contribute to the development of pharmaceutical products as an alternative and have been employed in many medical and pharmaceutical products as an alternative to synthetic agents.

4.1.3.1 Estimation of Total Phenolic Content

Folin–Ciocalteu was used to measure phenolic content by a calibration curve ($y = 0.821x-0.001$, $R^2=0.9938$) of gallic acid as a reference. The results were expressed in gallic acid equivalents (GAE) per gram dry weight of extracts.

The phenolic content of twelve methanol plant extracts ranged from 18.88±0.017 to 237.7±0.06mg GAE/g, representing an approximate four-fold difference. PGL, AAR, AZL, PPL, and SVF exhibited significant phenolic contents of 237.7±0.06, 188.66±0.120, 169.43±0.04, 157.50±0.06, and 102.74±0.06 mg GAE/g, respectively. In contrast, BCL, TPL, AIL, and FBP showed the lowest phenolic contents (18.88±0.017, 26.717±0.02, 32.234±0.03, and 37.629±0.011 mg GAE/g, respectively). A moderate range of total phenolic content was present in EHL, APL, and PBL of 51.138±007, 74.747±0.01, and 95.436±0.02mg GAE/g, respectively (**Figure 4.5**).

4.1.3.2 Estimation of Total Flavonoid Content

The results of the total flavonoid content (TFC) determined in the selected extracts are depicted in **Figure 4.6**. A calibration curve (y = 0.057x+ 0.0086, R^2=0.9915) of rutin (0–250µg/mL) was used to derive the results, which were expressed in rutin equivalents (RE) per gram dry extract weight. The total flavonoid content in methanol extracts of the twelve plants ranged from 32.087±0.010 to 228.63±0.08mg RE/g, exhibiting around a fourfold difference. PBL, PGL, and SVF exhibited significantly high flavonoid contents, with values of 228.63±0.08, 201.03±0.121, and 101.912±0.090mg RE/g, respectively. In contrast, the lowest flavonoid contents were observed in AAR (32.087±0.010mg RE/g), AZL (40.68±0.015mg RE/g), APL (43.315±0.010mg RE/g), and PPL (60.33±0.043mg RE/g). A moderate range of total flavonoid content was observed in FBP, EHL, BCL, AIL, and TPL with values ranging from 72.789±0.015 to 96.18±0.05mg RE/g.

Previously, several studies have been reported on the significant amounts of phenols and flavonoids in various extracts such as *A. precatorius* methanol leaf extract (Farhana et al. 2023), *Acalypha indica* ethanol leaf extracts (Tasmim et al. 2021), ethanolic extracts of *E. hirta* ethanol leaf extracts (Sudha & Padmini, 2023), *P. betle* methanol leaf extracts (Basit et al. 2023) and *P. guajava* methanol leaf extracts (Santhosh & Sarojini, 2024).

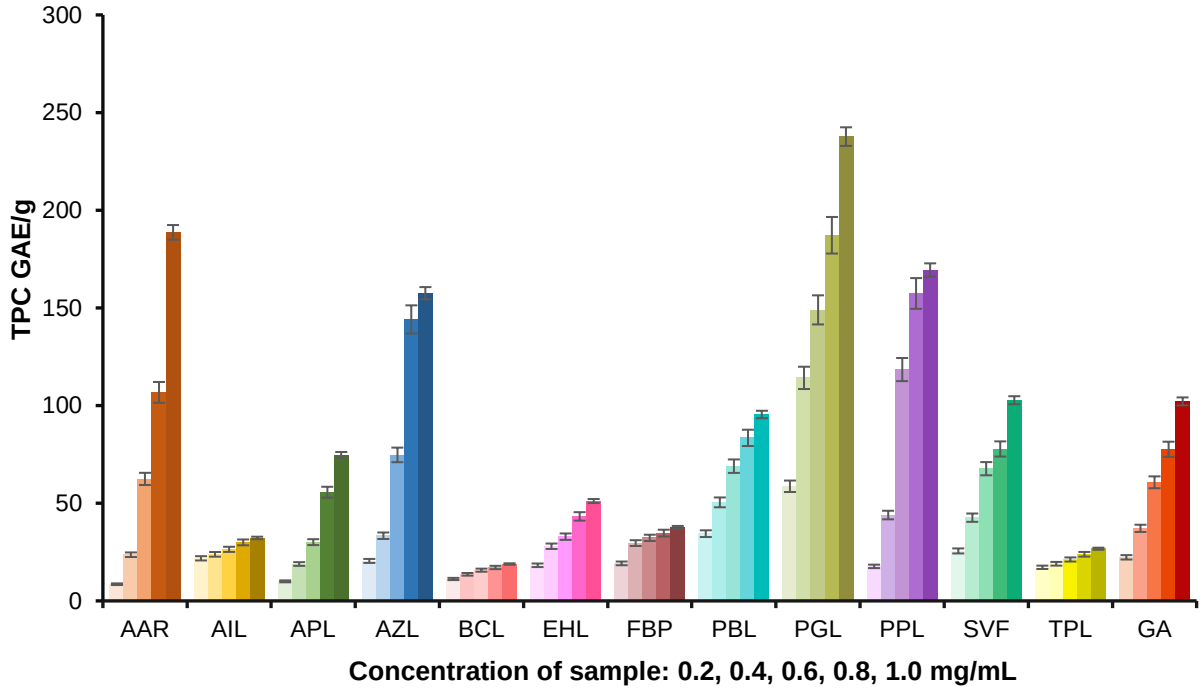

Figure 4.5. Total phenolic content (TPC) of selected plant extracts

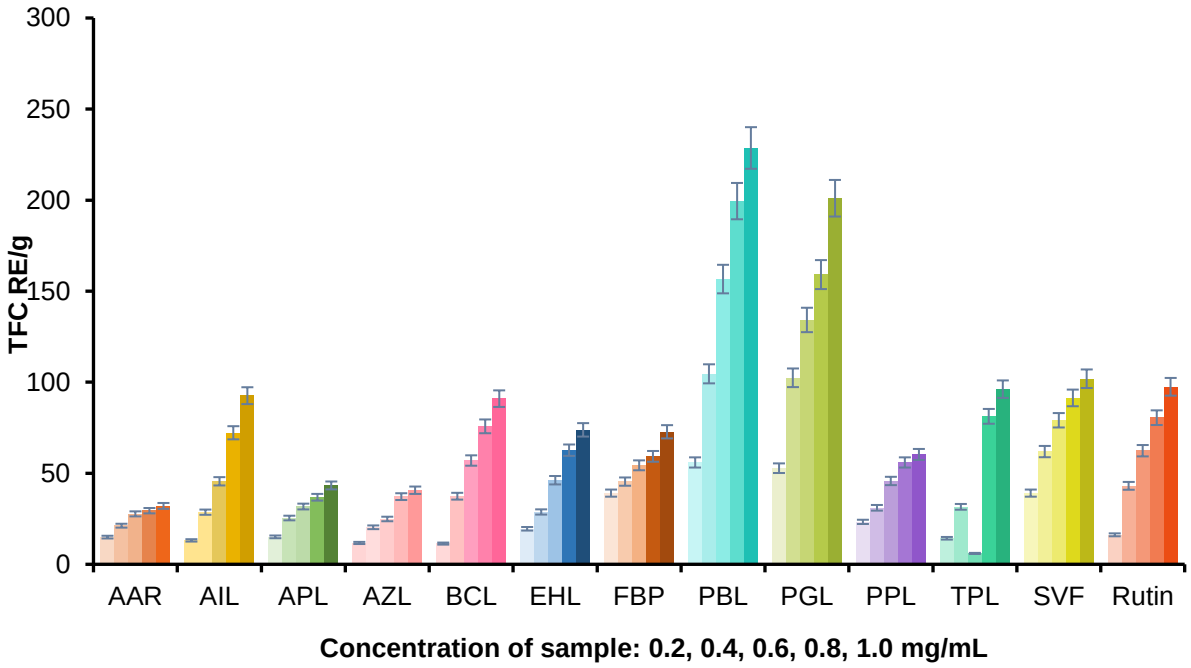

Figure 4.6. Total flavonoid content (TFC) of selected plant extracts

AAR-*Achyranthes aspera* Root, AIL-*Acalypha indica* Leaf, AZL-*Azadirachta indica* Leaf, APL-*Abrus precatorius* Leaf, BCL-*Barleria cuspidata* Leaf, EHL-*Euphorbia hirta* Leaf, FBP-*Ficus benghalensis* Prop root, PBL-*Piper betle* Leaf, PGL-*Psidium guajava* Leaf, PPL-*Pongamia pinnata* Leaf, TPL-*Tridax procumbens* Leaf, SVF-*Solanum virginianum* Fruit.

4.1.4 *In vitro* DPPH Radical Scavenging Assay

The onset and progression of multiple diseases have been linked to oxidative stress. ROS-induced oxidative damage can be effectively treated by supplementing natural antioxidants and strengthening the body's defense mechanism against free radicals (Kasote et al. 2015). Plants synthesize abundant sources of antioxidants, particularly, flavonoids, phenols, vitamin C, and tannins. These compounds exhibit a wide range of biological activities that protect against numerous chronic illnesses, like arteriosclerosis, cancer, and heart problems (Sharma & Patel, 2018). In the presence of radical scavengers, the free radical is neutralized, resulting in a decline in absorption and formation of reduced DPPH, accompanied by a loss of deep violet color (Asfaw, 2022). In this study, the antioxidant properties of the twelve plant extracts were evaluated using DPPH assay, with IC_{50} values reported in **Figure 4.7**.

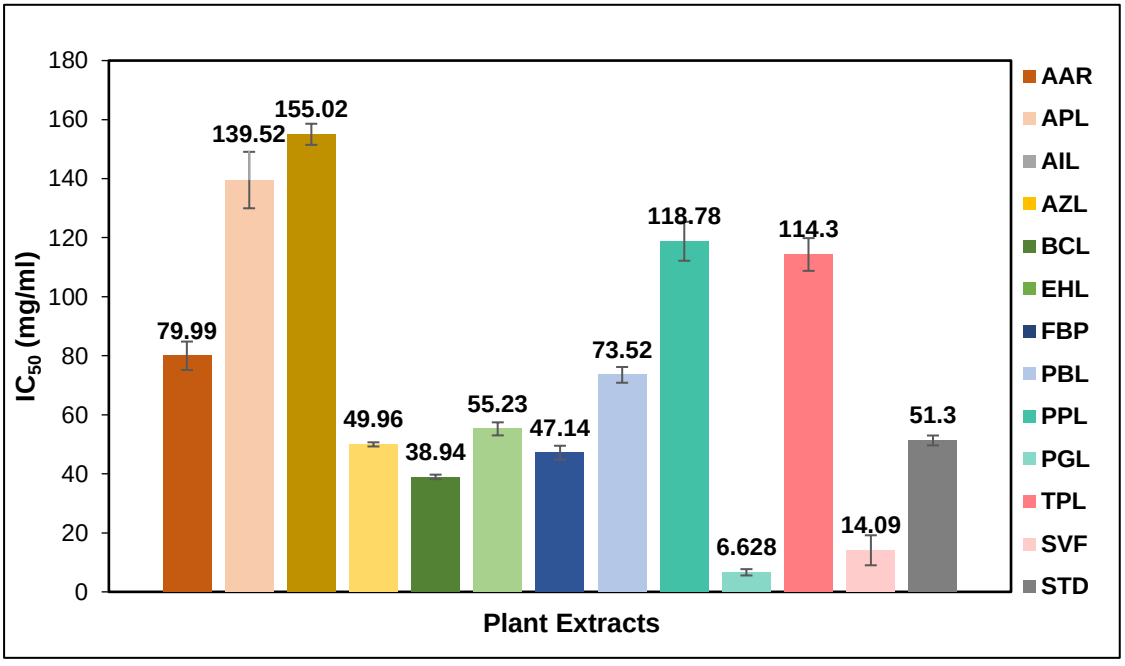

The IC_{50} values are represented in mg/ml. The expressed inhibitory concentration was statistically significant ($p<0.05$) among different plants

Figure 4.7. IC_{50} values of selected plant extracts

The DPPH radical scavenging activity of the plant extracts was comparable to that of the known antioxidant rutin. The results indicate significant inhibition ($p<0.05$) of different plant species investigated. The IC_{50} value, representing the

concentration of plant extracts required to scavenge 50% of free radicals was calculated to determine the antioxidant potency of each extract. A lower IC_{50} value indicated stronger antioxidant activity, while a higher value indicated weaker activity. The antioxidant activities of the plant extracts were ranked in the following order: PGL>SVF>BCL>FBP>AZL>EHL>PBL>AAR>TPL>PPL>APL>AIL.

According to the proposed scale, the extracts with IC_{50}<50mg/ml were highly active, those with IC_{50}<100mg/ml were moderately active, and those with IC_{50}>100mg/ml were considered low in antioxidant activity. Based on this scale, extracts of PGL (6.628±6.601mg/ml), SVF (14.09±5.08mg/ml), BCL (38.94±0.785mg/ml), FBP (47.14±20.02mg/ml), and AZL (49.96±0.705mg/ml) were classified as extracts with high antioxidant potency. In contrast, the extracts of EHL (55.23±2.210mg/ml), PBL (73.52±2.67mg/ml), AAR (79.99± 4.81mg/ml), and PPL (118.78±6.601mg/ml) exhibited moderate efficacy in scavenging capacity against DPPH when compared to the standard rutin. The remaining extracts, including TPL, AZL, and AIL, possessed relatively lower radical scavenging activity.

According to Farhana (2023), the methanol leaf extract of *A. precatorius* divulged excellent antioxidant properties compared to extracts obtained for ethanol, water, and petroleum ether. *P. betle* methanolic extracts (236±1.34mg TEAC/g) showed more potent radical scavenging activities than aqueous extracts (Basit et al. 2023). Similar findings have been reported by Santhosh & Sarojini, (2024) for *P. guajava*, which exhibited the strongest antioxidant activity with 86.24% activity at 250 µL of concentration, likely due to its high phenolic content and flavonoids, which have contributed significantly to anti-DPPH radical activity. Likewise, *T. procumbens* leaf methanol extracts exhibited anti-radical activity of 52.16% (Syed et al. 2020) and 52.63% (Patil & Pawar, 2018). The ethanol leaf extracts of *P. pinnata* showed 89% inhibition against DPPH radical at 125µg/ml concentration, which may have contributed to the availability of flavonoids and phenolic compounds (Sarje et al. 2020). These findings suggest that these plants with significant antioxidant properties may act as promising candidates for further exploration in developing antioxidant-rich formulations.

4.1.5 Antimicrobial Activities of Plant Extracts

4.1.5.1 Antimicrobial Activities of Plant Extracts on Clinical Cariogenic Isolates

The antibacterial screening of polyherbal crude extracts revealed that all tested bacterial pathogens were found to be sensitive to these extracts indicating their efficacy. However, the degree of sensitivity was influenced by the concentration of the extract and inhibition zone against the tested microorganisms. The results demonstrated that the extracts displayed significant antibacterial activity compared to antibiotics against the tested clinical isolates. The plant extracts were highly potent against all bacterial isolates at 10 mg/ml of concentration, which was equivalent to the efficacy of tested antibiotics. The antibacterial activity of the plant extracts was assessed against four Gram-positive bacterial strains, *S. mutans, S. salivarius, S. parasanguinis,* and *S. oralis,* as presented in **Table 4.3**.

The extracts AAR, EHL, PGL, SVF, BCL, FBP, and PBL demonstrated statistically significant ($p<0.0001$) inhibition against the bacterium, *S. mutans* with inhibition zones ranging from 18.3±1.52 to 24.0±1.00mm (**Figure 4.8**). Furthermore, *S. salivarius* was sensitive to the extracts SVF, EHL, AAR, PGL, and BCL which exhibited inhibition zones of 30.3±0.577*,* 26.0±4.58*,* 25.3±0.57, 22.6±1.52, and 17.6±1.52 mm, respectively (**Figure 4.9**). Extracts of EHL, PGL, BCL, and SVF also exhibited strong antibacterial activity against *S. parasanguinis* with inhibition zones of 22.6±1.52, 22.3±0.57, 20.0±1.00, and 19.3±0.57mm, respectively (**Figure 4.10**). *S. oralis* also exhibited inhibition zones ranging from 22.6±2.52 to 13.6±2.08mm in the extracts PGL, EHL, PBL, AAR, and SVF (**Figure 4.11**).

The antibacterial effectiveness of the extracts was assessed against three Gram-negative bacterial isolates such as *K. pneumoniae*, *P. aeruginosa*, and *A. baumanii* as presented in **Table 4.4**. The results showed that *K. pneumoniae* was significantly sensitive to extracts FBP, SVF, PGL, EHL, and BCL with inhibition zones ranging from 15.6±0.57 to 18±1.00mm (**Figure 4.12**). *P. aeruginosa* was resilient to most of the extracts mainly for EHL, PGL, BCL, AAR, and AIL which exhibited inhibition zones ranging from 20.3±0.577 to 27±2.51mm (**Figure 4.13**). *A. baumanii* was found to be sensitive to extracts EHL, BCL, FBP, PGL, AIL, and SVF with inhibition zones ranging from 21.6±1.52 to 24±1.00mm (**Figure 4.14**).

The results showed that the extracts BCL (19±1.00 mm), EHL (19±1.00mm), SVF (19±1.00mm), and APL (18.3±0.57mm) exhibited greater inhibition zones against the fungal strain *C. albicans* (**Figure 4.15**). The IZD results revealed that extracts FBP, EHL, BCL, PGL, and AIL were effective against Gram-negative isolates, while the fungal isolate was found to be sensitive towards the extracts BCL, EHL, APL, and SVF. The extracts of AZL, PPL, and TPL were found to have minimum inhibition effect against the tested microorganisms compared to the others. The commercial antimicrobial agents used in this study showed varying degrees of sensitivity and resistance against the tested microorganisms. The positive control of sodium fluoride (NaF) (10mg/mL) inhibited the growth of Gram-positive isolates including SMU (16.6±0.57mm), SSA (19.0±2.00mm), SPSA (18.0±1.00mm), and SOS (17.0±0.57mm), Gram-negative isolates such as KP (17.6±0.57mm), PA (15.3±0.57mm), AB (23.0±1.00 mm), and the fungus CA (16.5±1.00mm). In contrast, the negative control did not exhibit any inhibitory effects. The study revealed that most of the oral pathogens were highly susceptible to the methanolic extracts of AAR, BCL, EHL, FBP, PGL, and SVF indicating the presence of potentially active compounds with anti-cariogenic activity.

Our present findings correlated with Jebashree et al. (2011) who revealed the ability of *P. guajava* leaves to inhibit *S. mutans* and *C. albicans* at 5mg/disc with a diameter of 14 and 15mm. Similarly, Deshpande & Kadam, (2013) reported the ethanol leaf extract of *P. betel* exhibits a higher IZD of 20.6±1.12mm, than the aqueous crude extract of 8.3±0.53mm against *S. mutans*. Kuta et al. (2013), proved the appreciable activity of *E. hirta* methanol extract (10mg/mL) against *S. mutans,* and *P. vulgaris* with 6-11mm and 2-20mm, respectively.

Manikandan et al. (2017) reported that an aqueous extract of *F. benghalensis* prop root has moderate IZD against *S. mutans* (6mm) and *L. acidophilus* (10mm) at 250µl. In the present study, the antibacterial effectiveness of the extracts at different concentrations was able to inhibit the growth of selected oral pathogens that correlated with the findings of Yadav et al. (2020) who reported that the aqueous extract of *A. aspera* root (10mg/ml) exhibited IZD of 21 mm against *S. mutans*.

Table 4.3. Inhibitory zone diameter (mm) of selected plant extracts against Gram-positive oral clinical isolates

Conc. (µg/ml)	Plant extracts												Positive control
	AAR	**AIL**	**APL**	**AZL**	**BCL**	**EHL**	**FBP**	**PBL**	**PGL**	**PPL**	**TPL**	**SVF**	**NaF**
Streptococcus mutans													
25	11.0±1.00	10.0±0.00	9.30±0.57	0	9.00±0.00	11.3±0.57	0	0	11.0±1.00	0	0	9.00±0.00	0
50	15.0±1.00	11.6±1.52	11.6±0.57	0	11.6±0.57	14.0±1.00	12.3±0.57	11.3±1.52	13.6±1.15	10.0±0.00	10.3±0.57	11.6±0.57	9.3±8.32
100	19.0±1.73	14.0±1.00	14.0±1.00	0	14.0±1.00	17.0±1.00	14.3±1.154	9.30±8.32	17.0±1.00	10.6±0.57	12.3±0.57	15.3±0.57	12.3±0.57
150	**24.0±1.00**	16.6±0.57	17.0±1.00	10	18.6±0.57	**20.3±0.57**	**18.3±1.52**	16.6±4.6	**20.6±0.20**	14.3±1.15	15.0±1.00	**23.3±1.52**	**16.6±0.57**
Streptococcus salivarius													
25	11.3±1.15	0	0	0	0	14.3±2.08	9.60±0.57	0	12.6±1.15	0	0	19.0±1.00	0
50	15.0±1.00	0	0	10.3±0.57	10.6±0.57	18.6±2.30	10.6±0.57	0	15.3±1.52	0	0	22.3±0.57	10.0±1.73
100	20.3±1.52	11.3±1.15	10.3±0.57	12.0±1.00	13.6±1.52	22.3±3.78	12.6±0.57	11.6±0.57	19.0±2.00	11.6±0.57	8.30±7.23	26.3±0.57	12.6±0.57
150	**25.3±0.57**	13.6±0.57	14.6±0.57	13.6±0.57	17.6±1.52	**26.0±4.58**	16.0±1.00	14.6±0.57	**22.6±1.52**	13.3±0.57	14.6±0.57	**30.3±0.57**	19.0±2.00
Streptococcus parasanguinis													
25	11.6±0.57	0	11.0±1.00	0	12.3±0.57	13.0±1.00	10.0±0.00	15.6±0.57	10.0±0.00	0	0	0	0
50	14.3±0.57	0	13.3±0.57	10.3±0.57	13.3±0.57	16.0±1.00	12.3±0.57	17.3±0.57	12.3±0.57	0	0	0	11.3±0.57
100	15.6±0.57	0	15.0±0.00	12.0±1.00	15.6±0.57	19.0±1.00	14.3±0.57	20.6±0.57	15.0±1.00	11.3±0.57	11.6±0.57	14.3±0.57	16.3±0.57
150	18.0±1.00	14.0±1.00	17.3±0.57	13.6±0.57	**20.0±1.00**	**22.6±1.52**	16.6±0.57	18.0±1.00	**22.3±0.57**	14.6±0.57	14.3±0.57	19.3±0.57	18.0±1.00
Streptococcus oralis													
25	0	0	0	0	0	11.3±1.15	0	0	11.3±0.57	0	0	0	0
50	10.0±1.154	0	10.0±0.00	0	0	15.3±1.52	0	12.3±1.15	15.0±1.00	0	0	0	10.0±0.00
100	14.6±2.51	11.0±1.00	12.0±1.00	10.0±0.00	11.0±1.00	18.0±1.00	11.6±15.0	17.0±1.00	17.0±1.00	12.0±1.00	12.0±1.00	16.0±1.00	14.6±2.51
150	**19.0±1.00**	15.0±1.00	14.3±0.57	13.6±2.08	15.0±1.00	**21.0±1.00**	15.0±1.00	**20.0±1.00**	**22.6±2.52**	16.0±1.00	16.0±1.00	**18.3±0.57**	17.0±0.57
P value	<0.0001	<0.0001	<0.0001	<0.0001	<0.0001	<0.0001	<0.0001	<0.0001	<0.0001	<0.0001	<0.0001	<0.0001	<0.0001

The mean diameters of the inhibition zone (mm) are reported as mean values±standard deviation. A one-way ANOVA test with Tukey's post hoc test was performed to evaluate the statistical significance ($p<0.0001$) of multiple comparisons for each bacterial isolate. 0: No inhibitory effect. Noteworthy inhibition values are denoted in bold. AAR-*Achyranthes aspera* Root, AIL-*Acalypha indica* Leaf, AZL-*Azadirachta indica* Leaf, APL- *Abrus precatorius* Leaf, BCL-*Barleria cuspidata* Leaf, EHL-*Euphorbia hirta* Leaf, FBP-*Ficus benghalensis* Prop Root, PBL-*Piper betel* Leaf, PGL-*Psidium guajava* Leaf, PPL-*Pongamia pinnata* Leaf, TPL- *Tridax procumbens* Leaf, SVF-*Solanum virginianum* Fruit, Sodium fluoride (NaF) as positive control.

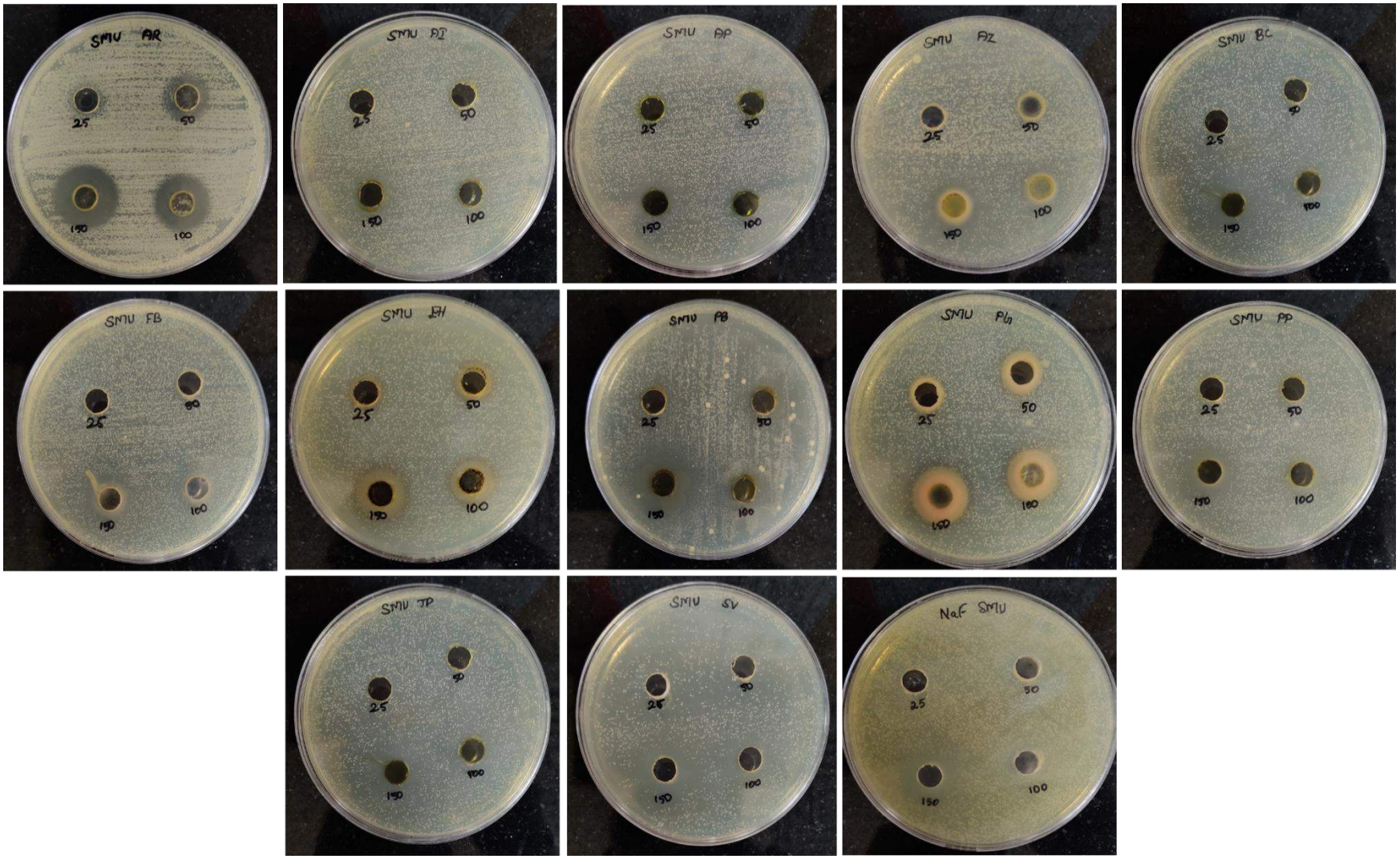

Figure 4.8. Antimicrobial activity of plant extracts against *Streptococcus mutans* (SMU)

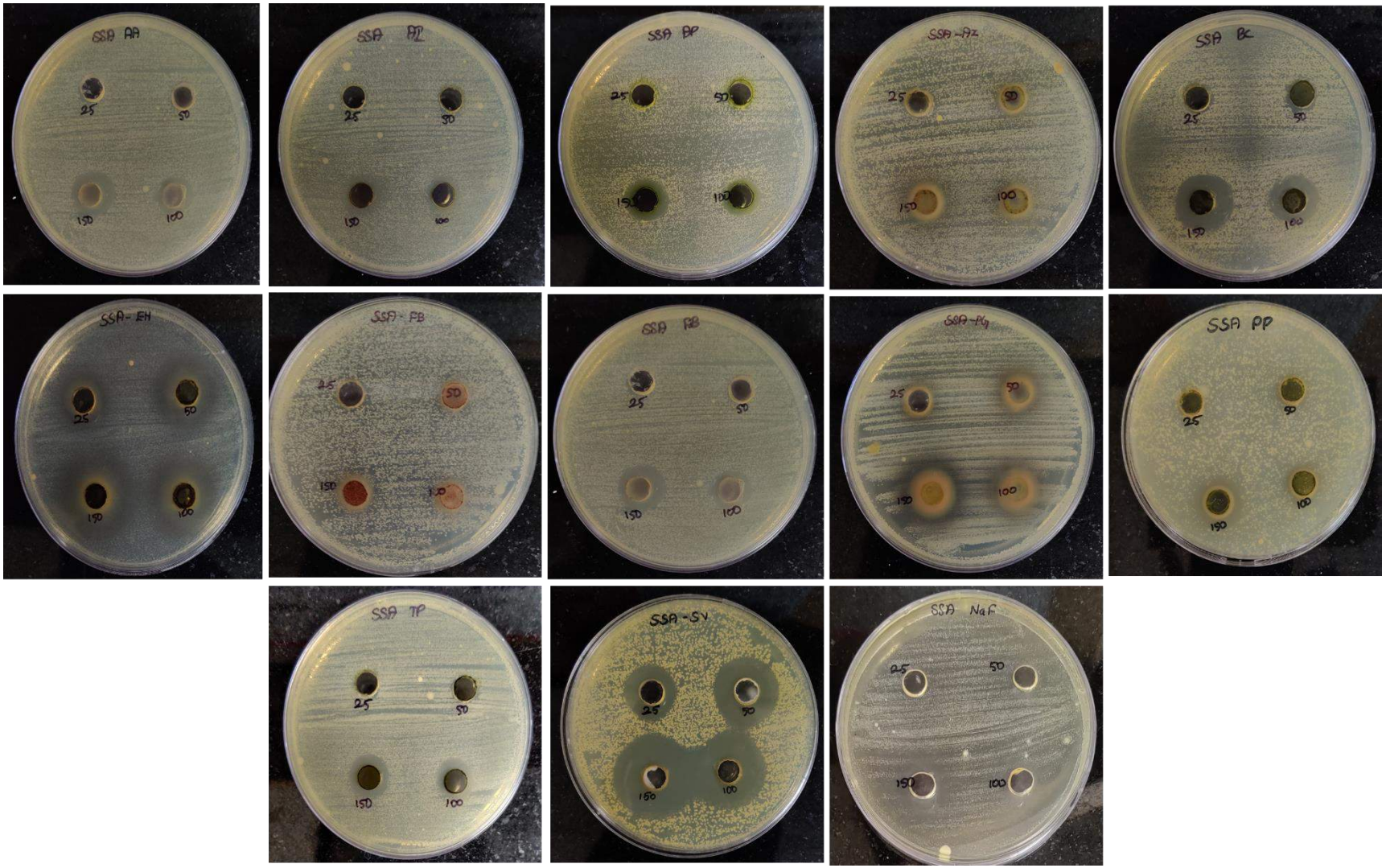

Figure 4.9. Antimicrobial activity of plant extracts against *Streptococcus salivarius* (SSA)

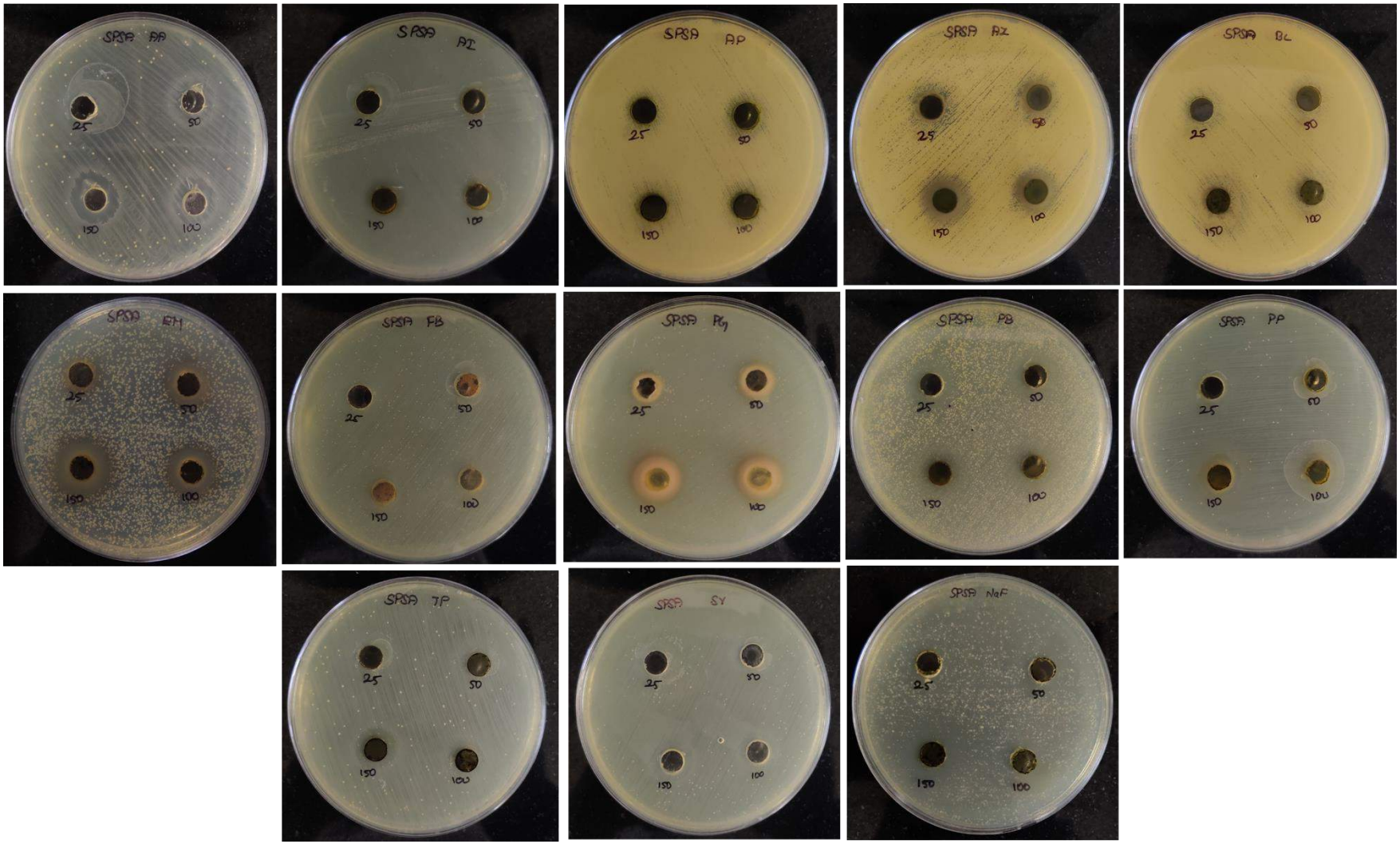

Figure 4.10. Antimicrobial activity of plant extracts against *Streptococcus parasanguinis* (SPSA)

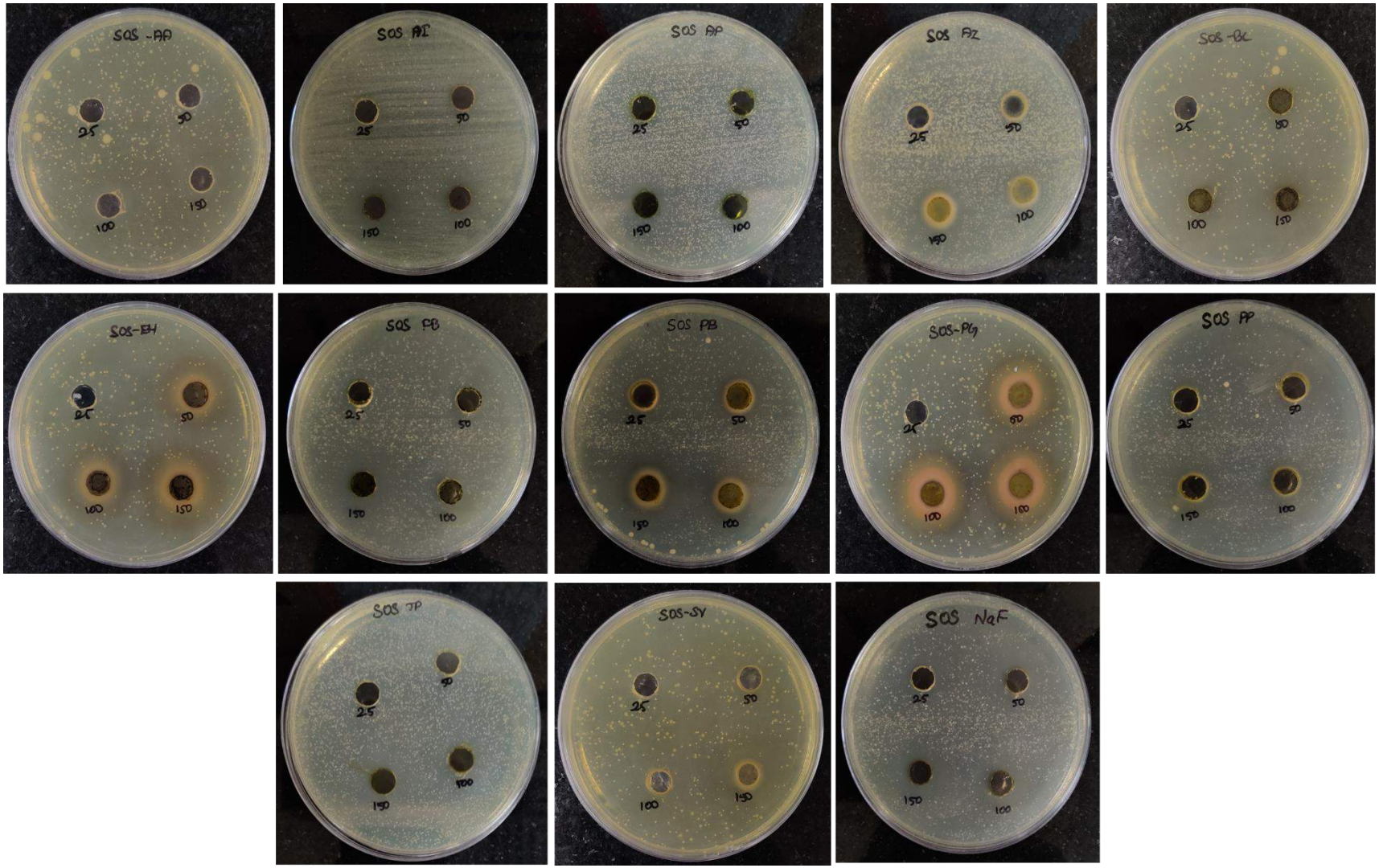

Figure 4.11. Antimicrobial activity of plant extracts against *Streptococcus oralis* (SOS*)*

Table 4.4. Inhibitory zone diameter (mm) of twelve plant extracts against Gram-negative and fungal oral clinical isolates

Conc. (µg/ml)	Plant extracts												Positive control
	AAR	**AIL**	**APL**	**AZL**	**BCL**	**EHL**	**FBP**	**PBL**	**PGL**	**PPL**	**TPL**	**SVF**	**NaF**
Klebsiella pneumonia													
25	0	0	0	3.30±5.77	0	3.30±5.77	0	0	3.30±5.77	0	0	6.60±5.77	0
50	0	0	0	11.0±0.00	10.6±0.57	7.60±6.65	8.00±6.92	0	11.0±0.00	0	0	13.0±0.00	10.6±0.57
100	11.3±0.57	12.3±0.57	11.6±0.57	12.0±0.00	13.3±0.57	13.6±0.57	13.0±0.00	11.3±0.57	12.6±0.57	6.60±5.77	12.0±1.00	3.00±1.52	13.3±0.57
150	14.0±1.00	14.3±0.57	13.6±0.57	13.6±0.577	15.6±0.57	15.6±0.57	**18.0±1.00**	14.3±0.57	16.0±1.00	12.3±0.57	13.6±1.52	16.6±1.52	17.6±0.577
Pseudomonas aeruginosa													
25	0	0	0	0	0	13.6±1.52	0	10.3±0.57	14.0±1.00	0	0	0	0
50	10.6±0.57	3.33±5.77	0	10.6±0.57	11.0±1.00	18.0±2.64	11.0±1.00	12.3±0.57	16.0±1.00	3.60±6.35	0	3.60±6.35	10.6±0.57
100	14.6±0.57	14.3±0.57	11.6±0.57	13.6±1.52	17.3±3.05	22.0±3.60	16.0±1.00	15.0±1.00	18.6±1.52	13.0±2.64	12.0±1.00	13.3±2.08	13.6±1.52
150	**20.6±1.154**	**20.3±0.57**	16.0±1.00	18.0±2.64	**22.3±3.055**	**27.0±2.51**	18.3±1.52	18.3±2.08	**23±2.64**	16.0±2.64	17.0±1.00	17.6±2.51	15.3±0.57
Acinetobacter baumanii													
25	0	0	6.60±5.77	0	0	11.6±1.52	0	3.30±5.77	11.6±0.57	0	4.00±6.92	0	0
50	0	7.60±6.65	12.0±1.00	6.60±5.77	7.60±6.65	14.6±1.52	11.6±0.57	11.6±0.57	14.3±0.57	11.0±1.00	12.0±12.64	11.6±0.57	11.6±0.57
100	14.0±1.00	18.6±1.52	17.0±1.00	17.0±1.00	18.6±1.52	18.6±1.52	13.6±0.57	16.6±1.52	17±1.00	14.0±1.00	18.6±1.15	16.6±0.57	18.6±1.52
150	18.6±1.52	**22.0±1.00**	20.6±0.57	20.3±0.57	**23.3±2.08**	**24.0±1.00**	**23.0±2.64**	**20.3±0.57**	**22.6±0.57**	21.3±0.57	22.0±1.00	**23.6±1.52**	23.0±1.00
Candida albicans													
25	0	0	0	0	0	0	0	0	0	0	0	0	0
50	11.0±1.00	0	0	0	0	11.0±1.00	0	0	3.33±5.77	0	0	10.6±0.57	10.0±0.57
100	13.3±0.57	11.6±0.57	11.6±0.57	12.3±0.57	13.6±0.57	14.0±1.00	12.3±0.57	12.6±0.57	13.6±0.57	13.0±1.00	12.3±0.57	14.3±0.57	12.6±1.52
150	15.3±0.57	13.0±0.00	18.3±0.57	17.6±0.57	**19.0±1.00**	**19.0±1.00**	17.6±0.57	18.3±0.57	17.3±0.57	16.3±0.57	14.6±0.57	**19±1.00**	16.5±1.00
P value	<0.0001	<0.0001	<0.0001	<0.0001	<0.0001	<0.0001	<0.0001	<0.0001	<0.0001	<0.0001	<0.0001	<0.0001	<0.0001

The mean diameters of the inhibition zone (mm) are reported as mean values±standard deviation. A one-way ANOVA test with Tukey's post hoc test was performed to evaluate the statistical significance (*p<0.0001*) of multiple comparisons for each bacterial isolate. 0: No inhibitory effect. Noteworthy inhibition values are denoted in bold. AAR-*Achyranthes aspera* Root, AIL-*Acalypha indica* Leaf, AZL-*Azadirachta indica* Leaf, APL- *Abrus precatorius* Leaf, BCL-*Barleria cuspidata* Leaf, EHL-*Euphorbia hirta* Leaf, FBP-*Ficus benghalensis* Proproot, PBL-*Piper betel* Leaf, PGL-*Psidium guajava* Leaf, PPL-*Pongamia pinnata* Leaf, TPL- *Tridax procumbens* Leaf, SVF-*Solanum virginianum* Fruit, Sodium fluoride (NaF) as positive control.

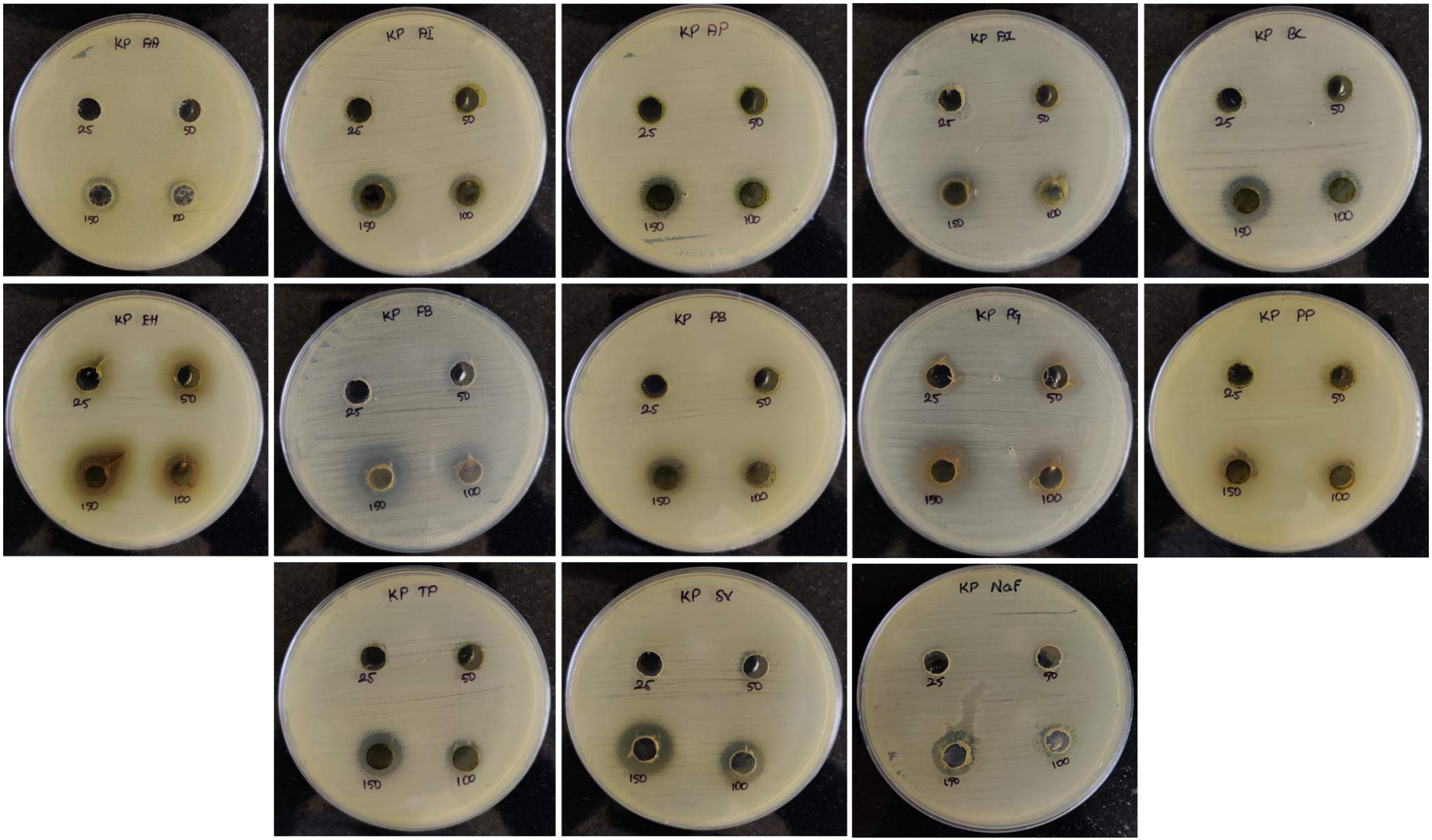

Figure 4.12. Antimicrobial activity of plant extracts against *Klebsiella pneumoniae* (KP)

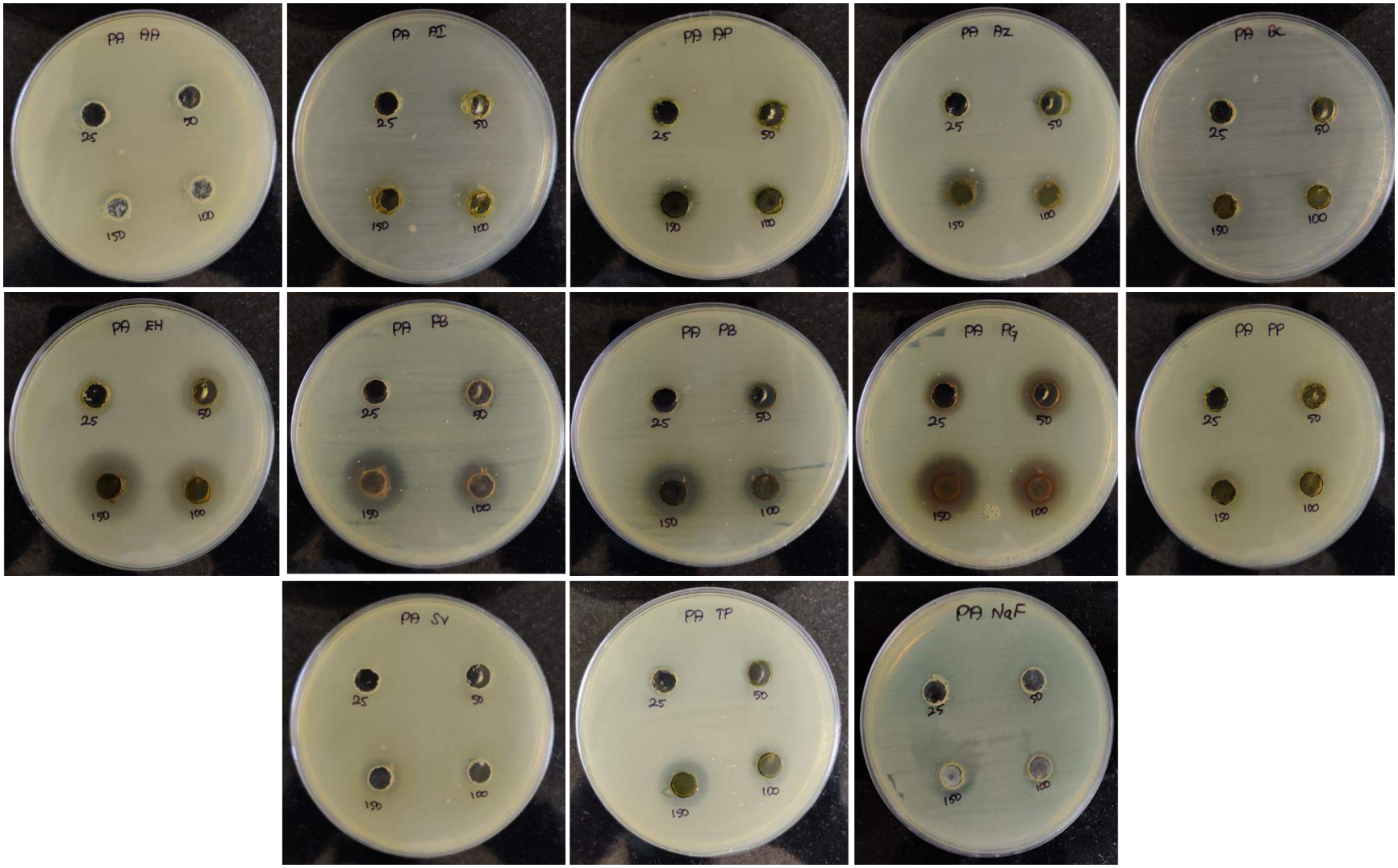

Figure 4.13. Antimicrobial activity of plant extracts against *Pseudomonas aeruginosa* (PA)

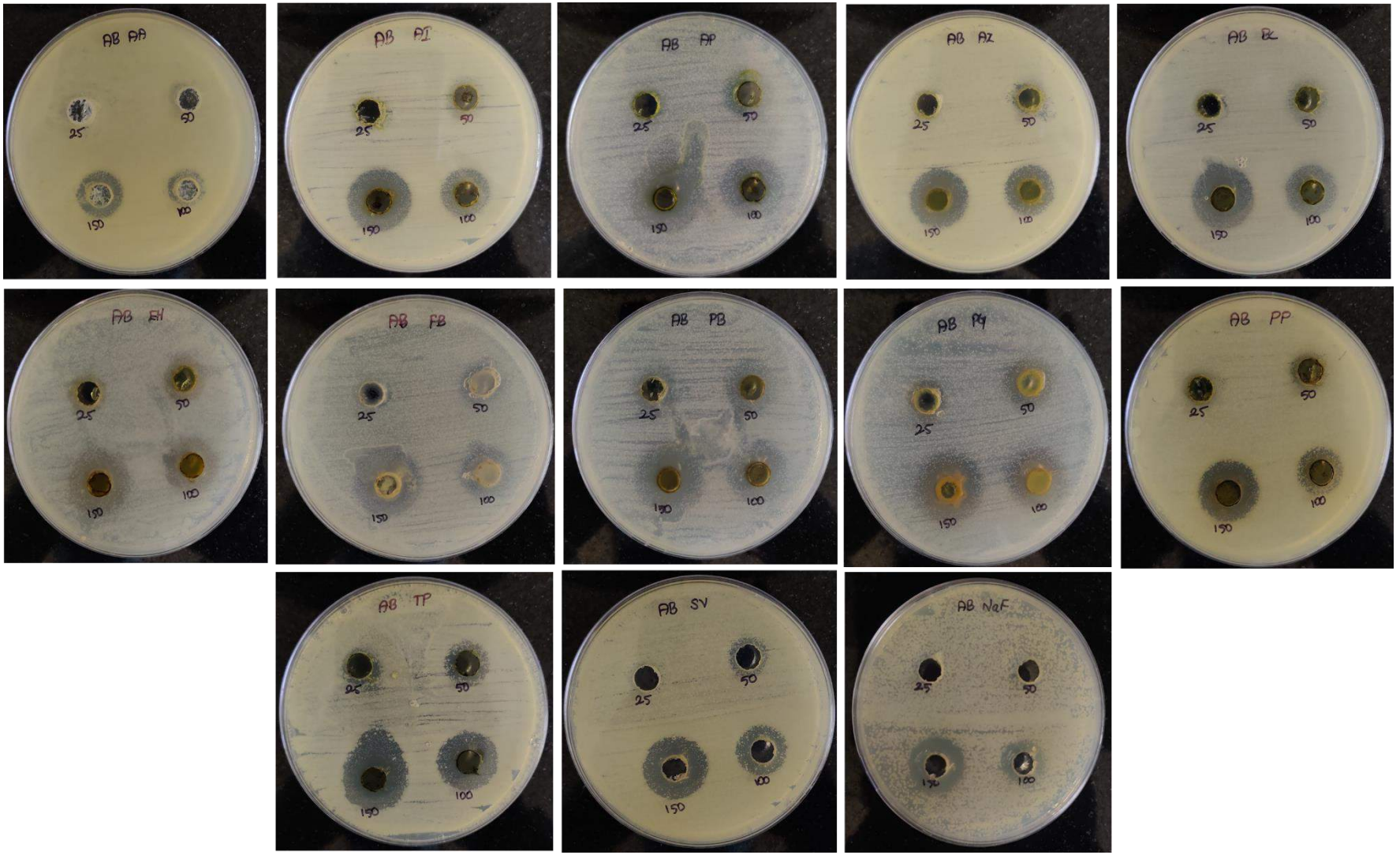

Figure 4.14. Antimicrobial activity of plant extracts agasinst *Acinetobacter baumannii* (AB)

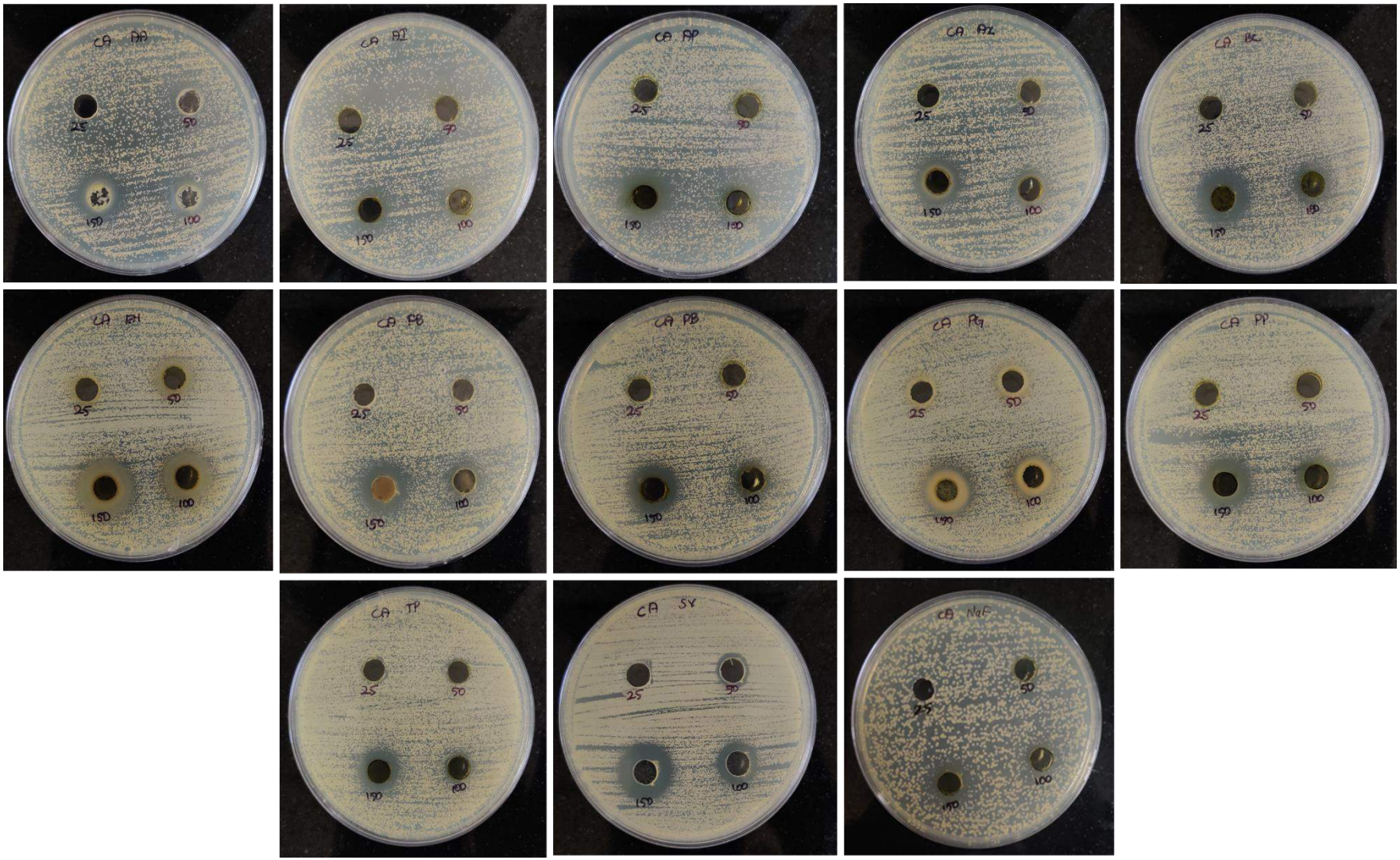

Figure 4.15. Antifungal activity of plant extracts against *Candida albicans* (CA)

Andika et al. (2023) reported the inhibitory effect of *A. precatorius* leaf alcoholic extract against the growth of *S. mutans* with IZD (12.2 mm), MIC (12.5mg/mL), and MBC (25mg/mL), which may be due to the presence of glycosides (abrusoside AD and abrusgenin), flavonoids and saponins (glycerin) that make them effective against the oral pathogen. Our results were supported by Rajaselvam et al (2023), who stated *S. virginianum* ethanolic seed extracts have active components to treat oral caries with strong antimicrobial activity on *S. mutans* (28mm) followed by *S. mitis* (22mm), *S. oralis* (21mm), *L. acidophilus* (16mm) and *P. aeruginosa* (14mm).

4.1.5.2 Determination of the MIC and MBC/MFC

All the plant extracts were screened for their microbial susceptibility studies using the micro broth dilution method as per the guidelines of the Clinical and Laboratory Standards Institute (CLSI). *In vitro* antimicrobial efficacies of several medicinal herbs against clinically isolated cariogenic bacteria were assessed by a two-fold serial dilution method. The minimal inhibitory concentration (MIC) and minimum bactericidal concentration/ minimum fungicidal concentration (MBC/MFC) values of twelve plant extracts against the bacteria range within 0.3125-20mg/ml are presented in **Table 4.5**.

Among the eight types of oral bacteria examined, Gram-positive isolates, *S. mutans, S. salivarius, S. parasanguinis,* and *S. oralis* were the most susceptible to AAR, BCL, EHL, FBP, PGL, and SVF which showed minimum inhibitory concentrations of 0.625-5mg/mL, while the MBC ranged 1.25-20mg/mL for the same. Gram-negative isolates *P. aeruginosa, K. pneumonieae,* and *A. baumanii* were more sensitive towards the plant extracts EHL, PBL, PGL, and SVF when compared to the other extracts, with the MIC range of 0.3125-2.5mg/mL. For *C. albicans*, the MIC value of 1.25mg/mL was noted in the plant extracts EHL, FBP, and PBL followed by the lowest MFC value of 2.5mg/mL. Extracts from AAR, BCL, EHL, FBP, PGL, and SVF demonstrated the lowest MIC (0.625-1.25 mg/mL) and MBC (1.25-2.5mg/mL) values, indicating their potential as effective natural antimicrobial agents against dental caries pathogens. This variation suggests that some extracts were more potent than others, and the efficacy of each extract was microorganism-specific.

Table 4.5. MIC and MBC/MFC of different plant extracts against oral pathogens

Plant extracts (mg/mL)	Bacterial isolates															
	SMU		SSA		SPSA		SOS		KP		PA		AB		CA	
	MIC	MBC	MIC	MBC	MIC	MBC	MIC	MBC	MIC	MBC	MIC	MBC	MIC	MBC	MIC	MFC
AAR	**1.25**	**2.5**	2.5	5	**1.25**	2.5	**1.25**	2.5	**0.625**	**1.25**	**0.625**	**1.25**	2.5	5	2.5	5
APL	5	10	2.5	5	2.5	5	2.5	5	2.5	5	10	20	2.5	5	2.5	5
ACL	5	10	5	10	2.5	5	2.5	5	1.25	2.5	2.5	5	2.5	5	2.5	5
AIL	5	5	5	10	5	10	1.25	2.5	1.25	2.5	2.5	5	2.5	5	2.5	5
BCL	2.5	5	**0.625**	**1.25**	1.25	5	1.25	2.5	1.25	2.5	1.25	2.5	2.5	5	**1.25**	**2.5**
FBP	**0.625**	**2.5**	1.25	2.5	1.25	2.5	1.25	2.5	1.25	2.5	**0.625**	**1.25**	**1.25**	**2.5**	2.5	5
EHL	2.5	5	2.5	5	2.5	5	2.5	5	1.25	5	**0.625**	**1.25**	2.5	5	**1.25**	**2.5**
PBL	5	10	5	10	5	10	2.5	5	5	10	2.5	5	2.5	5	1.25	2.5
PGL	**0.625**	**1.25**	1.25	5	**0.625**	**1.25**	1.25	2.5	2.5	5	**0.625**	**1.25**	2.5	5	5	10
PPL	5	10	5	10	5	10	2.5	5	1.25	2.5	2.5	5	2.5	5	2.5	5
TPL	5	10	5	10	5	10	2.5	5	1.25	2.5	5	10	2.5	5	2.5	5
SVF	**1.25**	**2.5**	2.5	5	2.5	5	2.5	5	2.5	5	**0.625**	**1.25**	2.5	5	2.5	5
NaF	2.5	5	2.5	5	2.5	5	2.5	5	1.25	2.5	0.625	1.25	0.625	1.25	2.5	5
DMSO	**NI**		**NI**		**NI**		**NI**		**NI**		**NI**		**NI**		**NI**	

AAR-*Achyranthes aspera* Root, AIL-*Acalypha indica* Leaf, AZL-*Azadirachta indica* Leaf, APL- *Abrus precatorius* Leaf, BCL-*Barleria cuspidata* Leaf, EHL-*Euphorbia hirta* Leaf, FBP-*Ficus benghalensis* Prop Root, PBL-*Piper betel* Leaf, PGL-*Psidium guajava* Leaf, PPL-*Pongamia pinnata* Leaf, TPL- *Tridax procumbens* Leaf, SVF-*Solanum virginianum* Fruit, Sodium fluoride (NaF) as positive control. MIC and MBC/MFC are expressed as mg/ml-noteworthy values denoted in bold. SMU-*S. mutans*, SSA-*S. salivarius*, SPSA-*S. parasanguinis*, KP-*K. pneumonieae*, PA-*P. aeruginosa*, AB-*A. baumanii*, CA-*C. albicans*. NI-No inhibition.

The minimum concentration, or MIC, is the lowest concentration of the chemical that prevents the growth of the bacteria. MBC is a complementary test for MIC, which depicts the minimum concentration of chemicals causing bacterial death. The MIC value of each tested plant extract exhibits differences in the inhibitory concentration, attributed to various secondary metabolites in the respective herbs. In our study, the antibacterial findings of *P. guajava* methanol extract against *S. mutans* and *C. albicans* are correlated with the findings of Jebashree et al (2011) who demonstrated that they exhibited inhibitory effects against *S. mutans* and *C. albicans* with MIC values of <0.076 and 0.625mg/mL, respectively.

Teanpaisan et al (2017) demonstrated the potential of *P. betle* leaf ethanol extract against *S. mutans* with a MIC and MBC of 1.56mg/mL and 3.17mg/ml, respectively which may be due to the presence of 4-chromanol (62.33%) and eugenol (17.10%). The results agree with Deshpande & Kadam, (2013) who reported a similar inhibitory effect of *P. betle* ethanol leaf extracts against *S. mutans* at a concentration of 5mg/mL.

4.1.5.3 Biofilm Eradication Potential of Plant Extracts

Using the crystal violet staining assay, the plant extracts exhibiting strong antimicrobial activity at the lowest concentrations were selected for their biofilm eradication testing. In the present work, the extracts of the plants exhibited varying degrees of inhibition on the biofilm-forming ability of cariogenic pathogens (**Figure 4.16**). The minimum biofilm eradication of the plant extracts AAR, BCL, EHL, FBP, PGL, and SVF at the MIC level ranged from 62.5 to 94.4% against the tested microbes. The plant extracts EHL, SVF, and AAR showed significant ($p<0.001$) biofilm inhibition at the MIC level against Gram-positive agents, including SMU, SSA, SPSA, and SOS. EHL exhibited 90% and 94.4% inhibition of SMU and SSA biofilm formation, respectively, followed by SVF (87 and 93.2%) and AAR (89.2 and 88.4%). In contrast, extracts BCL, EHL, FBP, and PGL demonstrated significant ($p<0.001$; $p<0.005$) inhibitory effects ranging from 86.2 to 93.6%, at MIC level (0.002-0.012mg/ml) against Gram-negative agents KP, PA, and AB. The extracts EHL and SVF also revealed promising inhibition of 82.6 and 80.2%, respectively against the fungal pathogen CA. These findings suggest that

the plant extracts possess potential biofilm inhibitory properties, warranting further investigation into their mechanism of action and potential benefits in combating microbial biofilm formation. The results indicated that extract EHL exhibited the highest biofilm inhibitory activity, followed by extracts PGL and SVF against all the cariogenic isolates. Extracts AAR, BCL, and FBP also showed significant biofilm inhibitory potential, despite higher concentrations. The secondary metabolites present in these plants exhibit antibiofilm effects due to specific biochemical characteristics. In addition to chemical composition, the antimicrobial activity of plant extracts is also determined by their physicochemical properties such as lipophilicity, solubility, and the presence of functional groups. Complex and diverse chemical constituents are mostly found in medicinal plant extracts and their synergistic combination with diverse biochemical activities enhances the efficacy of plant extracts.

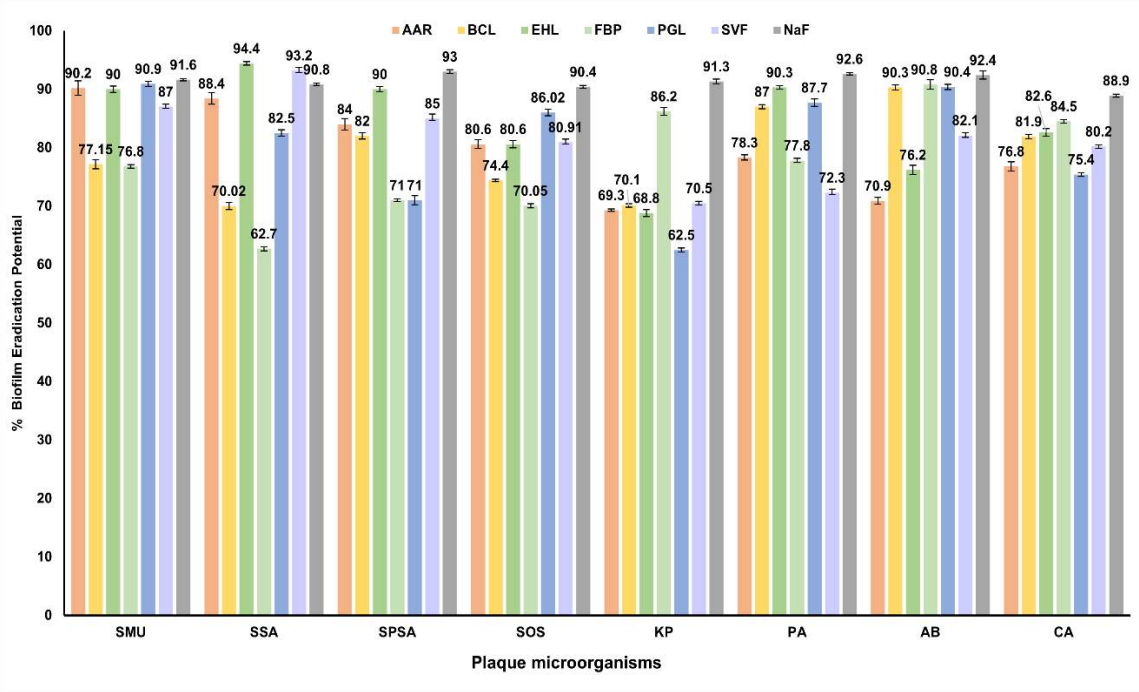

Plant extracts and sodium fluoride (NaF) at MIC using biofilm inhibition assay. The values were subjected to Tukey's post-hoc test ($p<0.05$). SMU- *S. mutans*, SSA- *S. salivarius*, SPSA- *S. parasanguinis*, KP- *K. pneumonieae*, PA- *P. aeruginosa*, AB- *A. baumannii*, CA- *C. albicans*.

Figure 4.16. Biofilm eradication potential of selected plant extracts against oral clinical isolates at the MIC level

The AAL, BCL, EHL, FBP, PGL, and SVF methanol extracts were evaluated for their biofilm eradication potential against eight oral clinical isolates, using a microtiter plate-based crystal violet assay. *S. mutans* is a key contributor to biofilm formation in the oral cavity, leading to dental caries. The capacity of these extracts to disrupt biofilms was quantified by measuring the reduction in biofilm mass after the treatment. Herbal extracts exhibited promising antibiofilm properties against a range of microorganisms. *A. aspera* root aqueous extract exhibited ≤94% biofilm inhibition capacity against *S. mutans* (Murugan et al. 2013). Similarly, a study by Gomashe et al. (2014) and Zayed et al. (2021) reported a strong antibiofilm activity against *S. mutans* by methanol extracts of *P. guajava* and alcoholic green tea extracts.

From the above findings, the twelve plant extracts expressed distinct profiles of estimated phytocompounds and antioxidants. Among them, the six plant extracts (AAR, BCL, EHL, FBP, PGL, and SVF) were selected for further studies due to their exceptional antimicrobial activity against cariogenic microorganisms at lower concentrations when compared to the other plant extracts. The difference in the phytochemical composition, antioxidant activity, and antimicrobial efficacy among the plant extracts can be attributed to the varying types and amounts of phytocompounds present in each extract which effectively suppress the growth of microbes. Hence, further studies will focus on these six plant extracts to identify the major bioactive compounds responsible for inhibiting *S. mutans* and to investigate the underlying molecular mechanisms using molecular docking and dynamic simulation.

PHASE II

4.2 *In silico* Identification of Potential Inhibitors from Selected Plant Extracts against Glucosyltransferase-C of *S. mutans*

S. mutans possesses several virulence factors, including a sucrose-dependent adhesion mechanism to form cariogenic biofilms. This process is mediated by glucosyltransferases (Gtfs), enzymes that break down the substrate sucrose into glucose and fructose synthesizing extracellular polysaccharides (EPSs) (Zhang et al., 2021) (Zhang et al. 2021). Inhibiting Gtfs has emerged as a promising therapeutic strategy for preventing the formation of cariogenic biofilm formation. *S. mutans* expresses three Gtf enzymes such as GtfB, GtfC, and GtfD, which synthesize glucans with varying solubility and linkages. GtfB (formerly known as GtfI) synthesizes mostly insoluble glucans with α-1,3-linked glucose. In contrast, GtfC (GtfSI) produces a mixture of insoluble and soluble glucans (α-1,6-linked glucose) while GtfD (GtfS) produces primarily soluble glucans (Atta et al. 2024). Insoluble glucans in the matrix of the biofilms facilitate bacterial adherence and aggregation on tooth enamel through structural and biochemical changes. These changes act as a protective barrier that shields bacteria from mechanical cleansing and host immune response. Soluble glucans, on the other hand, may be metabolized and consumed as an energy resource after the depletion of fermentable sugars in the mouth (Burne, 1998; Atta et al. 2024). As GtfC possesses more active binding sites compared to GtfB and GtfD, it acts as a promising target for the identification of phytocompounds that can effectively suppress SMU virulence.

4.2.1 Retrieval of Active Compounds from Selected Plant Parts

In the search for potential drug candidates against glucosyltransferase-SI (gtfC) of SMU, molecular docking proved to be the most direct and rational method. This method provides valuable insights into the interactions between molecules and biological targets, enabling them to elucidate the mode of action and potential efficacy. A total of 508 bioactive compounds, previously reported from six potential plants were retrieved from the online databases. Out of 508 phytocompounds, only 78 compounds met the criteria for a Drug likeness score (DL≥0.18). Hence, these 78 compounds were considered the key active

compounds responsible for the strong antibacterial activity, and these compounds corresponding to each herb are listed in **Table 4.6**. According to the Table, the highest number of compounds were found in PGL (41) followed by SVF (16), AAR (11), FBP (10), EHL (10), and BCL (4).

Table 4.6. Major bioactive compounds from the selected six plant parts

Plants	No. of Compounds	Compounds
AAR	11	Ecdysone, Oleanolic acid, Ecdysterone, Proanthocyanidin, Corrosolic acid, Ursolic acid, 20, 26-dihydroxy ecdysone, Stachysterone D, (25S)- Inokosterone, 22-acetonide, Stigmasta-5, 22-dien-3-ol.
BCL	4	Cycloeucalenol, β-Sitosterol, β-sitosteorl-β-D-glucose, Luteolin-7-O-glucoside.
FBP	10	Amyrin acetate, Dihydrobrassicasterol, Lanosterol, Lupenyl acetate, Epifriedelanol, β-progesterone, Stigmasterol, Sitosterol, Ergosterol acetate, 4,22-stigmastadiene-3-one.
EHL	10	Quercetin, Kaempferol, β-Sitosterol, β-Amyrin Acetate, Euphorbadienol, Pentagalloylglucose, Myricitrin, 2,4,6-Tri-O-galloyl-beta-glucose, Kaempferol-3-glucuronide, Euphorbol hexacosanoate.
PGL	41	Pyridoxine, Guavanoic Acid, Guavacoumaric Acid, Amritoside, Jacoumaric Acid, Goreishic Acid, Asiatic Acid, Quercetin, Ascorbic Acid, β-Ionone, Corosolic Acid, Strictinin, Amritoside, Casuarictin, Isoneriucoumaric Acid, Oleanolic Acid, Maslinic Acid, Guavin A, Guavin D, β-Sitosterol, Cianidanol, M6-Epi-β-Bisabolol, 6-Heptenoic Acid, Gentisic-Acid, Guaijavarin, Guavin-B, Guavin-C, Hyperoside, isoquercetin, Isostrictinin, Leucocyanidin, Oleanolic-Acid, Procyanidin-B1, Procyanidin B2, Procyanidin-B-3, Quercetin-3-O, Gentiobioside, Quercitrin, Stachyurin, Tellimagrandin-I, Ursolic-Acid.
SVF	16	Solasonine, Solamargine, Byzantionoside B, Citroside A, Matenoside A, Huzhangoside A, Huzhangoside B, Esculentin, Carpesterol, Campesterol, Daucosterol, Stigmasterol, Cholesterol, Sitosterol, Sitosteryl glucoside, β-solamargine.

AAR- *Achyranthes aspera* Root, BCL-*Barleria cuspidata* Leaf, FBP-*Ficus benghalensis* Proproot, EHL-*Euphorbia hirta* Leaf, PGL-*Psidium guajava* Leaf, SVF-*Solanum virginianum* Fruit.

4.2.2 Molecular Docking Studies

The 3D crystal structure of Glucosyltransferase-SI from *S. mutans* was obtained from RCSB PDB ID-3AIC. The protein consists of 8 chains (A, B, C, D, E, F, G, H) with a sequence length of 844 kDa. To identify the potential inhibitors predicted, 78 compounds were docked into the active sites of gtfC (Chain B and F) using extra precision (XP) glide mode. The binding affinity of all the compounds ranged from -14.534 to -0.373Kcal/mol, with chlorhexidine exhibiting a binding affinity of -4.394Kcal/mol.

Compounds with a binding affinity score greater than -7.0Kcal/mol were classified as *in silico* potential, while those with a score less than -7.0Kcal/mol were considered less active (Veeramachaneni et al. 2015). On this basis, 26 phytocompounds displayed a greater binding affinity (≥-7.0Kcal/mol) towards GtfC. The highly interacting ligands, along with their 3D and 2D interactions, are depicted in **Figure 4.17**. The data obtained as a result of molecular docking are shown in **Table 4.7**, along with the positive interactions between the target proteins, and the compounds, sorted by their docking scores. Among the plant extracts, PGL exhibited a strong binding affinity followed by EHL, SVF, AAR, BCL, and FBP. All ligands were docked against the GtfC active site, except for the compound huzhangoside A from SVF, which might be due to the unmatching binding for this compound.

The docking analysis identified that several PGL compounds exhibited strong binding affinity to GtfC. Guavin A, stachyurin, and guavin C exhibited strong binding affinity, with scores of -14.534, -13.44, and -13.388 Kcal/mol, respectively. Other compounds, including guavin D, amritoside, casuarictin, isostrictinin, guavin B, procyanidin B3, tellimargrandin-1, quercetin-3-O-gentiobioside, procyanidin B1, strictinin, procyanidin B2, leucocyanidin, and goreishic acid also showed notable affinity to GtfC with scores ranging from -11.5203 to -7.041 Kcal/mol. Four compounds from EHL, namely pentagalloylglucose, 2,4,6-tri-O-galloyl beta-glucose, myricetin, and kaempferol-3-glucuronide were identified with significant binding affinity to gtfC with the values of -11.8495, -11.654, -7.88509, and -7.71528Kcal/mol, respectively.

Ligand	3D-Interaction	2D-Interaction
PGL- Guavin A (-14.534Kcal/mol)		
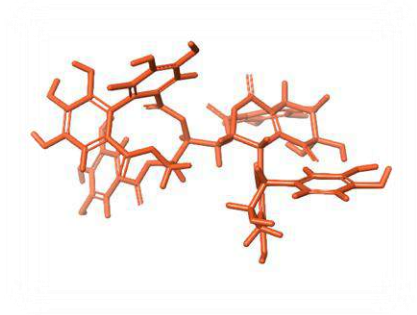		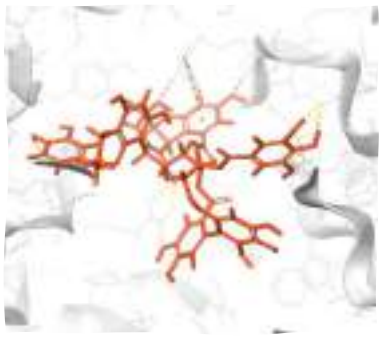
PGL- Stachyurin (-13.44Kcal/mol)		
	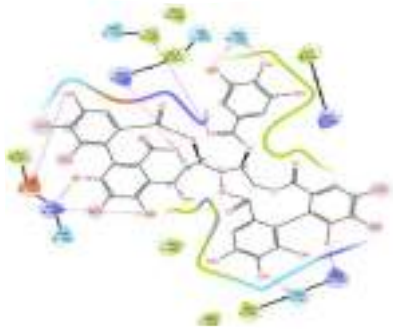	
PGL- Guavin C (-13.388Kcal/mol)		
		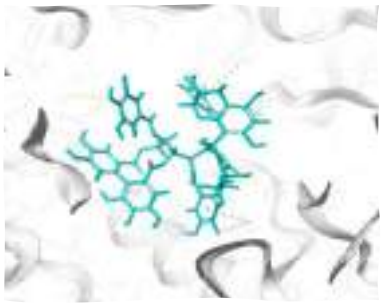
PGL- Guavin D (-11.5203Kcal/mol)		
		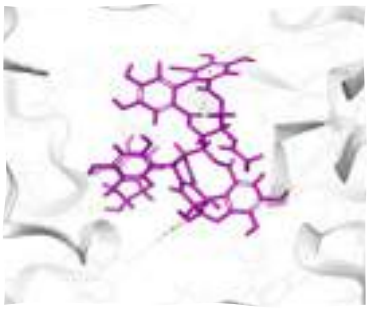

PGL- Amritoside (-11.15Kcal/mol)		
		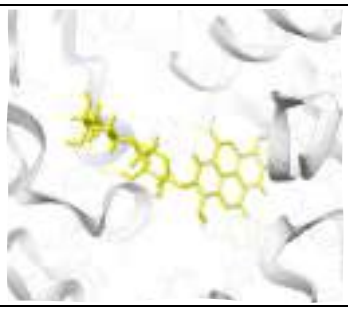
EHL- Pentagalloylglucose (-11.8495Kcal/mol)		
		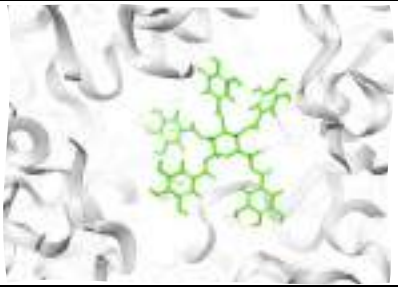
EHL- 2,4,6-Tri-O-galloyl beta-glucose (-11.654Kcal/mol)		
		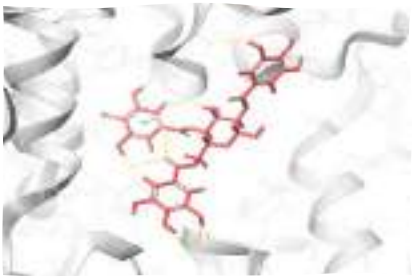
SVF- Solasonine (-9.618Kcal/mol)		
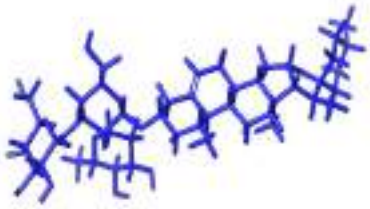	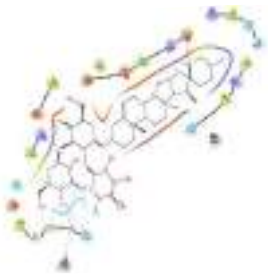	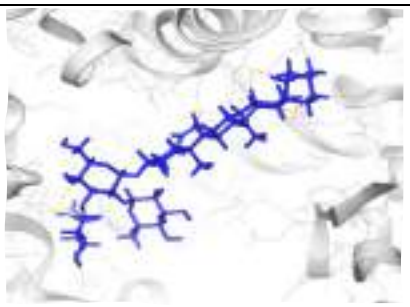
SVF- Esculentin (-8.251Kcal/mol)		
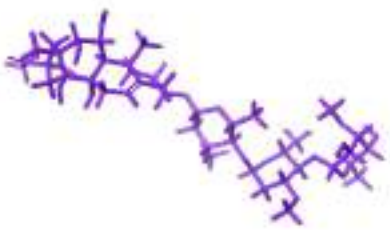		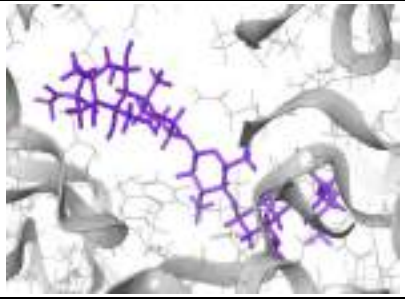

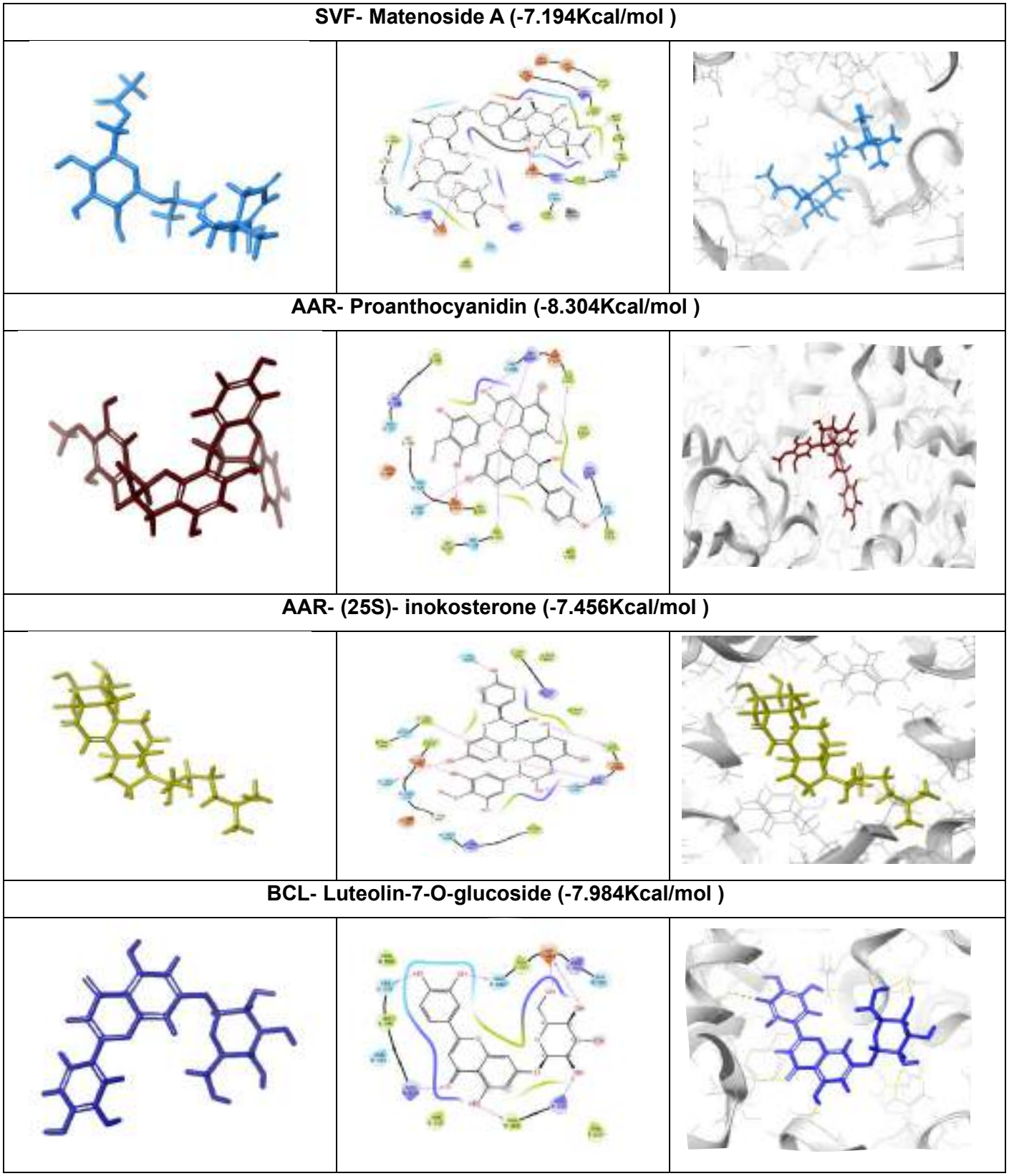

Figure 4.17. 2D and 3D Interaction of top hit ligands from the selected plants against GtfC

Furthermore, solasonine (-9.618Kcal/mol), esculentin (-8.251Kcal/mol), and matenoside (-7.194Kcal/mol), from SVF; proanthocyanidin (-8.304 Kcal/mol), 25(S) ionokosterone (-7.456Kcal/mol), from AAR and luteolin-7-O-glucoside (-7.984Kcal/mol) from BCL exhibited significant binding affinity to GtfC. All the compounds interacted with GtfC through various molecular interactions such as H-bonds, salt bridges, Pi-Pi stacking, and Pi cation interactions with the following residues of chain B: Tyr 519, Asn 563, Asp 424, Arg 425, Asn 537, Tyr 519, Ser 542, Mes 5001, Gly 429, Gly 428, Thr 426, Lys 977, Asp 597, and Chain F: Asn 563, Arg 425, Arg 538, Ala 423, Thr 422, Asp 424. The above major bioactive compounds identified from the plant extracts are mostly categorized under tannins, terpenes, flavonols, and phenolic compounds.

In particular, Guavin (A, C, and D) belongs to the hydrolyzable tannin (Yoshida et al., 2010), while stachyurin and casuaritcin are ellagitannins (Kusuki et al. 2023). According to the IMPPAT database, Goreishic acid is a triterpene, whereas pentagalloylglucose and 2,4,6-tri-O-galloyl beta-glucose are gallotannins. Kaempferol-3-glucuronide, myricetin, procyanidin B2, and leucocyanidin belong to the flavonol group. Phenols, flavonoids, and tannins synthesized by plants as a defense mechanism against microbial infections exhibit various biological activities including antioxidant and antimicrobial inhibitory effects (Biswas et al. 2013; Gorniak et al. 2019). Medicinal plants abundant in tannins (catechins, proanthocyanidins, ellagitannins, gallotannins, and epigallocatechin gallate) and, flavonoids (apigenin, quercetin, kaempferol, kurarinone, and morin) have shown to be highly active against oral pathogens. Over the past decade, several research has demonstrated that flavonoids, tannins, and major polyphenolic compounds, can inhibit the growth of cariogenic bacteria and prevent biofilm formation. These compounds have the potential to serve as alternatives to antibiotics, offering enhanced efficacy to overcome antibiotic resistance (Kovac et al. 2022).

The results of the present study are consistent with a recent investigation by Jauhar et al. (2023) on Propolis extract, which identified several compounds with strong docking abilities against glucosyltransferase (3AIC) and antigen I/II (3IPK). Similarly, Bhagavathy et al. ((2019) identified six active compounds from the GC-MS analysis of *Psidium guajava* leaf methanol extract, which exhibited

strong binding energies against glucosyltransferase, ranging from -69.76 to 53.16Kcal/mol. Uma Maheswari & Sankar, (2024) identified several compounds from *Murraya koenigii*, including koenigicine (-285.21 E-value), O-methyl murrayamine (-268.64 E-value), koenigine (-275.92 E-value), and murrayone (-240.26 E-value) which exhibited strong interactions with the glycosyltransferase protein of *S. mutans,* which coincides our work. Similarly, Wang et al. (2024) reported that six metabolites from *Lonicera japonica* flos possessed high negative binding energy against *S. mutans* biofilm-related proteins. Specifically, chlorogenic and oleanolic acid were found to disrupt the GbpC and adhesin P1 protein, respectively.

Table 4.7. The XP docking score of ligands from the selected plants against GtfC of *Streptococcus mutans*

S.No	PBCID	Protein/ Ligand	Plants	Docking Score (Kcal/mol)	Glide Energy	Glide score	Glide E model	Interaction	Amino acid Residues
1	73814546	Guavin A	PGL	-14.534	-74.551	-15.389	-102.144	H-bond, Pi-Cation, Salt bridge	B: ASP 424, ARG 425, TYR 978, F: ARG 425, ASP 424
2	157395	Stachyurin	PGL	-13.44	-66.073	-14.349	-94.844	H-bond, Salt bridge	B: TYR 519, ASN 563, ASP 424, ARG 425, F: ASN 563, ARG 425, ARG 538
3	472158112	Guavin C	PGL	-13.388	-75.321	-14.259	-107.24	H-bond, Pi-Cation, Salt bridge	B: ASP 597, ARG 540, LYS 600, ARG 596, ASP 380, LEU 382, LYS 977, F: ASP 380ARG 425
4	65238	Pentagalloylglucose	EHL	-11.8495	-11.826	-12.397	-136.845	H-bond, Pi-Pi Stacking, Pi-Cation	B: TYR 545, GLU 590, LYS 549, ASP 597, F: ARG 425, ASP 424, TYR 978, ASP 976, ASP 380
5	101460799	2,4,6-Tri-O-galloyl-beta-glucose	EHL	-11.654	-69.617	-12.376	-111.786	H-bond, Pi-Cation	B: THR 422, ARG 425, ALA 423, THR 426, F: TYR 519, ASP 424
6	73814547	Guavin D	PGL	-11.520	-68.474	-12.385	-89.908	H-bond, Pi-Cation, Salt bridge	B: LYS 549, ASP 424, ARG 425, F: ARG425, ASP 424, THR 426
7	73981613	Amritoside	PGL	-11.15	-59.696	-11.21	-82.975	H-bond	B: ALA 423, ASP 424, TYR 519, ASN 563,F: ARG 563, ARG 538
8	101601179	Casuarictin	PGL	-10.938	-61.913	-11.824	-95.316	H-bond, Salt bridge	B: ASP 597, ARG 596, ASP 593, GLU 590, F: ASP 380
9	13917513	Isostrictnin	PGL	-10.862	-63.114	-11.432	-79.797	H-bond, Pi-Cation, Salt bridge	B: ARG 538, SER 542, TYR 519, F: ARG 538, ASP 424, TYR 519, ARG 425
10	175616	Guavin-B	PGL	-9.862	-62.377	-10.589	-89.544	H-bond, Salt bridge	B: GLY 429, ARG 425, F: ARG 425, ALA 423
11	146798	Procyanidin-B-3	PGL	-9.827	-47.991	-11.665	-73.389	H-bond, Salt bridge, Pi-Pi Stacking	B: ASN 537, TYR 519, SER 542, F: ARG 425, ALA 423, THR 422
12	119247	Solasonine	SVF	-9.618	-59.55	-9.622	-65.767	H-bond, Salt bridge	B; MES 5001, GLY 429, GLY 428, THR 426, LYS 977, ASP 597
13	442690	Tellimagrandin	PGL	-9.606	-64.275	-10.244	-85.271	H-bond, Pi-Pi Stacking	B: ARG 425, TYR 519, TRP 517, F: ARG 425, ASP 424
14	5320834	Quercetin-3-o-gentiobioside	PGL	-9.324	-57.074	-9.359	-81.714	H-bond, Pi-Pi Stacking, Pi-Cation	B: ASP 424, THR 422, F: ASN 563, TYR 519, ARG 425
15	11250133	Procyanidin-b1	PGL	-8.802	-51.882	-9.025	-79.284	H-bond, Pi-Pi Stacking, Pi-Cation	B: TYR 519, SER 542, F: THR 426, TYR 519, ARG 425, ASP 424, ALA 423, THR 422
16	73330	Strictinin	PGL	-8.736	-56.675	-9.256	-88.501	H-bond	B: GLY 429, ARG 425, ASP 424, F: ARG 425, ASP 424. ALA 423

S.No	PBCID	Protein/ Ligand	Plants	Docking Score (Kcal/mol)	Glide Energy	Glide score	Glide E model	Interaction	Amino acid Residues
17	122738	Procyanidin B2	PGL	-8.645	-56.503	-8.868	-81.269	H-bond	B: TRP 517, ALA 423, TYR 519, ASN 563, F: ARG 425, ALA 423, ASN 563
18	108065	Proanthocyanidin	AAR	-8.304	-48.878	-8.527	-72.972	H-bond	B: ASP 424, ASN 563, TYR 519, F: ASN 563, ARG 425, ALA 423
19	188404	Esculentin	SVF	-8.251	-56.61	-8.251	-70.525	H-bond	F: ASP 424, ASP 976, ALA 983
20	71629	Leucocyanidin	PGL	-8.027	-42.955	-8.027	-53.441	H-bond	B: ALA 423, SER 542, F: ALA 423, THR 422
21	5280637	luteolin-7-O-glucoside	BCL	-7.984	-54.001	-7.984	-74.116	H-bond	B: SER 542, ARG 538, ALA 423, ARG 425, F: THR 422, ASP 424,
22	5281673	Myricitrin	EHL	-7.8850	-46.383	-7.9274	-63.4498	H-bond, Pi-Cation	B: THR 422, ARG 425, F: ALA 423, TYR 519
23	22846027	Kaempferol-3-glucuronide	EHL	-7.7152	-43.503	-7.751	-54.235	H-bond, Salt bridge	F: ALA 423, ARG 425, ASN 563, ARG 538
24	12358616	(25S)- inokosterone	AAR	-7.456	-46.412	-7.456	-59.471	H-bond	B: THR 422, ARG 425, ASN 563, F: ASN 563, ALA 423
25	163183907	Matenoside A	SVF	-7.194	-46.279	-7.194	-58.673	H-bond	B: ARG 425, F: THR 426, LYS 977, TYR 978, MES 5001
26	3081756	Goreishic acid	PGL	-7.041	-36.987	-7.044	-40.219	H-bond, Salt bridge	B: ARG 425, F: THR 426, TYR 519
27	5481224	Guaijavarin	PGL	-6.975	-46.423	-7.011		H-bond	B: ASN 563, F: ALA 423, ASP 424
28	21123946	20, 26-dihydroxyecdysone	AAR	-6.964	-42.225	-6.964	-56.205	H-bond	ASP 380, TYR 430, LYS 549, GLU 590, ASP 593
29	5280459	Quercitrin	PGL	-6.784	-40.769	-6.819	-61.405	H-bond, Pi-PI Stacking	B: ALA 423, ASP 424, ARG 425, F: ARG 425, TYR 519
30	119034	Asiatic acid	PGL	-6.758	-31.679	-6.766	-43.162	H-bond, Salt bridge	B: TRP 517, ASP 424, ARG B: 425, F: TYR 519
31	11700083	Jacoumaric acid	PGL	-6.695	-47.928	-6.703	-65.102	H-bond, Salt bridge	B: THR 636, LYS 549, F: ARG 425
32	5280804	Isoquercetin	PGL	-6.563	-42.733	-6.598	-55.812	H-bond, Pi-Cation	B: ARG 425, F: ARG 425, ASP 424
33	3469	Gentisic-acid	PGL	-6.528	-19.382	-6.528	-24.779	H-bond, Salt bridge	B: ARG 425, F: ASP 424, TYR 519
34	73611	Solamargine	SVF	-6.447	-55.818	-6.451	-81.035	H-bond, Salt bridge	B: GLN 553, LYS 549, ASP 597, F: ASP 424, ASP 976
35	14135395	ByzantionosideB	SVF	-6.415	-38.118	-6.415	-49.613	H-bond	B: ARG 425, F: THY 978, THR 426, MES 5001
36	5281643	Hyperoside	PGL	-6.094	-39.958	-6.129	-55.655	H-bond	B: ASP 424, ARG 425, TYR 519, F: ARG 425,
37	70699351	Sitosteryl glucoside	SVF	-6.083	-39.026	-6.083	-50.633	H-bond	B: ARG 425, ALA 423

S.No	PBCID	Protein/ Ligand	Plants	Docking Score (Kcal/mol)	Glide Energy	Glide score	Glide E model	Interaction	Amino acid Residues
38	9064	Cianidanol	PGL	-6.017	-37.639	-6.017	-48.821	H-bond, Pi-PI Stacking	B: ARG 425, F: TYR 519, THR 426, ASP 480, ALA 423
39	10100394	Isoneriucoumaric acid	PGL	-5.995	-49.42	-6.004	-85.239	H-bond, Salt bridge	B: LYS 600, ARG 596, GLU 590, ALA 548
40	19212	Ecdysone	AAR	-5.988	-41.236	-5.988	-52.514	H-bond	B: ARG 425, TYR 519, F: ARG 425, ASP 424
41	101211343	Guavanoic acid	PGL	-5.798	-38.218	-5.804	-51.367	H-bond, Salt bridge	B: ARG 425, F: TYR 519
42	5459840	Ecdysterone	AAR	-5.505	-40.864	-5.505	-52.633	H-bond	B: ASP 424, F: ARG 425, TYR 519
43	5280343	Quercetin	EHL	-5.471	-34.607	-5.51	-43.564	H-bond, Salt bridge	B: ARG 425, F: ASP 424, TYR 978
44	5280863	Kaempferol	EHL	-5.01	-33.75	-5.05	-43.943	H-bond, Pi-Pi Stacking	B: ARG 425, F: ARG 425, TYR 519, ASP 480
45	14312562	Citroside A	SVF	-5.278	-36.49	-5.278	-44.26	H-bond	B: TYR 545, GLU 590, ASP 597
46	70684796	22-acetonide	AAR	-5.193	-41.66	-5.193	-56.2	H-bond	B: TYR 519, F: THR 426, ARG 425
47	5742590	Daucosterol	SVF	-5.458	-39.533	-5.458	-53.89	H-bond	F: THR 426
48	15227299	Stachysterone D	AAR	-4.934	-40.703	-4.934	-46.261	H-bond	B: TYR 519, F: TYR 519, ASP 424
49	101211344	Guavacoumaric acid	PGL	-4.279	-56.13	-6.811	-43.892	H-bond	B: TYR 519, SER 542, F: ARG 425, THR 426, TYR 519
50	70705	6-Heptenoic acid	PGL	-4.913	-13.965	-4.918	-13.288	H-bond, Salt bridge	B: ARG 425, F: TYR 519
51	10494	Oleanolic acid	AAR	-4.819	-29.786	-4.827	-41.568	H-bond, Salt bridge	B: ARG 425, F: TYR 519
52	64945	Ursolic acid	AAR	-4.807	-33.459	-4.816	-44.173	Salt bridge	B: ARG 425
53	54670067	Ascorbic acid	PGL	-4.409	-21.909	-4.409	-23.677	H-bond, Pi-Pi Stacking, Pi-Cation	B: ARG 425, TRP 517, TYR 519, F: ARG 425, TYR 519
54	5997	Cholesterol	SVF	-4.176	-33.726	-4.176	-45.827	H-bond	B: SER 542
55	1054	Pyridoxine	PGL	-3.88	-23.361	-4.577	-27.678	H-bond	THR 426921
56	101690	Cycloeucalenol	BCL	-3.825	-37.653	-3.825	-50.118	H-bond	B: SER 542
57	12300148	6-Epi-beta-bisabolol	PGL	-3.646	-24.715	-3.646	-42.983	H-bond	THR 426
58	5364563	4,22-stigmastadiene-3-oness	FBP	-3.298	-27.817	-3.298	-37.726	H-bond	B: TYR 519
59	5994	Beta-progesterone	FBP	-2.872	-31.343	-2.872	-34.774	H-bond	B: ASN 563, F: ALA 423, ASP 424
60	173183	Campesterol	SVF	-2.722	-23.245	-2.722	-34.016	H-bond	B: ARG 425
61	10863111	Euphorbadienol	EHL	-2.46	-27.03	-2.46	-30.388	-	-

S.No	PBCID	Protein/ Ligand	Plants	Docking Score (Kcal/mol)	Glide Energy	Glide score	Glide E model	Interaction	Amino acid Residues
62	6436903	Ergosterol acetate	FBP	-2.384	-25.711	-2.384	-35.481	H-bond	B: ARG 425, F: TYR 519
63	5280794	Stigmasta-5, 22-dien-3-ol	AAR, SVF	-2.211	-26.161	-2.211	-32.831	H-bond	F: TYR 978, LYS 977
64	92157	Lupenyl acetate	FBP	-2.145	-31.313	-2.145	-33.796	-	-
65	92842	Amyrin acetate	FBP	-2.122	-34.184	-2.122	-44.365	-	-
66	119242	Epifriedelanol	FBP	-2.093	-30.591	-2.093	-35.996	H-bond	F: ALA 423
67	92156	Beta-Amyrin acetate	EHL	-2.01	-32.561	-2.01	-41.543	-	-
68	6918774	Corrosolic acid	AAR	-1.417	-37.772	-5.689	-48.13	H-bond, Salt bridge	B: ARG 425, F: TYR 519, THR 426
69	222284	Beta sitosterol	EHL, BCL, PGL, FBP	-2.724	-21.01	-2.724	-30.418	H-bond	B: ARG 425
70	5283637	Dihydrobrassicasterol	FBP	-2.159	-26.57	-2.159	-32.028	H-bond	F: LYS 977, TYR 978
71	246983	Lanosterol	FBP	-0.578	-20.236	-0.578	-23.568	-	-
72	21155918	Carpesterol	SVF	-2.71	-43.278	-2.71	-60.574	H-bond, Pi-Cation	LYS 549, ARG 596, TYR 430
73	638014	Beta-Ionone	PGL	-1.059	-20.421	-1.059	-23.568	H-bond	B: TYR 545, F: ARG 425
74	101280172	Euphorbolhexacosanoate	EHL	-0.373	-55.683	-0.373	-32.831	-	-
75	49799269	Huzhangoside B	SVF	-5.294	-27.523	-5.319	-32.561	H-bond, Salt bridge	B: ARG 425, F: TYR 519
76	5481224	Guaijavarin	PGL	-6.975	-46.423	-7.011	-62.996	H-bond	B: ASN 563, F: ALA 423, ASP 424
77	73659	Maslinic acid	PGL	-1.024	-34.158	-3.58	-46.157	H-bond, Salt bridge	B: ARG 425, F: TYR 519

4.2.3 Molecular Dynamic Simulation

Molecular dynamic simulation (MDS) is employed to determine Newton's classical equation of motion, and the intermolecular protein-ligand interaction with a specific time, temperature, volume, density, and pressure (Martinez, 2015). MDS results revealed that the protein-ligand complex of Guavin A, the top-hit compound with the gtfC protein of *S. mutans,* exhibited the highest negative binding energy (-14.534Kcal/mol) during the 100ns simulation. The simulation was further validated using the MDS Desmond model to explore molecular flexibility, stability, and structural behavior. The generated root mean square deviation (RMSD) and root mean square fluctuation (RMSF) demonstrated the conformational changes and dispersion of ligand structure from the protein backbone (Prasasty et al. 2020; Martinez, 2015; Rairez & Caballero, 2018).

The resulting RMSD values presented in **Figure 4.18 a & b** for protein Cα-backbone, and heavy atoms were initiated at 2.47Å at 0 ns and remained stable up to 4.74 Å at 26 ns. After 26ns, the ligand fell into close contact with the protein and maintained a stabilized complex up to 80ns at 6.90 Å. The PL complex exhibited fluctuations between 2-3ns followed by a stable conformation until 80ns. However, beyond 80ns, the ligand detached from the protein, resulting in increasing conformational fluctuations until the end of the 100ns simulation period. This protein structure demonstrated minimal fluctuations throughout the simulation.

Further, root-mean-square-fluctuation (RMSF) values (**Figure 4.19a**) were computed to determine protein flexibility. The protein RMSF values for Cα atoms ranged from 1.5 to 6.0 Å, indicating no significant residual fluctuations. The alpha-carbon backbone is represented by the blue spectrum while the red spectrum represents the ligands. The Y-axis measures angstrom (Å) and the X-axis measures nanoseconds (ns). The simulation results showed that the protein's α -helical and β-strands persisted over 90% of the simulation time and the green line indicated the protein interaction with the ligand.

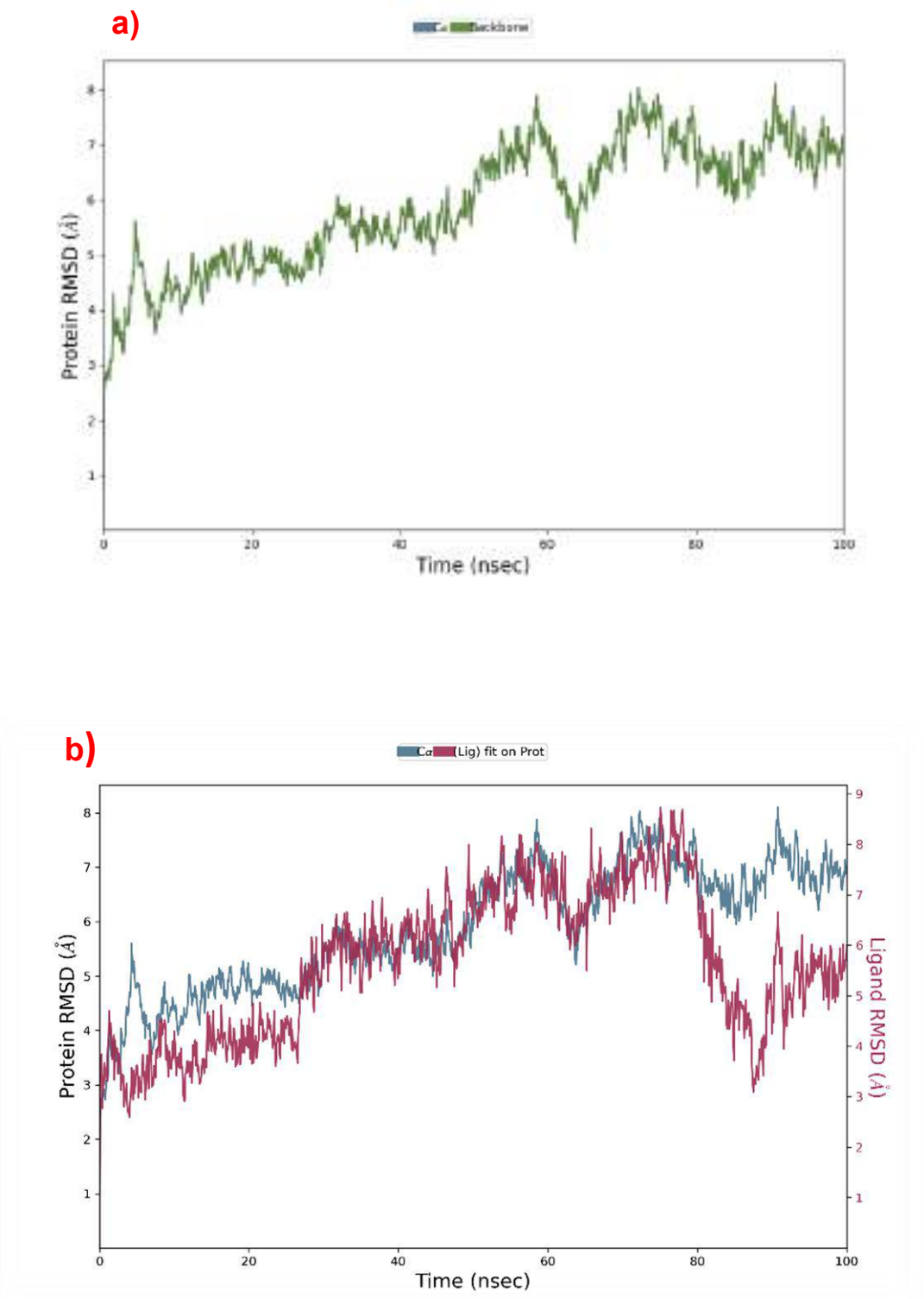

Figure 4.18. Root means square deviation (RMSD) of glucosyltransferase a) apoprotein and b) gtfC-Guavin A complex

The ligand contacting region was observed from 1.82 to 2.76 Å with the amino acid residues, THR, VAL, and GLU at chain B and from 2.01 to 2.57 Å with ILE, GLY at chain F. Guavin A formed ionic bonds, hydrogen bonds, and hydrophobic interactions with the catalytic domain of the gtfC protein. The ligand analysis in **Figure 4.19b** depicted the interactions between the ligand fragments and the protein. A total number of 88 heavy atoms in Guavin A were found to be present, indicating a stable binding mode. The histogram (**Figure 4.20**) showed the number of amino acids interacting with Guavin A, with the X-axis denoting the position of amino acids in the protein, and the Y-axis denoting the interaction fraction scale. The interactions between Guavin A and GtfC protein are depicted in **Figure 4.20** showing hydrogen bonds in green, hydrophobic interactions in lavender, strong ionic bonds in pink, and water bridges in blue color.

Guavin A also formed strong ionic bonds with crucial amino acids in GtfC protein, such as Arg425, Arg538 (chain B), Arg425, Arg538, and Lys549 (chain F) of gtfC with the frame count of 53, 8, 37, 28, and 124 respectively. Twenty-one amino acid residues interacted with H-bond in chain B: Asp380 (8), Asp424 (472), Asp425 (877), Thr426 (18), Gly429 (72), Asp480 (591), Trp517 (49), Ser578 (403), Tyr519 (314), Lys977 (2), and Chain F: Lys977 (157), Tyr978 (218), Asp424 (216), Arg425 (786), Thr426 (14), Tyr519 (98), Arg540 (31), Tyr545 (454), Lys549(12), Gln553(77), Tyr978 (4), and hydrophobic interactions occurred among Arg425 (435), Tyr430 (144), Asp424(736), Tyr519(2), and Arg596 (16). The protein-ligand contact analysis (**Figure 4.21),** showed, that Arg425 (chain F) highly interacted with hydrogen bonds (70%) throughout the simulation time, followed by Lys549 (39%), Asp424 (58%), Ala423 (58%) in chain F and Ala423 (49%), Asp480 (58%), Arg425 (46%), Asp424 (58%), Ser518 (46%) in chain B.

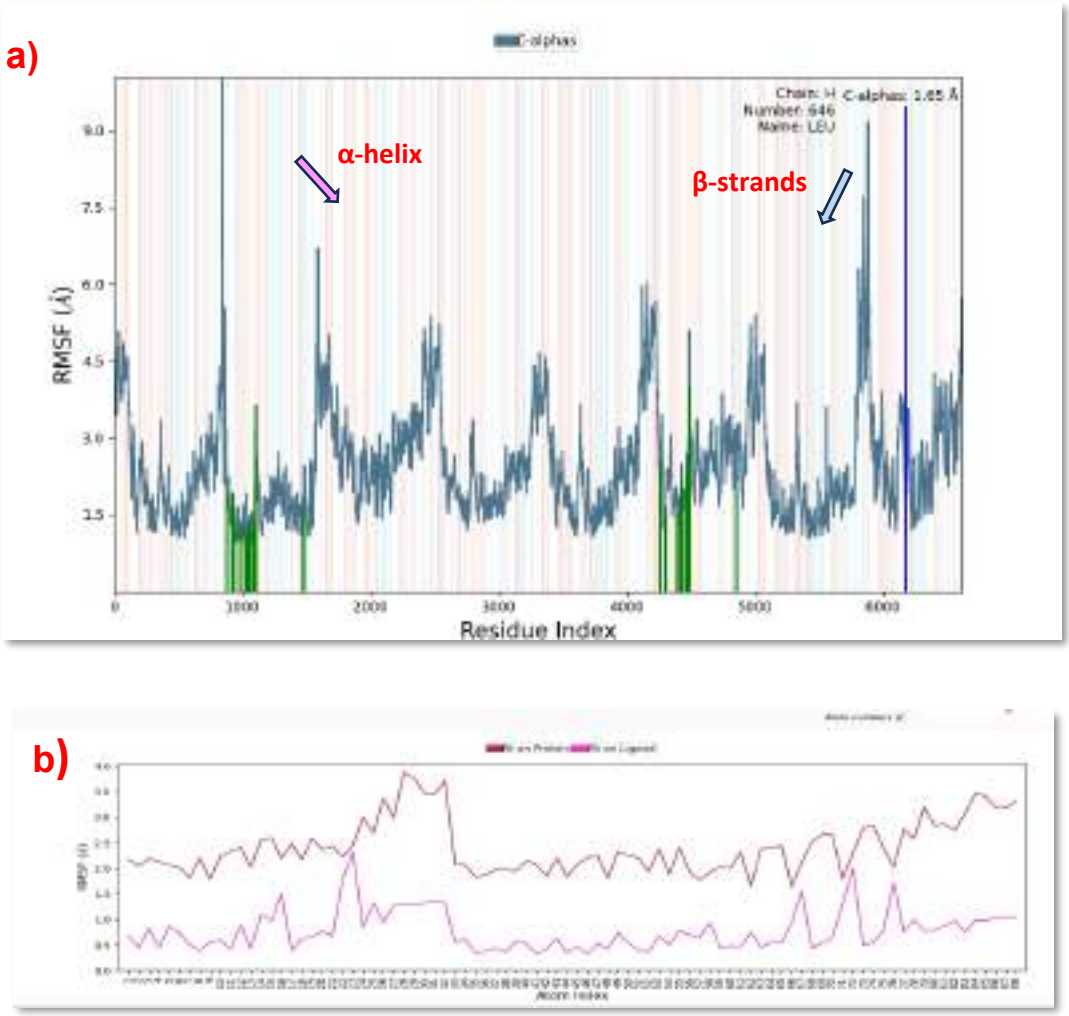

Figure 4.19. a) Root mean square fluctuation (RMSF) plot of glucosyltransferase and Guavin A and b) Ligand-Protein fit

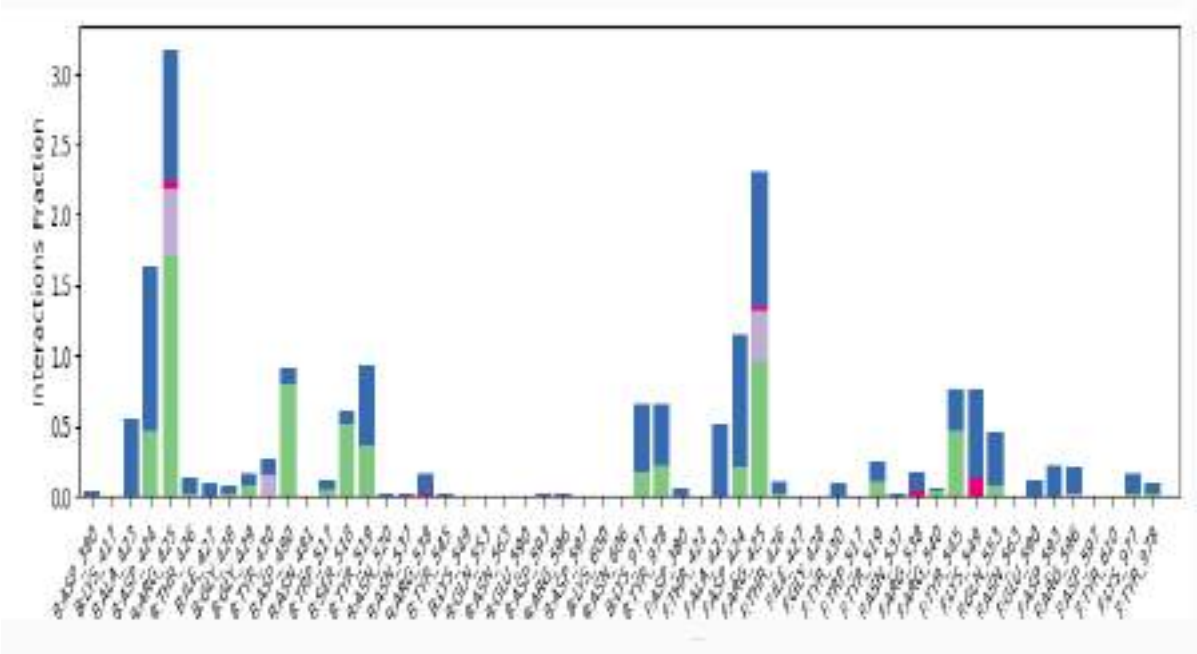

Figure 4.20. Histogram showing count of interaction in glucosyltransferase and Guavin A

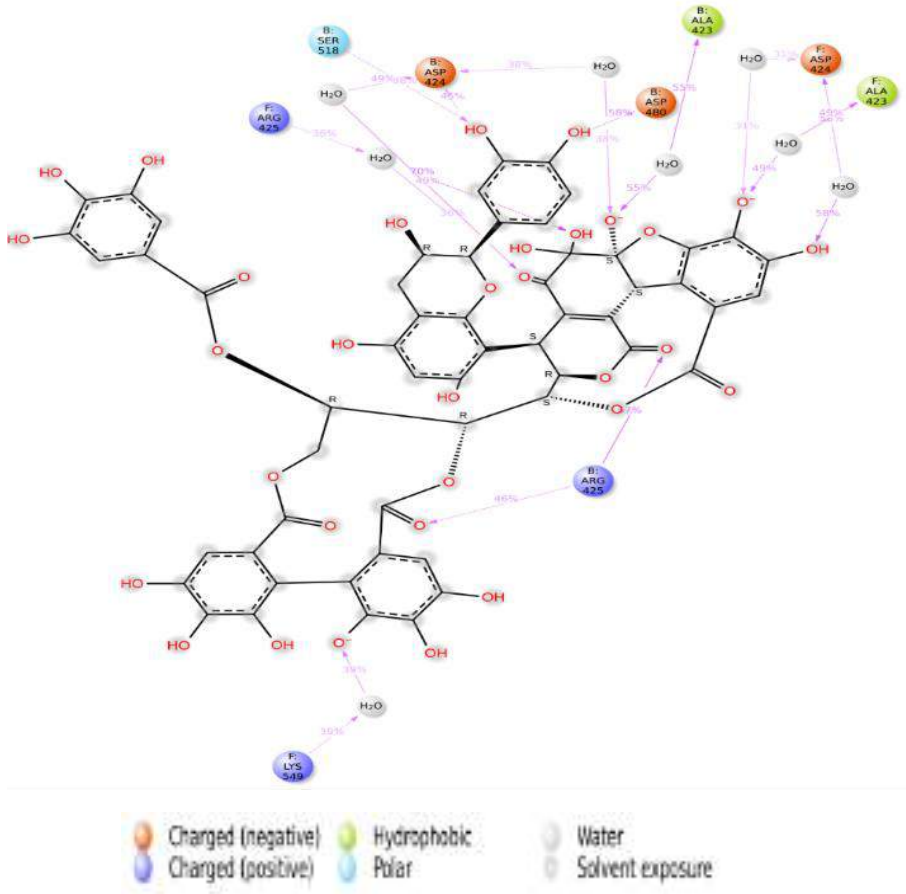

Figure 4.21. Interaction percentage of glucosyltransferase amino acids with the Guavin A

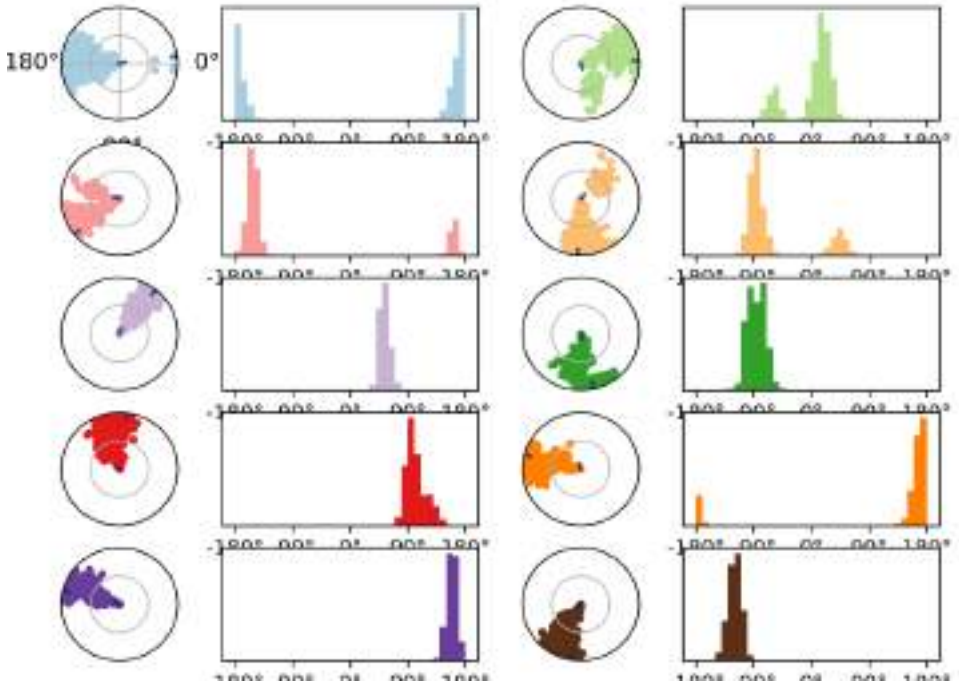

Figure 4.22. The torsion angle plot represents the potential energy of the ligand

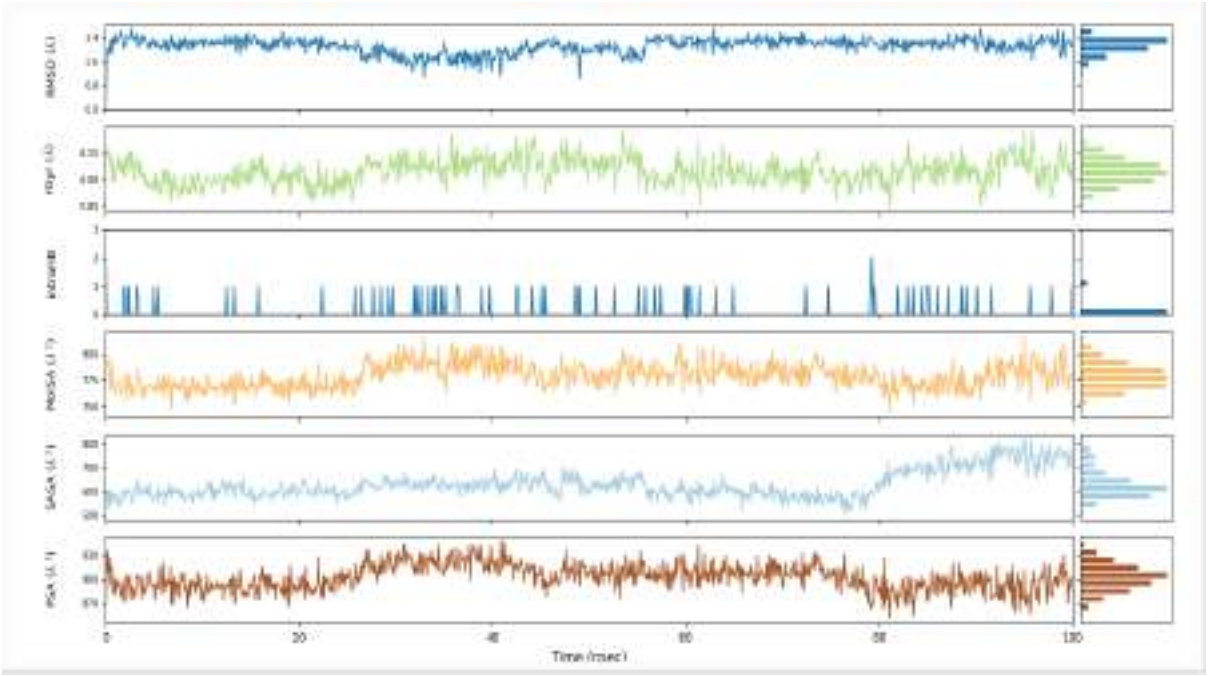

Figure 4.23. Ligand properties of Guavin A

The ligand properties confirmed that Guavin A exhibited stable interactions and intact binding with the gtfC protein throughout the 100ns simulation time, indicating its strong potential for SMU inhibition and dental caries prevention. It is evident from this that all the substrate and ligand-bound complexes exhibited stable RMSD plots with alpha-helices and beta-strands percentages providing valuable insights into substrate-ligand binding dynamics. The torsion angle plot (**Figure 4.22**) illustrated the relationship between the torsion angle and the potential energy of the ligand, predicting rotatable bonds throughout the 0 to 100ns simulation trajectory. The potential ligand values (**Figure 4.23**) displayed various properties, including RMSD, the radius of gyration, molecular surface area (MolSA), solvent accessible surface area (SASA), polar surface area (PSA), and intramolecular hydrogen bonds, and are expressed in Kcal/mol, determine the protein-bound conformation of the ligand.

Based on this search strategy, a novel adhesion inhibitory molecule against cariogenic isolates, can be identified to develop an effective formulation through a selection pipeline. Likely, Guavin A exhibited a stable interaction with active sites (Arg425, Arg538, and Lys549) of GtfC with strong ionic bonds representing its strong biofilm eradication efficacy. Similarly, the triterpenoid compound ursolic acid had strong hydrogen (Tyr430, and Asp909) and hydrophobic interactions with the novel active sites of Gtf's (Trp517, Leu433, Leu434, and Phe907), which plays a key role in the formation of biofilm. Ursolic acid proves its efficiency in disrupting the adhesion and aggregation of mature biofilms formed by SMU (Liu et al. 2021).

In this study, the identification of potential glucosyltransferase (GtfC) inhibitors from various phytochemical compounds was carried out through *in silico* molecular docking analysis. It explored numerous phytochemical compounds strongly bonded to the active sites of the GtfC enzyme of SMU*,* exhibiting significant interactions with key amino acid residues involved in the enzyme's catalytic activity. These compounds arise as potential candidates for further *in vitro* and *in vivo* experimental validation against SMU to combat plaque formation and eradication. The natural presence of these compounds in medicinal plants with low toxicity levels and high therapeutic activity highlights their potential exploitation in dental caries prevention.

Among 1,50,000 commercially screened compounds, a novel quinoxaline derivative, 2-(4-methoxyphenyl)-*N*-(3-{[2-(4-methoxyphenyl) ethyl] imino}-1,4-dihydro-2-quinoxalinylidene) ethanamine was identified as an effective inhibitor against gtfC. This compound also disables the catalytic function of *S. mutans*, making it a promising lead for developing novel anti-cariogenic agents (Ren et al. 2016). Rivera-Quiroga et al (2021), reported the anti-adhesion properties of a novel molecule ZINC19835187 towards the surface protein (Ag I/II) of *S. mutans* suggesting the stability of the protein-molecule complex that interacted with the residues Leu553, Asp554, Thr586, Val587, Lys811, Lys812, Asn814, Ile815, Trp816 through H-bond for 300ns simulation time. Similarly, the flavanone compound kurarinone is strongly coupled with *S. mutans* biofilm-forming enzyme Sortase A, compared to the standard chlorhexidine for 100ns (Salmanli et al. 2021).

To sum up phase II, out of 508 retrieved bioactive compounds present in the selected six plants (AAR, BCL, EHL, FBP, PGL, and SVF), 78 compounds met the criteria for drug-likeness and further docked against glucosyltransferase-C of *S. mutans*. Among them, 16 compounds from PGL, 4 compounds from EHL, 3 compounds from SVF, 2 compounds from AAR, and a single compound from BCL exhibited a greater binding affinity (≥-7.0Kcal/mol) towards the gtfC. However, FBP exhibited a lower binding affinity (-3.298Kcal/mol) towards glucosyltransferase-C which might be due to the structural differences, and to uncover its strong antibacterial activity against *S. mutans* further research is needed to assist with other binding proteins of *S. mutans*. Guavin A from PGL displayed the highest binding energy and was further validated using a molecular dynamics study which expressed stability for 80ns during a 100ns simulation period. Hence, all six plants were taken into account for the formulation of polyherbal dentifrice which was carried out in phase III.

PHASE III

4.3 Preparation and Evaluation of Polyherbal Dentifrice (PHDF)

Ayurveda, India's traditional system of medicine has promoted the utilization of herbs to prevent and treat various human ailments. The Ayurvedic principle emphasizes preventive care and health restoration (National Institutes of Health, 2005). Herbal medicine can be used single or in combination with other herbs, a concept called 'Polyherbalism'. This approach is endorsed in Ayurvedic literature, such as the '*Sarangdhar Samhita'* particularly when single-herb formulation fails to achieve the desired effect (Srivastava et al. 2012). Optimizing the proportions of different herbs in a polyherbal formulation can enhance therapeutic effectiveness through synergistic actions at lower dosages reducing toxicity. The combination of herbs in a specific ratio can boost the therapeutic benefits of polyherbal medicine due to the presence of diverse phytoconstituents (Dwivedi & Daspaul, 2013). The existence of bioactive compounds like alkaloids, phenols, glycosides, saponins, flavonoids, tannins, salicylic acid, and terpenes in different plants and polyherbal formulation has been related to their potent antimicrobial activity (Aziz et al. 2017; Aladejana, 2023).

The lack of clear experimental design in preparing polyherbal formulations can lead to poor consistency, stability, and productivity (Politis et al. 2017; Das & Dewanjee, 2018). Therefore, optimizing polyherbal combinations using the design of experiments (DoE) can efficiently develop effective pharmaceutical dosage forms with potent antimicrobial activity (Lamberti et al. 2022). Factorial design optimization ensures the assessment of all possible combinations of factors, evaluating the effect of each factor with minimal runs, and also elucidating correlations between variables and responses in pharmaceutical formulation development (Singh & Ahuja, 2002; Vandervoort & Ludwig, 2002). With this background, this phase aims to optimize the extract concentration of six potent antimicrobial plants with a synergistic ratio followed by the development and evaluation of polyherbal formulation in combating cariogenic microorganisms.

4.3.1 Design of Experiments (DOE) Modeling to Determine Synergistic Antibacterial Combinations of Plant Extracts

The six plant extracts namely, AAR, BCL, EHL, FBP, PGL, and SVF were combined in different ratios using the software, MODDE. The PLS model exhibited remarkable performance with a high regression coefficient (R^2= 0.945) indicating a strong positive correlation between the predicted and actual values. A Q^2 value, of 0.660 significantly exceeds the threshold of 0.10 (Bhatia et al. 2016), demonstrates the models' strong predictive accuracy and reliability. The model's strong reproducibility (0.53) and validity (0.52) indicated effective experimental control, low error rates, and a reliable model fit. These results validated the selected PLS as a highly dependable, efficient, and accurate predictive tool, aligning with the research findings of Bhatia et al. (2016).

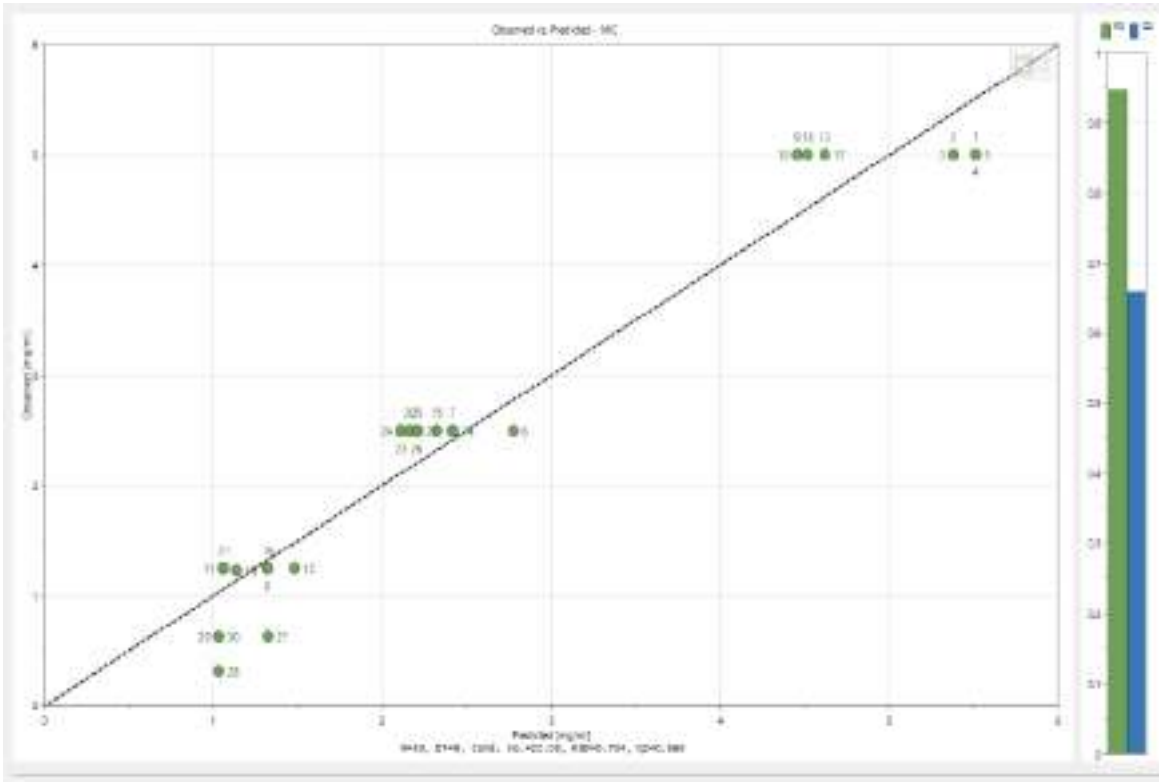

Figure 4.24. Observed vs Predicted plot of the MIC value of different combinations of plant extracts.

Table 4.8. The predicted ratio for methanol extracts proportion in combination using RSM

Exp. Name	The predicted ratio for methanol extracts proportion in combination						Observed MIC values	Predicted MIC
	PGL	SVF	EHL	FBP	BCL	AAR		
N1	5	0	0	0	0	0	2.5	5.56544
N2	0	5	0	0	0	0	5	5.39513
N3	0	0	5	0	0	0	5	5.66763
N4	0	0	0	5	0	0	5	5.53138
N5	0	0	0	0	5	0	5	5.39513
N6	0	0	0	0	0	5	2.5	2.7626
N7	2.5	2.5	0	0	0	0	2.5	2.13423
N8	0.5	0	2.5	0	0	0	0.625	0.722678
N9	0.5	0	0	2.5	0	0	5	4.15413
N10	0.5	0	0	0	2.5	0	5	4.31477
N11	0.5	0	0	0	0	2.5	0.625	0.322518
N12	0	2.5	2.5	0	0	0	1.25	0.923477
N13	0	2.5	0	2.5	0	0	5	4.35493
N14	0	2.5	0	0	2.5	0	1.25	1.24476
N15	0	2.5	0	0	0	2.5	2.5	2.43129
N16	0	0	2.5	2.5	0	0	2.5	1.85311
N17	0	0	2.5	0	2.5	0	5	4.19429
N18	0	0	2.5	0	0	2.5	5	4.29055
N19	0	0	0	2.5	2.5	0	0.625	0.538982
N20	0	0	0	2.5	0	2.5	0.625	0.635246
N21	0	0	0	0	2.5	2.5	0.625	0.795885
N22	1.25	0.625	0.625	0.625	0.625	0.625	1.25	1.67778
N23	0.625	1.25	0.625	0.625	0.625	0.625	1.25	1.55612
N24	0.625	0.625	1.25	0.625	0.625	0.625	1.25	1.75078
N25	0.625	0.625	0.625	1.25	0.625	0.625	1.25	1.65345
N26	0.625	0.625	0.625	0.625	1.25	0.625	1.25	1.55612
N27	0.625	0.625	0.625	0.625	0.625	1.25	0.625	0.681837
N28	1.25	1.25	1.25	2.5	2.5	2.5	0.3125	0.28817
N29	2.5	2.5	2.5	1.25	1.25	1.25	0.3125	0.28817
N30	1.25	1.25	1.25	1.25	1.25	1.25	0.3125	0.28817

Table 4.9. ANOVA results in the optimal design of the formulation

MIC	DF	SS	MS (variance)	F	p	SD
Total	30	288.94	9.63135			
Constant	1	177.481	177.481			
Total corrected	29	111.459	3.84342			1.96046
Regression	20	105.325	5.26627	7.72714	0.002	2.29483
Residual	9	6.13376	0.681528			0.825547
Lack of Fit	--	--	--	--	--	--
Pure error	0	0	0			--
	N=30	Q2 =	0.660	Cond.no=	22.08	
	DF=9	R2 =	0.945	RSD =	0.8255	
	Comp.= 2	R2 adj. =	0.823			

DF-Degree of Freedom, SS-Sum of Squares, MS-Mean Squares, F-F value, p-p value, SD-Standard Deviation.

Table 4.8. presented the optimized results of thirty experimental runs with various ratios of plant extracts and their corresponding MIC values. All 30 combinations exhibited antimicrobial activity (MIC≤1mg/ml), with the six plant combinations emerging as a particularly effective formulation, demonstrating potent antimicrobial activity against *S. mutans* at low MIC values. **Figure 4.24** represented the best model fit, with observed vs predicted values closely aligned around the line. To determine the optimal combination with better antimicrobial activity, a response axial plot was generated from the data presented in **Table 4.9**. The axial plot displayed varying colors for varying antimicrobial activity, and the blue region indicated the most effective six plant combinations that achieved the lowest MIC (0.3125mg/ml) and highest antimicrobial activity against *S. mutans.* The predicted MIC values denoted those combinations with higher proportions of EHL, PGL, SVF, and a lower proportion of AAR, BCL, and FBP, yielded optimal results. Three combinations within the blue region of the response contour plot (**Figure 4.25**) were selected, and the MIC assays were performed experimentally, to validate the prediction of the PLS model. The experimental results confirmed the model's reliability and fitness, with a strong correlation (r=0.73), between experimental and predicted MIC values for all combinations (**Figure 4.26**).

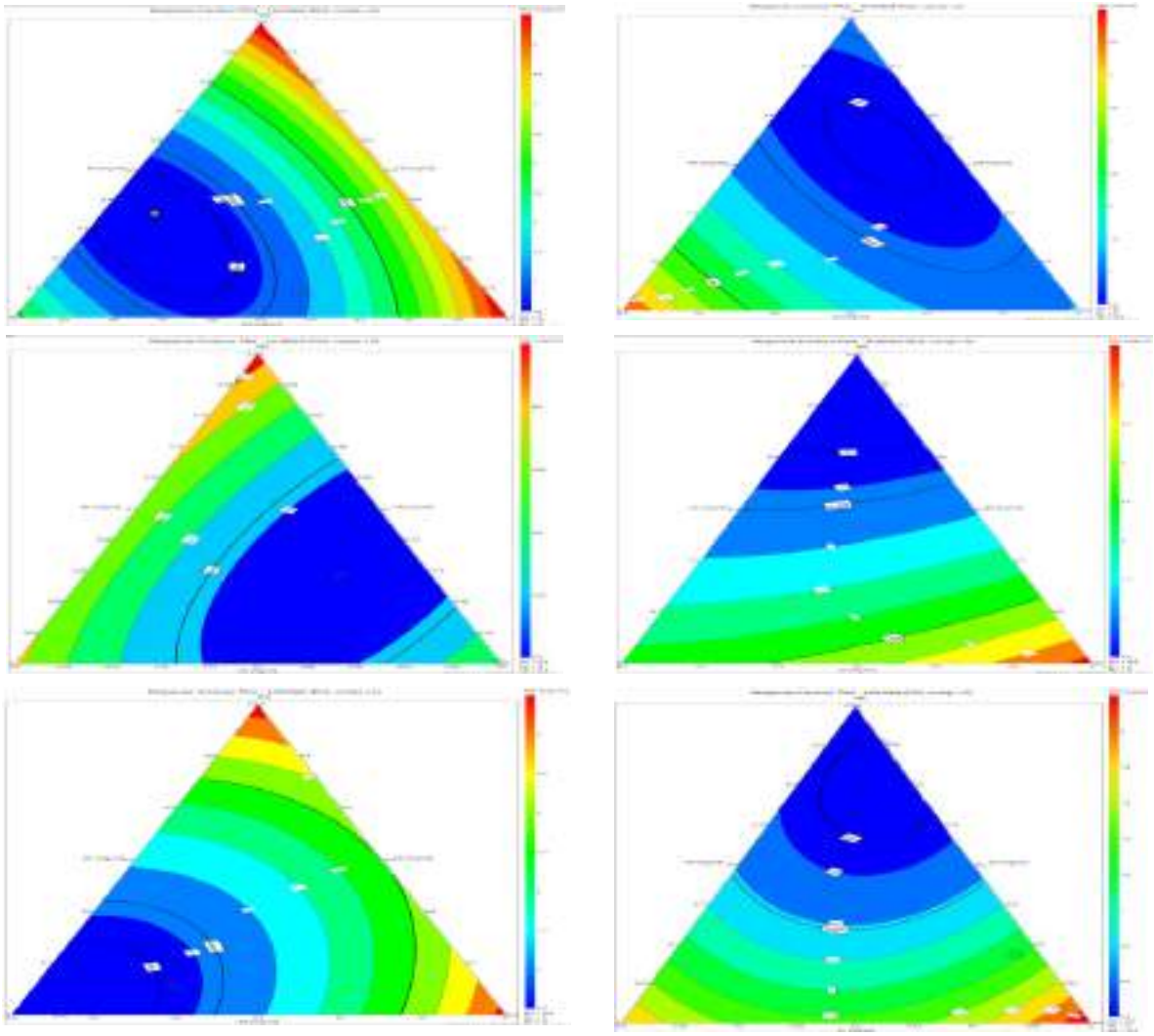

Figure 4.25. Response contour plot showing different combinations of six plant extracts in MIC against *S. mutans.*

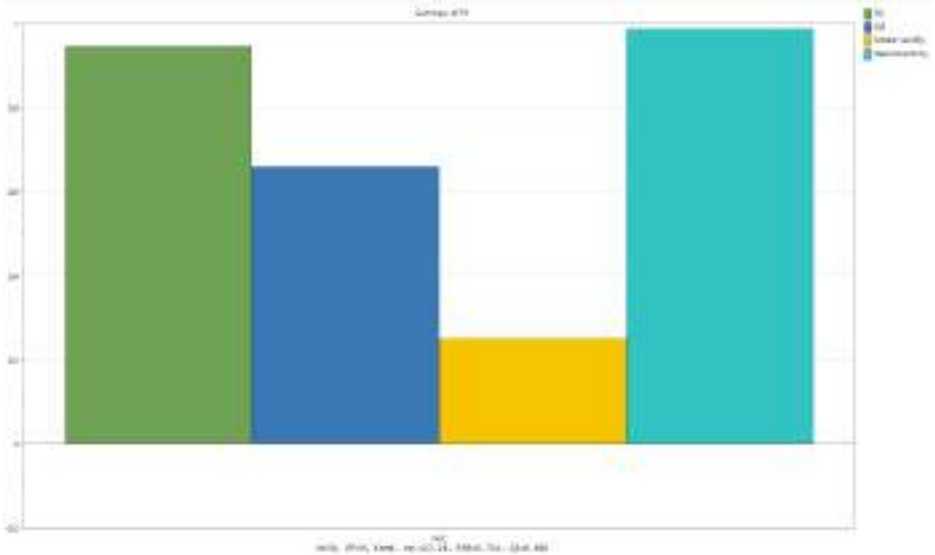

Figure 4.26. Summary of fit plot

In this study, DoE optimization software (MODDE 9.1) was employed to identify the optimal combinations of herbal extracts. This enabled systematic evaluation of the interactions between different herbal extracts, accelerating the development of novel antimicrobial agents with improved efficacy, reduced toxicity, and cost-effectiveness. Similar to our study, Mapeka et al (2024), reported enhanced antimicrobial activity against six common foodborne pathogens, and synergistic action was observed in the combination of *Rosmarinus officinalis* (59.5%) with either *Syzygium aromaticum* (40%) or *Salvia officinalis* (0.5%) methanol extracts, resulting in potent activity against *B. cereus with* a MIC of 0.17mg/ml. Their results also showed a strong predictive accuracy, with a correlation (r-value) of 0.73 between the predicted and experimental data. A study by Tanisha et al (2024) demonstrated the potent synergistic effect of combining seed-aqueous extracts of *Nelumbo nucifera, Chenopodium quinoa,* and *Salvia hispanica* in an equivalent ratio (1.5mg/ml). The combination exhibited significantly the highest activity in reducing obesity and diabetes in diet-induced obese diabetic mice with notably low toxicity.

4.3.2 Preparation of Polyherbal Dentifrice (PHDF)

For the preparation of an effective polyherbal dentifrice, the methanolic extracts of six antimicrobial agents, AAR, BCL, EHL, FBP, PGL, and SVF underwent optimization and lyophilization at -40ºC for 48h. Additional excipients include powders of *Syzygium aromaticum* flower bud, *Mentha piperita* leaf, *Acacia nilotica* leaf, *Centella asiatica* leaf, *Abrus precatorius* leaf, *Cinnamomum verum* bark, *Sapindus trifoliatus* nut, licorice root, xylitol, pink salt, myrrh, and coconut shell charcoal, sourced from the local markets. The excipients were selected based on a thorough literature review and an examination of the labels of commercially available tooth care products, ensuring their efficacy and safety in dental care applications. Visual inspection and particle size analysis confirmed the uniformity of the developed formulation, showing consistent color, texture, and particle size throughout the batch, with no visible inconsistencies. Based on the literature review and optimized proportions, the composition of the developed formulation is summarized in **Table 4.10.**

Tablet 4.10. Composition of ingredients used in polyherbal dentifrice

Ingredients		Quantity (mg/Tablet)
Therapeutic agent	*Achyranthes aspera*-root	**5**
	Barleria cuspidata-leaf	**5**
	Ficus benghalensis-prop root	**5**
	Euphorbia hirta-leaf	**10**
	Psidium guajava-leaf	**10**
	Solanum virginianum-fruit	**10**
Anti-inflammatory	Licorice	**45**
Astringent	Myrrh	**50**
Analgesic	Peppermint (*Mentha spicata*)	**50**
Remineralizing	Gotu Kola (*Centella asiatica*)	**10**
Sweetening	Xylitol	**50**
Natural abrasiveness	Pink salt	**50**
Whitening agent	*Abrus precatorius* leaf	**45**
	Coconut shell charcoal	**35**
Flavoring agents	*Cinnamomum verum*	**50**
Foaming agent	Soapnut- *Sapindus trifoliatus*	**30**
Binding agent	Starch	**50**
	Total weight	**510 mg**

Figure 4.27 Formulated polyherbal dentifrice (PHDF)

The tablet's weight (510mg) was optimized for stability and compression. The active polyherbal extract (45mg) was deliberately kept low to ensure precise dosing. The remaining 465mg consisted of excipients that enhanced tablet performance. This formulation is consistent with industry standards, ensuring a consistent and effective dose. The tablet formulations were prepared using the direct compression method, incorporating the above ingredients mentioned in **Table 4.10**. to promote oral health and hygiene. **Figure 4.27** represents the formulated polyherbal dentifrice and fifty tablets were successfully prepared in a single batch. Then, the tablets underwent different evaluation parameters like appearance, surface texture, hardness, weight variation, friability, and disintegration. The results presented that the combined powders of the herbal extracts were suitable for the formulation of the tablet, highlighting the innovative potential of this approach in the development of herbal-based pharmaceuticals.

Many researchers have formulated a polyherbal toothpowder using different kinds of herbal ingredients mainly composed of neem, clove, cinnamon, mint, and rock salt with the addition of other excipients that satisfy all required properties to treat halitosis, bacterial plaque formation, and staining (Sanap et al. 2024; Dakhurkar et al. 2019). As an eco-friendly substitute to commercial toothpaste, similar research was conducted by Sheeba et al (2024) using clove, cinnamon, ginger, amla, and stevia by direct compression method in a 250mg dosage of toothpowder tablet to improve oral hygiene. Moreover, polyherbal kinds of toothpaste composed of several natural extracts are highly active against *S. mutans* and prevent tooth decay with all the desired properties due to the presence of phytoconstituents like alkaloids, flavonoids, glycosides, phenols, and tannins (Sharma et al. 2014; Narayanasamy et al. 2023).

4.3.3 Evaluation Parameters for Polyherbal Dentifrice (PHDF)

4.3.3.1 Organoleptic Evaluation

Organoleptic parameters confirmed the identity of the plant extracts and added excipients (**Table 4.11**).

Appearance: The final herbal toothpowder exhibited a uniform light brown color with a fine, smooth texture. There were no visible lumps or color variations, suggesting effective mixing and consistent quality.

Odor: The toothpowder emitted a pleasant, aromatic fragrance characterized by the dominant scent of clove and peppermint, which are known for their refreshing and antiseptic properties. The natural aroma was well-balanced, with no overpowering or unpleasant odors detected.

Table 4.11. Organoleptic evaluation of PHDF

Organoleptic Evaluation	
Test	**Observation**
Color	Light brown
Odor	Aromatic
Taste	Sweet & salt
Texture	Fine
Appearance	Powder
Abrasiveness	Good

Taste: Preliminary taste tests indicated a mild, herbal flavor with a refreshing aftertaste, contributing to a pleasant user experience. The taste of the developed dentifrice was found to be sweet and salty.

Pandharinath Dakhurkar et al. (2019) formulated an herbal tooth powder using the dried powders of clove, cinnamon, pepper, neem, babul, arjuna, triphala, ritha, lodhara, vavding, pudina, tulsi, kala namak, madhunashini, and licorice which resulted in a brown color powder with a distinct odor, sweet and bitter taste.

4.3.3.2 Physiochemical Evaluation

The results of the physiochemical evaluation are mentioned in **Table 4.12**.

Determination of pH Value: The pH of a solution indicates the concentration of hydrogen ions (H+) relative to a standard solution, as an indicator of its level of acidity and alkalinity. The pH of the herbal toothpowder was found to be 7.2±0.3, indicating a neutral to slightly alkaline nature. This pH range is favorable for oral health as it helps maintain the mouth's natural balance and prevents enamel erosion.

Moisture Content: The moisture content of the herbal tooth powder was found to be 1.32±0.2%, which falls within the acceptable range for dry herbal powders. Low moisture content minimizes the risk of microbial growth and enhances the product's shelf life.

Hardness and Thickness: The polyherbal toothpowder tablets were evaluated using a Pfizer Hardness Tester to determine the average hardness of the tablet. A total of randomly selected 10 tablets were tested and the recorded hardness value was found to be below the acceptable range (<3kg/m^2), thus PHDF tablets failed the test representing their minimal hardness with a thickness of 5mm diameter.

Table 4.12. Physiochemical evaluation of PHDF

Physiochemical Evaluation	
Test	**Observation**
pH	7.2±0.3
Moisture Content	1.32±0.2%
Hardness	Fail
Thickness	5mm
Friability	0.6%
Foamability	3ml

Friability and Foamability: The friability test assessed the tablet's ability to resist abrasion and breakage under stress, simulating the handling that occurs during packaging, transportation, and use. The friability of polyherbal toothpowder tablets was tested using an iNWEKA friability tester. A pre-weighed sample of 20 tablets from each batch was subjected to 100 revolutions in friability at 25rpm. The formulated tablets were weighed again and calculated for the weight loss in percentage. The friability values for all batches were below the acceptable limit of 1% threshold, indicating that the tablets possess excellent mechanical strength, abrasion resistance, and durability enabling them to withstand handling and transportation without significant physical degradation or weight loss. The formulated PHDF produced 3ml of foam when mixed with water.

Bharathi et al (2020) and Sheeba et al (2024) reported similar pH (6), moisture content (1.06%), and low friability of the formulated herbal toothpowder, which correlate to our present findings.

4.3.3.3 Rheological Evaluation

The results of the rheological evaluation are represented in **Table 4.13**.

Table 4.13. Rheological evaluation of PHDF

Rheological Evaluation		
Test	**Observation**	**Inference**
Angle of Repose	58º39’	Poor flow
Bulk Density	2.127g/cm^3	-
Tapped Density	3.03g/cm^3	-
Carr’s index	29.80 %	Cohesive
Hausner’s ratio	1.42g/cm^3	Good flow
Disintegration	3 min 15 sec	-

The Angle of Repose: The flow characteristics of the herbal toothpowder were assessed using the fixing funnel method. The measured angle was 58º39’, which falls above the range indicating poor flowability.

Bulk and Tapped Density: The bulk and tapped densities of toothpowder were determined to be 2.127 g/cm^3 and 3.03 g/cm^3, respectively.

Carr’s Index: The polyherbal powder exhibited a Carr’s index of 29.80%, indicating poor flowability. The obtained results confirmed that the polyherbal toothpowder tablet possesses acceptable compressibility and good mechanical strength despite having minimal hardness. These tablets were designed for chewing to facilitate the release of active ingredients for brushing. The formulated toothpowder tablets were found to be a better alternative to toothpaste for maintaining oral hygiene.

Hausner’s Ratio: The results expressed around 1.42g/cm^3 indicated good to fair flowability, suggesting that the powder is moderately cohesive and free-flowing suitable for tablet compression processes.

Disintegration Test: All the toothpowder tablets tested demonstrated a satisfactory disintegration time of 3 minutes 15 seconds, within the acceptable time range. This result met the pharmacopeial requirements, ensuring that the chewable tablets disintegrate effectively upon brushing, releasing the active ingredients to produce the intended therapeutic effect. Here dissolution test is not applicable as it is a polyherbal formulation and contains many chemical constituents.

Weight Variation Test: All the chewable tablets tested fell within the acceptable range, with deviations between -0.56 and 1.62%. This uniformity in weight ensures consistent dosing and quality, demonstrating a well-controlled manufacturing process that meets the required standards.

Table 4.14. Weight variation test

S. No	Individual weight (mg)	Weight variation (mg)	Weight deviation (%)
1	502.4	2.4	0.48
2	508.1	8.1	1.62
3	496.5	4.5	-0.7
4	497.2	3.8	-0.56
5	494.0	6	-1.2
6	500.5	0.5	0.1
7	503.7	3.7	0.74
8	490.0	10	-2
9	497.8	3.2	-0.44
10	497.7	3.3	-0.46
11	507.6	3.4	1.52
12	503.0	3	0.6
13	505.5	5.5	1.1
14	506.9	6.9	1.38
15	504.3	4.3	0.86
16	499.2	1.8	-0.16
17	505.7	5.7	1.14
18	498.7	8.7	-0.26
19	499.1	1.9	-0.18
20	501.2	1.3	0.24
	Average weight		**500.995**

The results of the rheological evaluation are on par with the findings of Bharathi et al (2020) and Sanap et al (2024), who demonstrated the bulk density (4 gm/ml), and angle of repose (48º74') which showed good flow properties and good packing ability of the developed toothpowder. The quick disintegration time reported by Sheeba et al. (2024) coincides with our results indicating minimum hardness and easy crushing. Similarly, Phuke et al (2024) reported that the weight variation test for all the dentifrice formulations (F1-F4) met the pharmacopeial limit with weights ranging from 400-450mg and deviations within the acceptable 5% limit.

Storage Stability Assessment: A three-month storage stability assessment of the toothpowder tablets demonstrated that the tablets retained their pH, moisture, and physical integrity, within acceptable limits under both accelerated and long-term storage conditions. These results indicated that the chewable tablets remain stable, safe, efficacious, and of high quality throughout their shelf life under recommended storage conditions (**Table 4.15**).

Table 4.15. Storage stability assessment of the developed polyherbal dentifrice

Assessment condition	Temperature (ºC) /Relative Humidity (RH)	Observation			
		pH	Moisture content	Friability	Color
0 day	32±2ºC/65±5%	7.4	1.30%	0.32%	Light brown
1st month	04±0.5ºC/no RH 25±0.2ºC/60±5% 30±2.0ºC/65±5%	7.3 7.0 7.2	1.15% 1.29% 1.28%	0.21%	
2nd month	04±0.5ºC/noRH 25±0.2ºC/60±5% 30±2.0ºC/65±5%	7.3 7.4 7.5	1.30% 1.25% 1.17%	0.18%	
3rd month	04±0.5ºC/noRH 25±0.2ºC/60±5% 30±2.0ºC/65±5%	7.2 7.1 7.3	1.21% 1.24% 1.29%	0.45%	

Stability testing of polyherbal tablets is crucial, as it determines their shelf life and storage conditions. This implies assessing the tablet's stability under different environmental conditions such as temperature and humidity followed by analyzing the efficacy and state of change in the required parameters (Zarvandi et al. 2017).

4.3.4 Cytotoxicity Evaluation of PHDF

The mortality rate of the brine shrimps at various observation intervals and concentrations of PHDF were represented in **Table 4.16**. The results indicated that PHDF exhibited low toxicity at the tested concentrations. After 24h of incubation, 1-5 out of 30 shrimps were found dead at the highest concentration. The PHDF showed a 17% mortality rate at a concentration of 1500µg/ml, suggesting its safety for therapeutic uses. The standard potassium dichromate ($K_2Cr_2O_7$) showed a significantly lower LC_{50} value of 29.15µg/ml.

Table 4.16. Cytotoxicity of PHDF using brine shrimp assay

Sample (1mg/mL)	Concentration (µg/ml)	Mortality of Brine shrimp (no. of shrimps dead) (hours)					
		1	2	4	6	24	% Mortality (24h)
PHDF	**100**	0	0	0	1	1	3
	250	0	0	0	0	2	7
	500	0	0	0	0	3	10
	1000	0	0	0	0	4	13
	1500	0	0	0	0	5	17
Control $K_2Cr_2O_7$	**1 (mg/ml)**	30	-	-	-	-	100
Blank	Saline water	0	0	0	0	0	0

The brine shrimp lethality assay has significantly matched the toxicity data of rat models and humans which proves consideration of this assay as a valuable preceding one (Zivkovic et al. 2016; Da Silveira Carvalho et al. 2017). A larger presence of phytoconstituents in herbal extracts may retain subsequent cytotoxic effects (Sampaio et al. 2021). Thus, evaluating the safety and related toxic effects of herbal drugs necessitates user preference and scientific evidence (Saad et al. 2017).

Artemia salina has been extensively employed in evaluating the acute toxicity of herbal materials, natural products, pesticides, heavy metals, and metal complexes (Banti & Hadjikakou, 2021). Nerdy et al (2021) reported the LC_{50} value of green and red betel ethanolic leaf extracts as 44.975µg/mL and 31.556µg/mL respectively, suggesting potential for anticancer properties. Similarly, Waghulde et al (2020) found that the combined extracts of *Annona reticulata* with *Allium fistolisum* and *Brassica oleraceae* exhibited enhanced efficacy against the shrimp larvae compared to individual plant extracts, indicating a synergistic effect of bioactive compounds that contribute to their pharmacological effects.

4.3.5 Atomic Absorption Spectrometric Analysis of PHDF

Plant extracts used in dosage form can pose serious health problems if contaminated with heavy metals. According to Saper et al (2008) approximately 21% of tested Ayurvedic formulations contained unacceptable levels of heavy metals including lead, mercury, and arsenic. To ensure safety, it is mandatory to analyze heavy metals in plant extract or powder. The findings demonstrated the absence of heavy metals like arsenic, lead, cadmium, and mercury in the formulated PHDF. In contrast, the presence of essential minerals like calcium, potassium, and magnesium was detected with estimated concentrations of 7867, 8209, and 2387mg/kg, respectively (**Table 4.17**).

Table 4.17. Atomic absorption spectrometric analysis

Test Parameters	Test Results
Arsenic (As)	ND
Cadmium (Cd)	ND
Lead (Pb)	ND
Mercury (Hg)	ND
Calcium (Ca)	**7867 mg/kg**
Potassium (K)	**8209 mg/kg**
Magnesium (Mg)	**2387 mg/kg**

ND: Not Detected

The excessive intake of non-essential heavy metals including cadmium, arsenic, lead, and mercury are proven to be toxic to human health due to their

high specific gravity which leads to many chronic diseases (Jomova et al. 2024). The exposure of these metal toxins from oral care products has become a concern in recent years (Vella & Attard, 2019; Ogidi & Agbo, 2021). World Health Organization (WHO), and the United States Environmental Protection Agency (USEPA) have published a permissible limit of these toxic metals. Our present sample polyherbal dentifrice (PHDF) demonstrated the presence of no such toxic metals, which ensures its safety for daily usage. Our study is in contrast to several relative studies that have detected these metals in developed dentifrices (Ogidi & Agbo, 2021; Lawi et al. 2023;). Furthermore, the availability of essential minerals like calcium, potassium, and magnesium in a dentifrice can significantly enhance oral health. These minerals facilitate remineralization, fluoride uptake, pH balance, and inhibition of nerve response to external stimuli (Najeeb et al., 2016). These minerals when in combination may coordinate to build hard tooth enamel and maintain bone density.

4.3.6 Cost Analysis of Polyherbal Dentifrice

Table 4.18. Temporary cost analysis of the developed PHDF

Requirements	Amount in Rs.
Herbal Extracts	500/-
Excipients	75/-
Manufacturing and production cost	800/-
Total amount (500 Tablets)	1375/-
The cost of 50 Tablets	137/-

The temporary cost analysis was done for the formulated PHDF **(Table 4.18**). The total cost of the product was calculated based on the expenses of raw materials (herbal powders and binding agent), and production cost which includes solvent usage, lyophilization of plant extracts, and tablet compression. The expenses incurred for the development of formulation were estimated to be Rs.137/pack (50 tablets) and Rs. 2.74 for each tablet. This cost analysis underscores the need to balance quality and cost efficiency to develop a product that appeals to consumers and sustains market success.

This phase demonstrated that the combined extract of PGL, EHL, and SVF at higher ratios and BCL, AAR, and FBP at lower ratios exhibited significant synergistic effects on *S. mutans* with lower MIC. With this combination, a polyherbal toothpowder tablet was formulated by adding required excipients, then directly compressed into a tablet form to ensure consistent therapeutic effect and user-friendliness. The resulting polyherbal dentifrice was light brown with a characteristic odor and taste, exhibited minimal hardness, possessed good mechanical strength, and remained stable for three months during the evaluation. Additionally, the PHDF possessed low toxicity and contained essential minerals that contributed to effectiveness and oral hygiene. Therefore, the PHDF was further validated for its anti-cariogenic efficacy to treat dental caries which was discussed in the next phase.

PHASE IV

4.4. Anticariogenic Efficacy of Formulated PHDF

Dental caries remains a widespread, untreated health concern globally, affecting approximately 2.5 billion people, with a prevalence rate of 14.6% in the last decade, particularly affecting socially underserved communities (Elamin & Ansah, 2023). Effective prevention relies on individual-based preventive care management, including a low-sugar diet, and gentle oral hygiene practices that can reduce cavities, promote oral health, and prevent various ailments (Nath et al. 2023). Dental plaque, mainly composed of Gram-positive and Gram-negative bacteria, plays a significant role in tooth decay. *S. mutans,* a Gram-positive bacterium, is a primary etiological agent responsible for dental caries (Selvaraj et al. 2024). The virulence of *S. mutans* is strongly associated with acid production, pH reduction, biofilm formation, and tooth enamel demineralization.

Although various chemical and mechanical methods have been employed to eliminate plaque formation, traditional medicine-based mechanical plaque removal has proven to be effective and harmless. Brushing is a common oral hygiene technique practiced worldwide and serves as a valuable complement to this approach, mechanically removing plaque and good oral health. This practice dates back to the Egyptians who developed toothpowder around 3000- 5000 BC using natural ingredients: egg shells, animal bone ashes, charcoals, horns, etc., (Deepak et al. 2024). Many oral hygiene products, such as toothpaste, rely on preservative agents like paraben and sodium benzoate to maintain their texture. Intrast, toothpowder tablets are therapeutically more effective and require no chemical substances due to their abrasiveness, dry texture, and compressed form. In addition, these tablets in precise dosages are convenient for brushing, eco-friendly with zero plastic packaging, and retain hygiene storage (Sheeba et al. 2024).

Research on the biological activities of herbal products has significant implications mainly in the pharmaceutical, health, food, and cosmetic industries. Numerous species of plants, and plant compounds applied in the formulation has gained attention for its antimicrobial potential, which was well documented by recent reviewers Khameneh et al (2019), Chassagne et al (2021), Ekiert & Szopa

(2023). Hence, this phase focuses on the antimicrobial efficacy of developed PHDF to combat cariogenic microorganisms, eradicate biofilms, mitigate pH levels, and inhibit hydrophobic interactions against caries-causing organisms.

4.4.1 Determination of Inhibitory Zone Diameter, MIC, and MBC/MFC

The antimicrobial efficacy of the formulated polyherbal dentifrice was evaluated against tested clinical isolates, revealing notable differences in effectiveness (**Figure 4.28**). The PHDF, marketed standard (MS) and sodium fluoride (NaF) demonstrated substantial inhibition zones with 21.6±1.15mm, 13.0±1.00mm, and 13.6±1.52mm respectively for *S. mutans*, 21.0±1.00mm, 13.0±1.00mm, and 13.0±1.00mm, respectively for *S. salivarius*, 21.1±0.57mm, 11.0±1.00mm and 14.6±0.57mm, respectively for *S. parasanguinis*, and 21.6±1.52mm, 12.0±0.00mm, and 10.6±0.57, respectively for *S. oralis*, at 150µg/ml, indicating strong antibacterial activity. Similarly, the PHDF, MS, and NaF showed notable inhibitory effects against Gram-negative isolates such as *K. pneumoniae* (22.0±0.00mm, 15.0±1.00mm, and 13.3±2.88, respectively), *P. aeruginosa* (23.6±2.3mm, 16.3±0.57mm, and 14.3±0.57mm, respectively), and *A. baumannii* (23.6±2.88mm, 12.3±0.57mm, and 14.0±1.00mm, respectively). Likewise, the fungal pathogen *C. albicans* also exhibited a significant inhibition zone of 20.6±0.57mm for PHDF, 15.3±0.57mm for MS, and 14.6±0.57mm for NaF. The IZD results of PHDF expressed impartial inhibition against all the tested clinical isolates when compared to the marketed standard and sodium fluoride demonstrating effective prevention of bacterial growth (**Table 4.19**).

The effectiveness of herbal oral care products such as herbal mouth rinse formulated by Loganathan et al (2024) using the aqueous leaf extracts of *Ocimum tenuiflorum* and *Ocimum gratissimum* and three commercial herbal-based mouth rinses (OX, Pesona, and Watsons) evaluated by Teh et al. (2015) exhibited significant antibacterial activity towards *S. mutans* and *Lactobacillus spp. and S. mutans, S. sobrinus, L. salivarius*, and *C. albicans,* respectively. Polyherbal toothpaste formulated by Mohankumar et al (2013) exhibited substantial antibacterial activity against *S. mutans* and *L. acidophilus* suggesting that these products can be a valuable adjunct to conventional oral care products in preventing and controlling oral diseases.

Table 4.19. Inhibitory zone diameter (mm) of PHDF, marketed standard, and NaF against oral clinical isolates

Inhibitory Zone Diameter (mm)			
Oral isolates	**PHDF**	**Marketed Standard (MS)**	**Sodium Fluoride (NaF)**
SMU	**21.6±1.15**	13.0±1.00	13.6±1.52
SSA	**21.0 ±1.00**	13.0±1.00	13.0±1.00
SPSA	**21.1±0.57**	11.0±1.00	14.6±0.57
SOS	**21.6±1.52**	12.0±0.00	10.6±0.57
KP	**22.0±0.00**	15.0±1.00	13.3±2.88
PA	**23.6±2.30**	**16.3±0.57**	14.3±0.57
AB	**23.6±2.88**	12.3±0.57	14.0±1.00
CA	**20.6±0.57**	15.3±0.57	14.6±0.57

The values expressed as mean±SD.

SMU-*S. mutans*, SSA-*S. salivarius*, SPSA-*S. parasanguinis*, KP-*K. pneumonieae*, PA-*P. aeruginosa*, AB-*A. baumanii*, CA-*C. albicans*

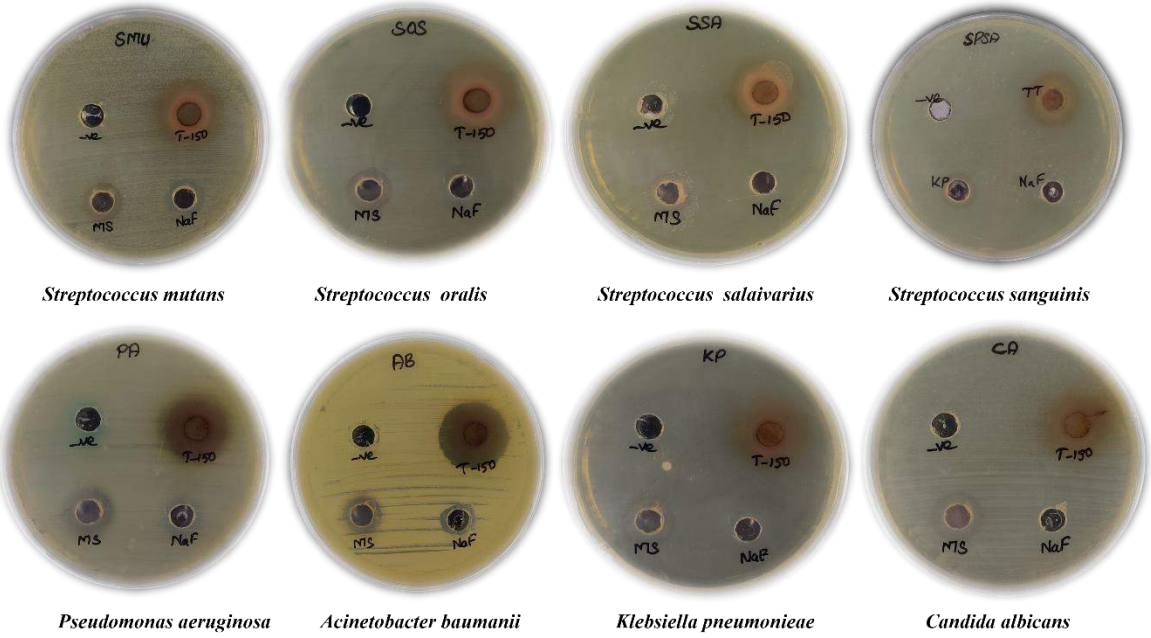

Figure 4.28. Antimicrobial efficacy of PHDF compared with a marketed standard against oral clinical isolates

The MIC of PHDF against the eight oral pathogens ranged from 0.3125 to 1.25mg/ml and MBC/MFC ranged from 0.625 to 2.5mg/ml. For instance, PHDF demonstrated the lowest MIC and MBC values against *S. parasanguinis* (0.3125 and 0.625 mg/mL), respectively, followed by *S. mutans*, *S. salivarius*, *K. pneumoniae*, *P. aeruginosa, and A. baumannii,* (0.625 and 1.25mg/mL), respectively, for higher concentrations of 1.25 and 2.5mg/ml were required for *S. oralis* and *C. albicans*, respectively. These findings indicated that PHDF inhibited microbial growth at lower concentrations, while higher concentrations are necessary to achieve bactericidal or fungicidal effects (**Table 4.20**).

Table 4.20. MIC, MBC, and MFC of PHDF against oral clinical isolates

Oral isolates	PHDF		STD		NaF	
	MIC	MBC	MIC	MBC	MIC	MBC
SMU	0.625	1.25	5	10	2.5	5
SOS	1.25	2.5	5	10	5	10
SSA	0.625	1.25	2.5	5	1.25	2.5
SPSA	0.3125	0.625	2.5	5	2.5	5
KP	0.625	1.25	2.5	5	2.5	5
PA	0.625	1.25	2.5	5	1.25	2.5
AB	0.625	1.25	5	10	5	10
CA	1.25	2.5	2.5	5	2.5	5

The values are presented in mg/ml.

SMU-*S. mutans*, SSA-*S. salivarius*, SPSA-*S. parasanguinis*, KP-*K. pneumonieae*, PA-*P. aeruginosa*, AB-*A. baumanii*, CA-*C. albicans*

Studies have consistently demonstrated the effectiveness of herbal care in preventing and controlling oral diseases. Two clinical studies proved that neem extract toothpaste/gel effectively reduced the level of *S. mutans,* plaque formation, and gingivitis equivalent to the effect of chlorhexidine gel (Selvaraj et al. 2020). Prepared herbal tooth powder exhibited potent antimicrobial activity against tested bacteria and fungi with significant zones of inhibition observed against *S. mutans* and *C. albicans* providing evidence for the therapeutic benefits and antimicrobial properties of herbal-based oral care products, supporting their use in oral health maintenance (Asokan et al. 2020)

4.4.2 Effect of PHDF on Cell Surface Hydrophobicity of *S. mutans*

The hydrophobic interaction of *S. mutans* contributes to the primary attachment to tooth enamel, a hydrophobic surface that results in the accumulation of biofilm and plaque. The hydrophobic index of *S. mutans* was estimated by the microbial adhesion to hydrocarbons (MATH) test which involves treating the cells of *S. mutans* at different MIC concentrations (1/8MIC, 1/4MIC, 1/2MIC, and MIC) of PHDF in the presence of the toluene and comparing with the control group.

The control group exhibited high hydrophobicity, with over 77% of cells aggregation with the surface hydrocarbon and the aqueous phase showed high affinity for the tested hydrocarbon toluene, resulting in their removal from the aqueous phases. In contrast, the PHDF treated, significantly reduced the hydrophobic indices of the *S. mutans* in a concentration-dependent manner at 1/8MIC, 1/4MIC, 1/2MIC, and MIC from 66.7, 50.5, 28.5, and 12.4%, respectively. The efficacy of PHDF was slightly more effective than the standard NaF (30.8%) at the MIC level (P<0.0001) as depicted in **Figure 4.29**.

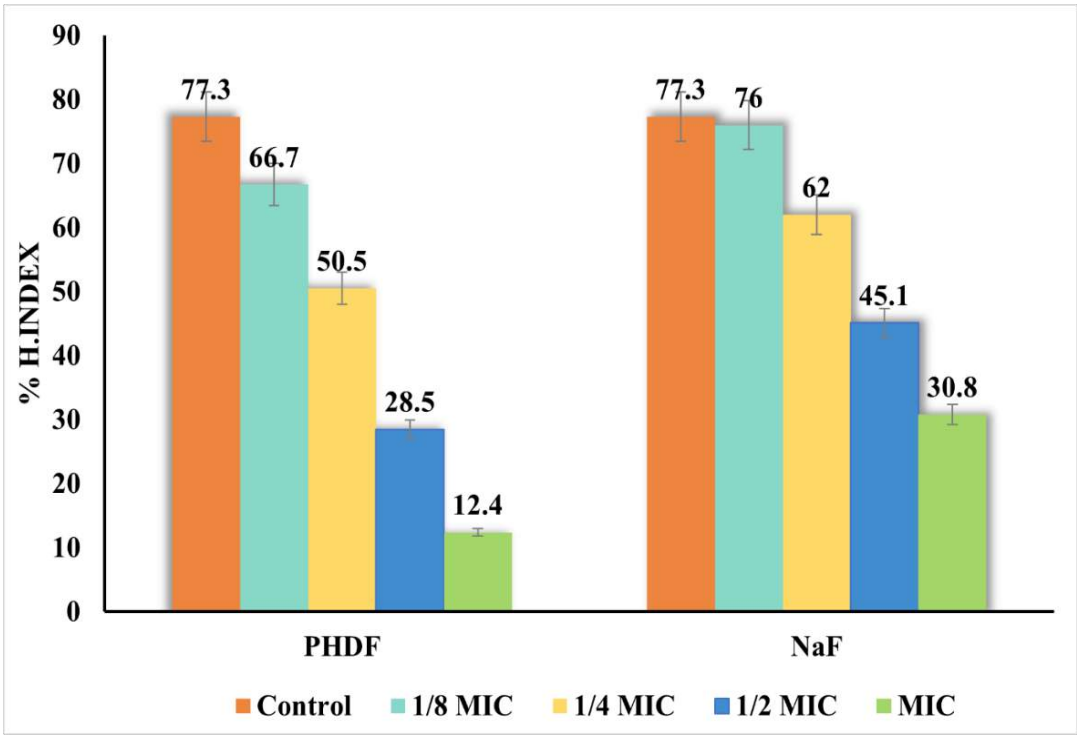

Figure 4.29. Hydrophobic interaction of formulated PHDF against *S. mutans*

Despite the use of antibiotics and chemical agents in dentistry, *S. mutans* remains multidrug-resistant due to its hydrophobic nature enabling tooth surface adherence (Chowdaiah et al. 2019). However, herbal extracts offer a promising solution by modifying *S. mutans* hydrophobicity, thereby reducing virulence and pathogenicity (Matsumoto-Nakano et al. 2009). Exposure to ¼ MIC of ethanolic extracts from *Streblus asper*, *Cymbopogon citratus*, and *Syzygium aromaticum significantly* hindered the hydrophobicity of *S. mutans* ATCC 25,175, CSM06, and CSM25, while 1/2 × MIC of these extracts reduced the hydrophobicity indices to less than 50% (Karnjana et al. 2023). The essential oils have shown promise in reducing the hydrophobic nature of *S. mutans.* Oregano essential oils (OEOs) 1/16 MIC significantly decreased the hydrophobic nature of *S. mutans* ($p<0.05$) (Yuan et al. 2023). Additionally, *Thymus vulgaris* (linalool), *Thymus zygis,* and *Thymus vulgaris* (Carvacrol) exhibited inhibitory rates of 21.66%, 42.21%, and 56.72% at 1/2 MIC (Park et al. 2023).

4.4.3 Effect of PHDF on Glycolytic pH Drop

The cariogenic pathogen *S. mutans* is a potent glycolytic acid producer that rapidly metabolizes dietary glucose, causing a significant drop in oral pH from 7.0 to 4.0, and leading to tooth decay (Matsui & Cvitkovitch, 2010). The activity of PHDF on different MIC values (1/8 MIC, 1/4 MIC, 1/2 MIC, and MIC) on the production of acid by *S. mutans* was examined. Initially, the pH of all MIC values ranged from 7.3 to 7.5. After 24h the negative control pH decreased to 4.0, indicating the acid production of *S. mutans*. In contrast, PHDF at MIC, inhibited acid production, maintaining 7.0 pH even after 24 h of incubation.

At 1/8 MIC, PHDF, reduced the acidity of the bacterial environment showing a pH of 4.8, while the positive control (NaF) group suppressed the acid production at MIC concentration, exhibiting a final pH of 7.3 with a significant difference $P<0.001$ (**Figure 4.30**). These findings, clearly demonstrated that PHDF inhibits acid production by *S. mutans* in a dose-dependent, with higher concentrations of PHDF preventing acid production and maintaining a neutral pH.

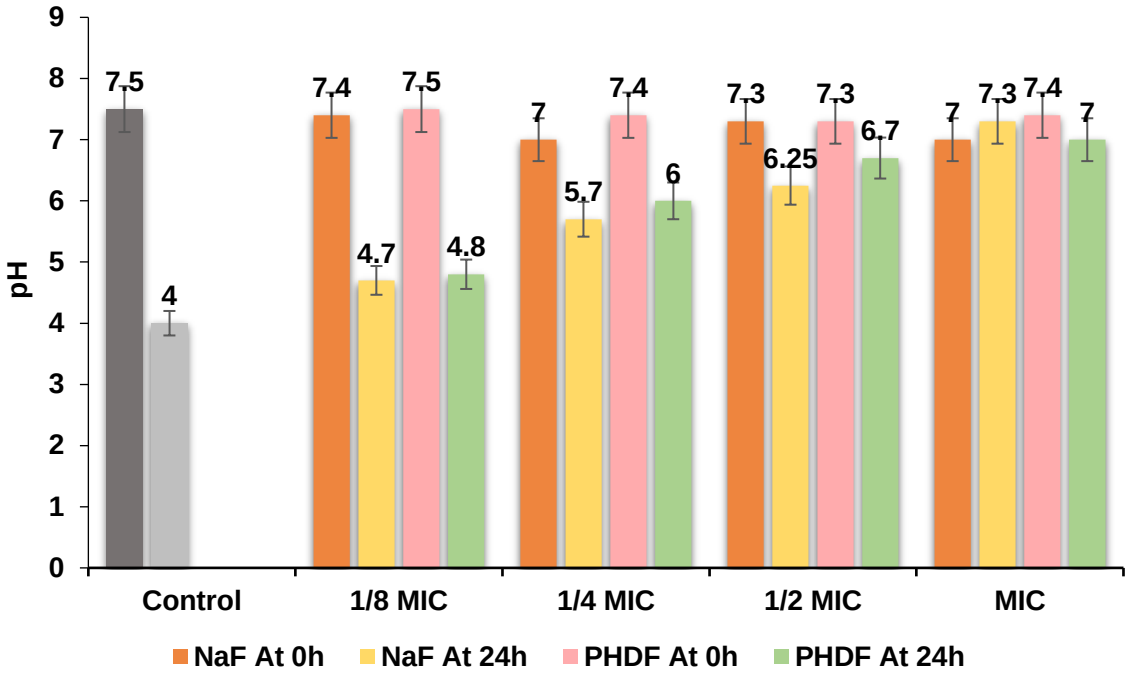

Figure 4.30. Acidogenic mitigation of *S. mutans* by formulated PHDF

Natural herbs have been scientifically reported to be non-toxic and effective in combating the virulence factors of *S. mutans* for treating periodontal diseases, halitosis, mouth ulcers, and cancers (Sidhu et al. 2020). Thai herbal formulations significantly inhibited acid production by *S. mutans* through quorum sensing inhibition, thereby preventing a significant drop (Sanpinit et al. 2022). The essential oils of *Origanum vulgare* L. (OEO1) and *Origanum heracleoticum* L. (OEO2) inhibited organic acid production by *S. mutans* at MIC concentration, maintaining initial pH. In contrast, the negative control pH dropped from 7.01 to 4.17, and the positive control pH was 6.94 at 1/2 MIC after 24h of incubation (Yuan et al. 2023). These results are on par with our findings which proved the efficacy of natural herbs in the inhibition of acid production by *S. mutans* thereby preventing a significant drop, ultimately contributing to a healthy oral environment.

4.4.4 Biofilm Eradication Potential of PHDF

The action of PHDF at 1/8 MIC, 1/4 MIC, 1/2 MIC, and MIC against the biofilm-forming cariogenic isolate *S. mutans* inhibited most of the biofilms attached to the flat-bottomed 96-well plate. PHDF exterminated the biofilm aggregation of *S. mutans*, inhibiting 94.87% of biofilm formation at MIC concentration, 76.87% at

1/2 MIC, and 29.05% and 39.52% at 1/8 MIC and 1/4 MIC, respectively. In addition, the impact of PHDF on the degradation of biofilm activity was comparable to NaF-positive control, achieving 91% activity, with high statistical significance (P<0.0001) (**Figure 4.31**).

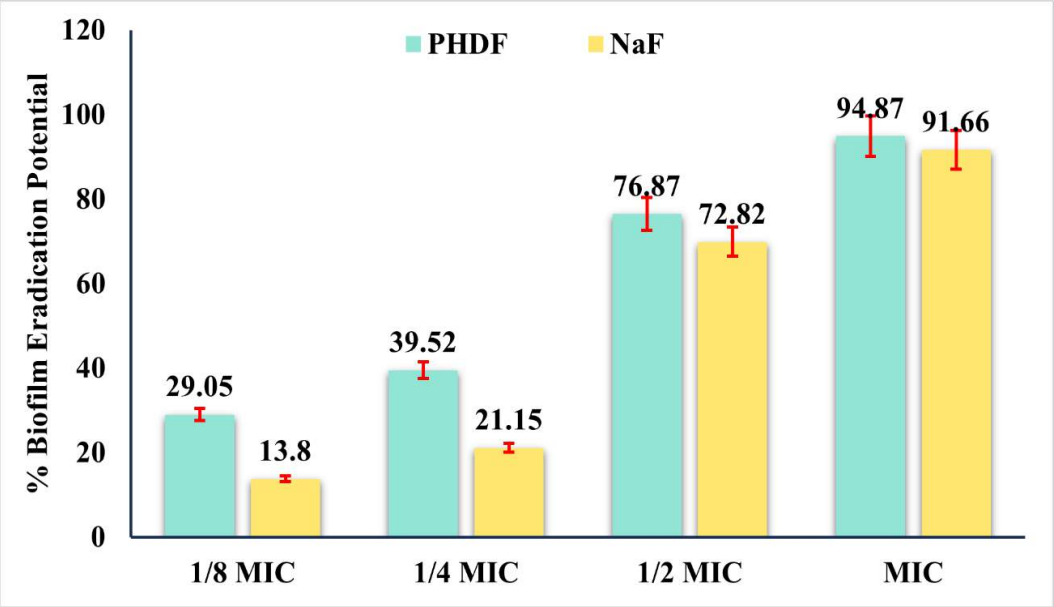

Figure 4.31. Effect of PHDF and Sodium fluoride (NaF) on SMU biofilm assessed by crystal violet staining assay

The eradication of the formed biofilm of SMU was further analyzed using a resin tooth model. The different MIC levels of PHDF significantly detached the biofilm formed on the resin tooth after 24h of incubation. The cleaning ability of the formulated PHDF was also evident and observed to be dose-dependent when compared to NaF using safranin staining displayed in **Figure 4.32 a & b**. The Polyherbal toothpowder tablets are considered a viable alternative to toothpaste for improving oral hygiene, combining effectiveness with ease of use.

Various plant extracts and their products have demonstrated potent antimicrobial and anti-biofilm activities against oral pathogens, particularly *S. mutans*. A mouthwash prepared using the extracts of *Rosa damascena* flower petals, *Coleus amboinicus* leaves, *Psidium guajava* leaves, and *Phyllanthus acidus* fruits expressed excellent antimicrobial activity against *S. mutans, E. faecalis, S. aureus, E. coli, and C. albicans*. and disrupted *S. mutans* biofilm formation (Sakthivel et al. 2024).

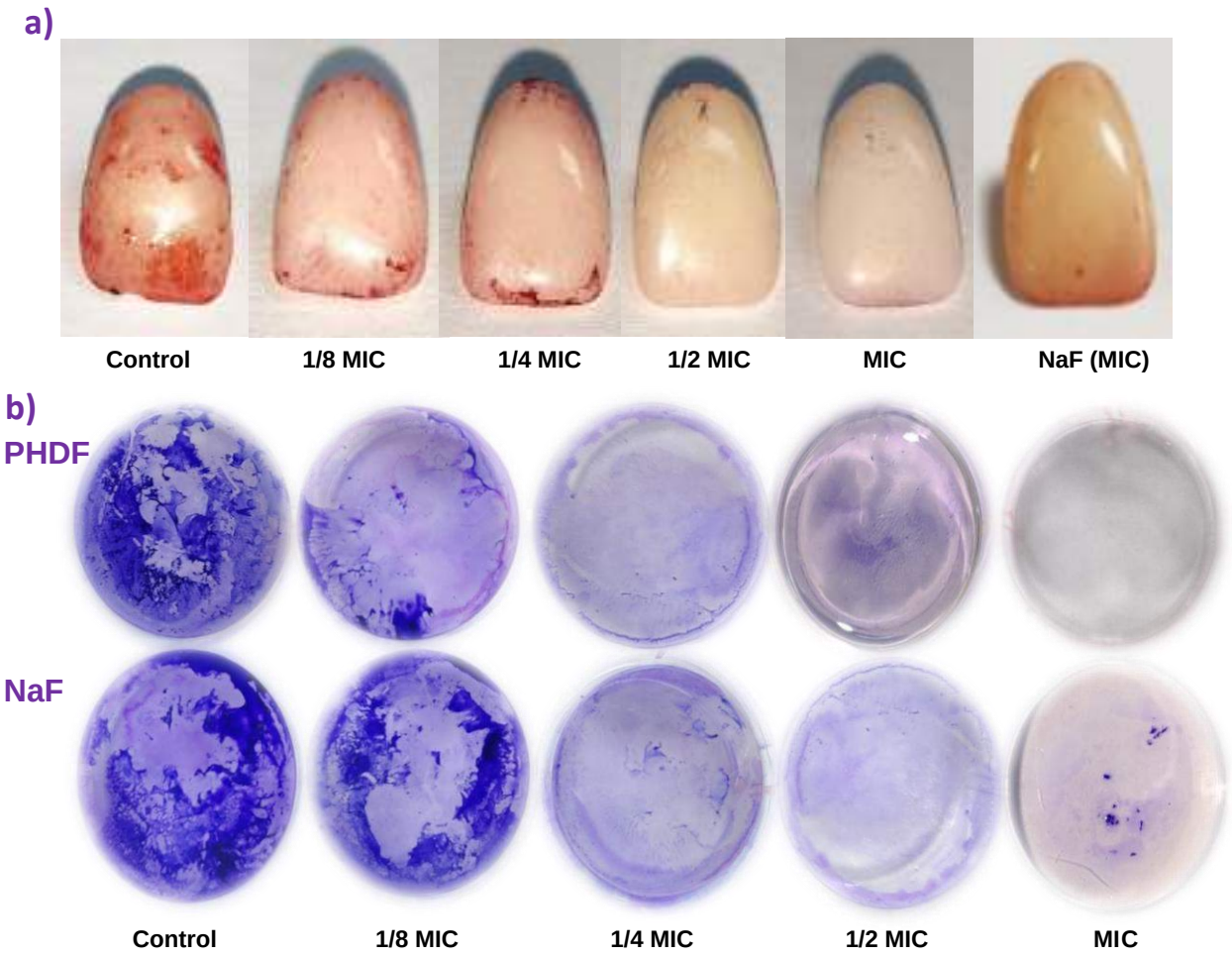

Biofilm formation assays using a) artificial resin teeth and b) 96-polystyrene well plates at 37ºC for 24h under anaerobic conditions. Concentrations ranged from 1/8 MIC, 1/4 MIC, 1/2 MIC, and MIC. NaF (MIC) was used as a control.

Figure 4.32. Inhibition of preformed biofilm of SMU by PHDF and Sodium fluoride (NaF) using a) resin teeth model, b) 96-well polystyrene plate

The methanol extract of *Salvadro persica* inhibits *S. mutans* biofilm formation with a minimum biofilm inhibitory concentration (MBIC) of 10 mg/ml (Balhaddad et al. 2021). The methanol extracts of *Cistus creticus*, *Cistus monspeliensis*, *Rosmarinus officinalis*, *Salvia sclarea*, and *Thymus longicaulis* significantly inhibited *S. mutans* biofilm formation at different concentrations (Hickl et al. 2018). Similarly, Cho et al (2022) reported a novel compound 3'3"-dihydroxy-(-)-matairesinol from the heartwood of *Juniperus chinensis*, effectively disrupts the *S. mutans* biofilm formed on the resin teeth surface showing similar effectiveness to the standard 0.1% NaF.

4.4.5 SEM Analysis of PHDF Treated *S. mutans* Biofilms

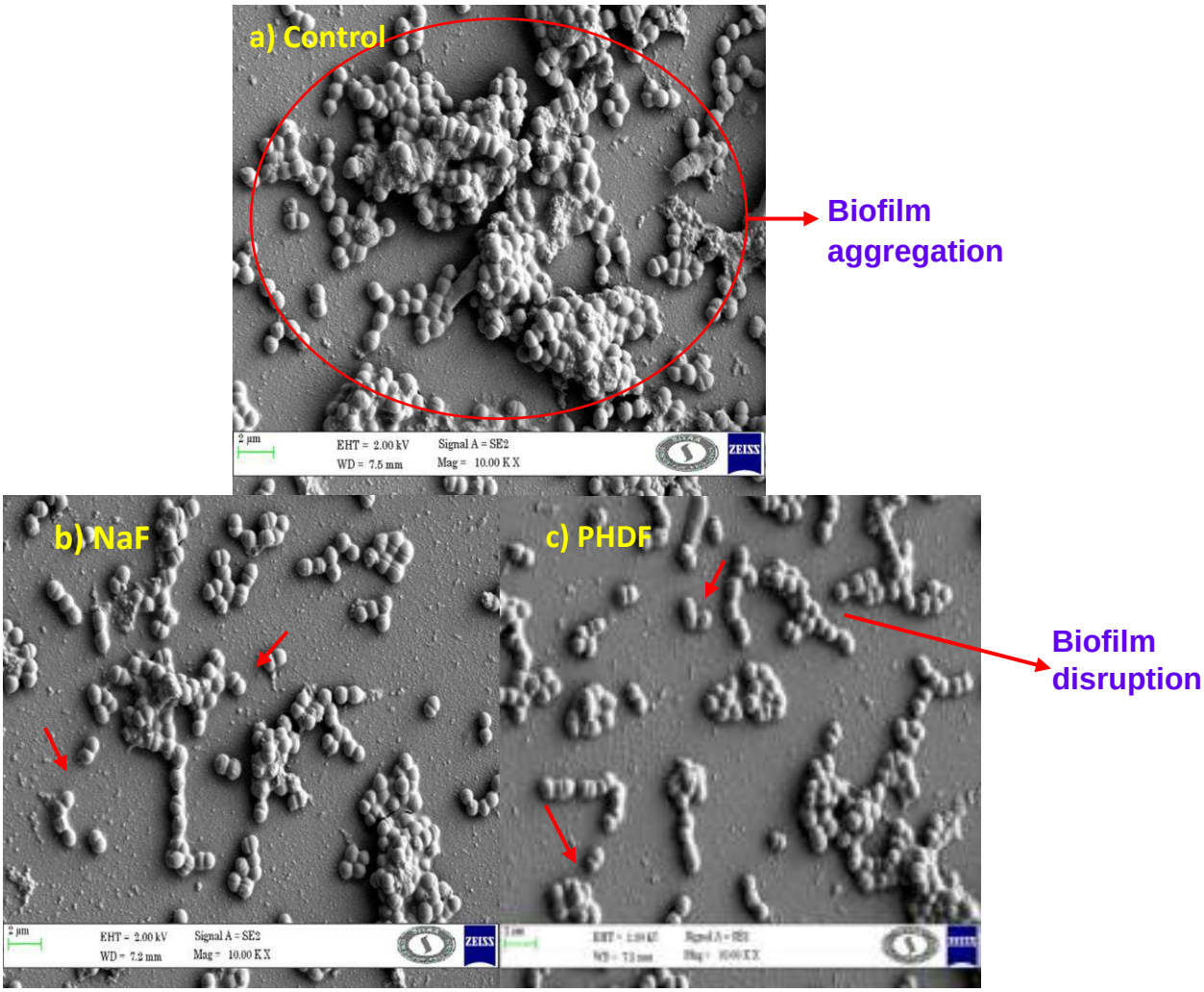

Figure 4.33. Micromorphology of *S. mutans* biofilms at the MIC level a) Control, b) NaF Treated, and c) PHDF Treated

The effect of PHDF and NaF against *S. mutans* biofilm was examined using SEM. The untreated biofilm composed of aggregated cocci in the chains and pairs, revealed matured bacterial biofilm attaching to the base material after 24 hours. In contrast, PHDF treatment significantly decreased the formation of *S. mutans* biofilm on the base material which was observed from SEM images shown in **Figure 4.33** demonstrating comparable efficacy to NaF in inhibiting *S. mutans* biofilm formation. Moreover, the biofilm images taken at 1000X magnification were incorporated to measure the total surface area of biofilm attached to the glass slide using ImageJ software. The percentage area of biofilm coverage was calculated by counting the pixel corresponding to a bacterial

presence in the image. The results illustrated that the untreated control biofilms comprised 39.03% of surface area, whereas sodium fluoride and PHDF treated significantly reduced biofilm coverage to 15% and 18.6%, respectively.

Recent studies have demonstrated the efficacy of natural extracts in eradicating *S. mutans* biofilm, which causes structural changes and degradation of accumulated biofilms as observed through SEM imaging. Formulated AgNps from the ethanolic extracts of *Streblus asper, Cymbopogon citratus, and Syzygium aromaticum* at the MIC level visualized the structural change and eradication of accumulated biofilm of *S. mutans* observed using SEM images (Karnjana et al. 2023). The synergistic combination of *H. natalensis* and *Camellia sinensis,* as well as tea tree and peppermint essential oil treated on enamel block at 1/2 MIC, displayed a detached cocci and degraded cell surface of *S. mutans* when observed through SEM imaging when compared to the untreated sample which indicated a dense group of aggregated biofilms (Henley-Smith et al. 2024).

The outcome of the phase IV results revealed the mechanism of action of PHDF formulation in treating dental caries. *In vitro* findings demonstrated that the formulated PHDF is highly effective in inhibiting the growth of tested oral pathogens and eradicating the biofilm formation of *S. mutans* at its MIC level when compared to the marketed standard and NaF. This might be due to the synergistic effects of combined plant extracts and multiple phytoconstituents present in PHDF. These findings suggest that the formulated PHDF is a potent anti-cariogenic agent, capable of protecting the oral cavity from cariogenic microorganisms and preventing tooth decay when used for daily brushing. To further understand the interaction of these drug molecules and disease targets with their effects on human physiology, a network pharmacology approach was employed in phase V.

PHASE V

4.5 Validation of Therapeutic Activity of PHDF Against Dental Caries Through the Network Pharmacology Approach

The formulated polyherbal toothpowder tablet offers a promising herbal remedy for preventing and treating primary dental caries by inhibiting the growth of cariogenic microorganisms. By providing scientific validation, this research reinforces the traditional use of medicinal plants, paving the way for their safe and effective long-term application. Our *in vitro* findings demonstrated that the bioactive compounds present in the six plants (AAR, BCL, EHL, FBP, PGL, and SVF) exhibited better antimicrobial efficacy towards cariogenic organisms. To further elucidate the mechanisms underlying the anti-cariogenic effects of the polyherbal formulation, we applied a network pharmacology approach to investigate the interactions between its bioactive components and target genes involved in dental caries using *in silico* tools.

4.5.1 Deciphering the Repairing Mechanism of PHDF for Dental Caries

Polyherbal medicine comprises natural compounds that provide therapeutic and preventive benefits, providing an alternative to commercial antibiotics for the prevention and treatment of dental caries. The unique chemical structures and major biological activities of phytocompounds make them effective against dental caries. Network pharmacology compiles comprehensive data to understand the overall interactions between the compounds and human biological targets. This emerging discipline integrates the tools of bioinformatics, pharmacological, and molecular biology tools to elucidate the mechanisms of action and interaction between drugs, targets, and disease (Nogales et al. 2022; Jiashuo et al. 2022). With this pharmacological network approach, the present study aims to investigate the molecular mechanism by which polyherbal compounds combat dental caries, focussing on the identification of potential targets, mechanism of action, and pathway involved in dental caries formation. The findings are further validated through a multi-faceted approach using *in vitro, vivo,* and *silico* experiments, that include bioinformatics tools such as gene ontology, pathway enrichment analysis, and molecular docking simulations.

4.5.2 Screening of Potential Targets of Active Components in PHDF

The potential 78 compounds mentioned in section 4.2.1 were considered the key active compounds for their strong antibacterial activity. To identify their potential interactions, target fishing was done to screen the effective targets (*Homo sapiens*) associated with dental cavities using the SuperPRED 2022, Swiss Target Prediction, Malacards, Comparative Toxicogenomic Database (CTD), and Gene Expression Omnibus Database (GEO). Based on the gift and influence score the targets were filtered and about 24779 targets were retrieved from Mala cards (56), CTD (14373), and GEO (13298) databases. Once the targets were retrieved from these individual databases, the key targets common to all these databases were identified. A total of 9 key targets (MMP9, MMP3, MMP13, IL6, 1L1B, CA4, CA6, ACE, and ALB) were identified to be common to all databases and integrated using the Venny tool. (**Figure 4.34** and **Table 4.21**). These findings suggest that targeting these genes with PHDF could be an effective way for treating dental caries throwing light on its underlying mechanisms.

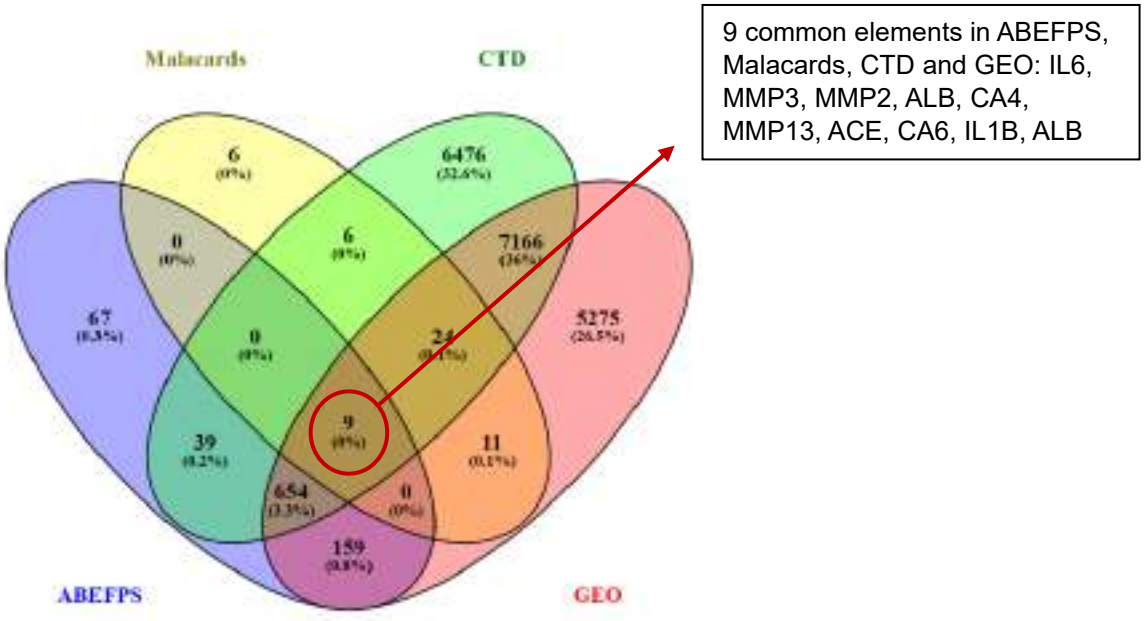

Figure 4.34. Venn diagram showing intersection targets of ABEFPS active compounds and dental-related genes

ABEFPS: **A**-*Achyranthes aspera*, **B**-*Barleria cuspidata*, **E**-*Euphorbia hirta*, **F**-*Ficus benghalensis*, **P**-*Psidium guajava*, **S**-*Solanum virginianum*; **GEO**:Gene Expression Omnibus database; **CTD**: Comparative Toxicogenomic Database.

Table 4.21. Potential Targets of Components of PHDF

Gene Symbol	Gene Name
MMP3	Matrix Metalloproteinase-3 (Stromelysin-1)
MMP2	Matrix Metalloproteinase-2 (72 kDa type IV Collagenase)
MMP13	Matrix Metalloproteinase-13 (Collagenase 3)
IL1B	Interleukin-1 Beta
IL6	Interleukin-6
CA4	Carbonic anhydrase-4
CA6	Carbonic anhydrase-6
ALB	Serum albumin
ACE	Angiotensin-converting enzyme

Matrix metalloproteinases (MMP2, MMP3, and MMP13), Interleukin 1-Beta (IL1B), Interleukin-6 (IL6), Albumin (ALB), Angiotensin-converting enzyme (ACE), Carbonic anhydrase-4 (CA4), and Carbonic anhydrase-6 (CA6) are the key targets of PHDF, found to be highly associated with dental caries. Several studies have identified the association between specific key proteins, and the formation and progression of dental caries. Matrix metalloproteinases (MMPs) are membrane-bound enzymes, that hydrolyze components of extracellular matrix (ECM). It plays a vital role in demineralizing and destroying the components of the extracellular matrix and is activated by bacterial acids, therefore progressing tooth decay (Chaussain-Miller et al. 2006). MMPs are mostly found in saliva, gingival crevicular fluid, and odontoblast (Jain & Bahuguna, 2015). MMP3, a stromelysin found in demineralized human dentin, functions as a proteoglycanase, leading to proteoglycan destruction (Salman et al. 2024). According to Benli et al. (2021), MMP2 initiates secondary caries, irrespective of its restorative material. A meta-analysis showed a significant association between genetic variation in MMP13 and the risk of dental caries (Molaei & Motahari, 2022).

Cytokines play an important role in the immunopathogenesis of dental caries. Cytokines such as IL1B and IL6, mediate inflammation and immune responses. A systemic review and meta-analysis identified that, among children and young adults with active dental caries, the cytokine IL-6 was found to be most dominant present in their saliva (Alarcón-Sánchez et al. 2024). IL1B (Interleukin 1 Beta) plays a significant role in the progression of dental caries by promoting inflammation in response to bacterial infection (Stefanovic et al. 2021).

Salivary albumin, (ALB) is not directly associated with caries it may indirectly influence oral health by altering the composition of saliva, suggesting that modulating this protein could help prevent caries (Nireeksha et al. 2017). ACE inhibitors are primarily associated with hypertension and heart conditions, that cause dry mouth (xerostomia) as a side effect, increasing the risk of dental caries. Valtellini & Ouanounou, (2023) discussed the importance of managing oral health in hypertensive patients, including those on ACE inhibitors, to mitigate the risk of dry mouth and subsequent dental caries. Carbonic anhydrases, specifically CA4 and CA6, play an important role in maintaining the pH balance of saliva. They neutralize the acids produced by bacteria in the mouth, which helps in the prevention of tooth decay. Al-Mahdi et al. (2023) in their study identified that the individuals with dental caries have higher levels of CA4 and CA6 in their saliva compared to those without caries.

4.5.3 Analysis of Protein-Protein Interaction (PPI) Network

Analyzing the protein-protein interaction (PPI) network provides valuable insights into complex biological processes and disease mechanisms. Studying protein interactions can help identify and elucidate key proteins, disease causes, potential treatments, protein relationships, and the development of targeted therapies. PPI network analysis facilitates the identification of multiple targets, enabling the development of effective treatments for complex diseases. A total of 9 potential targets were input into the STRING database to illustrate their relationships. The Protein-Protein Interaction (PPI) network between the target proteins is depicted in **Figure 4.35**, which consists of 9 nodes and 21 edges; representing interactions between target proteins. Network analysis exhibited an average node degree of 4.67, which corresponds to the average number of

interactions (at the score threshold) per protein. The average local clustering coefficient is 0.802 with a PPI enrichment value of 1.82e-06 demonstrating the network's connectivity and significance.

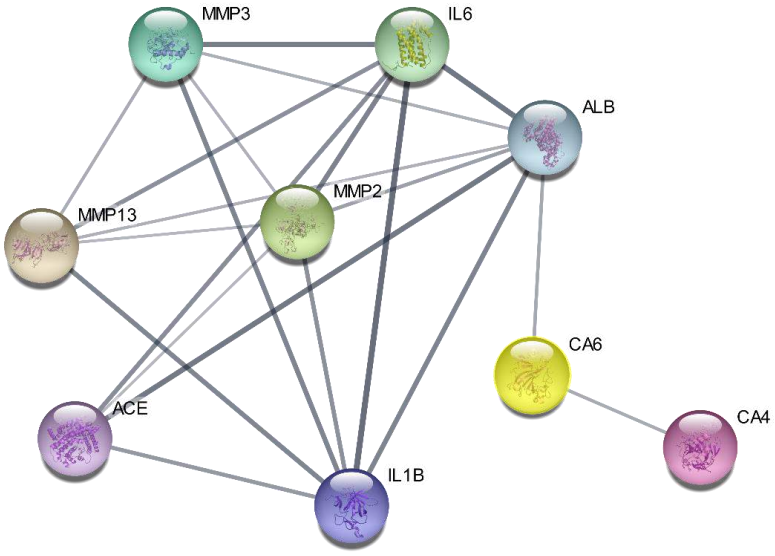

Figure 4.35. Protein-protein interaction (PPI) network of key targets

Exploring protein-protein interaction facilitates a better understanding of the role of specific enzymes and immune responses involved in the progression of tooth decay. This ensures the development of targeted treatments and preventive measures, improving oral health outcomes (Peres et al. 2019).

4.5.4 Compound Target Network Construction

A compound-target interaction network system was constructed to understand the interaction between the compounds and their putative targets. As shown in **Figure 4.36,** the network comprised 78 active compounds connected to 9 putative targets through 516 edges. The putative targets were denoted by purple nodes, while the active components were denoted by blue nodes.

The edges showed how they interact with one another. In this network, the active compounds of selected plants AAR, BCL, EHL, FBP, PGL, and SVF were found to interact with multiple targets. These results imply that the active biochemical compounds of the formulation might have a synergistic effect on these targets of dental caries. The degree of node distribution showed that PGL had the highest degree of 38, followed by AAR (16), SVF (15), FBP *and* EHL (11),

and BCL (5). The compound degree distribution revealed that procyanidin B1 and B2 had the highest of 7, followed by corrosolic acid, quercetin, kaempferol, guavacoumaric acid, isonericoumaric acid, leucocyanidin, guajiverin, hyperoside, isoquercetin, quercetin-3-O-gentiobioside, citroside of 6. Subsequent compounds showed decreasing degrees such as oleanolic acid, ursolic acid, coumaric acid, goreishic acid, gentisic acid, esculentin, carpesterol of 5, ecdysone, luteolin-7-O-glucoside, guavanoic acid, asiatic acid, guavin A, guvain D, guavin C of 4, stigmasterol, β-Sitosterol, pentagalloylglucose, myricitrin, 2,4,6-Tri-O-galloyl-beta-glucose, sitosterol, Beta-ionone, maslinic acid, amritoside, Guavin B, quercitrin, solasonine, solamargine connected of 3, acenotide, euphorbolhexacosanoate, euphorbadienol, dihydrobrassicasterol, ergosterol, 6-heptanoic acid, strictinin, stachyurin, tellimagrandin, campesterol, daucosterol of 2 degrees, and the remaining compounds with 1 degree.

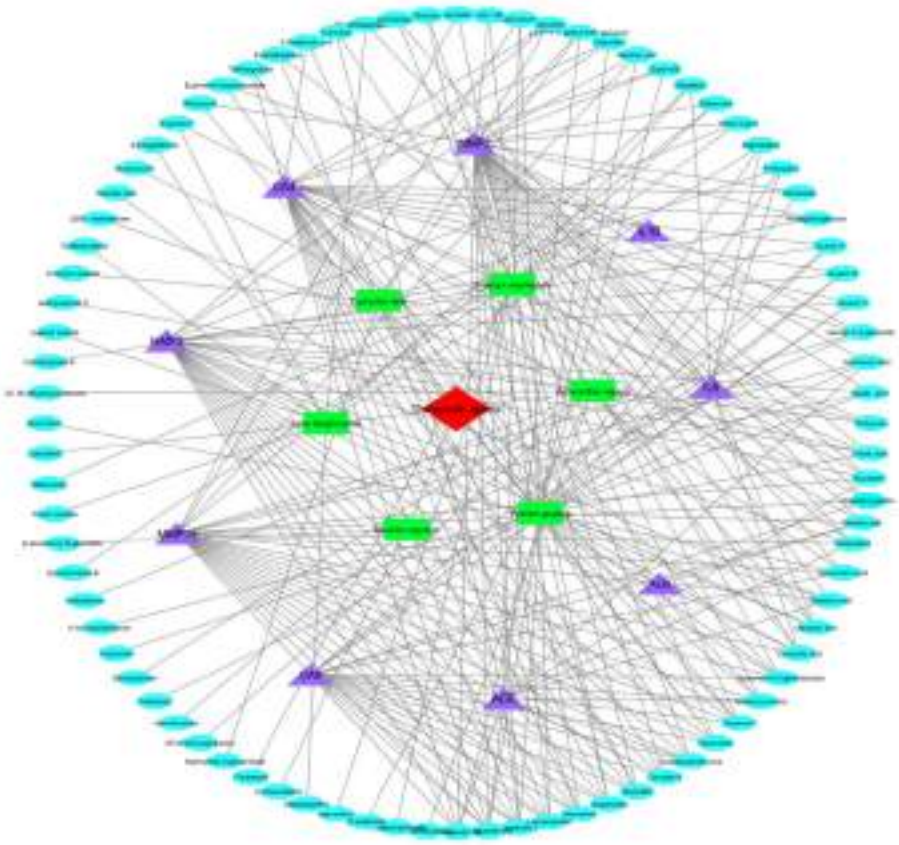

Figure 4.36 Compound- target network

Green color indicates herbs; purple color indicates potential targets of dental caries;
Blue color indicates potential compounds of PHDF

Our results identified the compounds, procyanidins specifically B1, B2, and B3 as highly connected compounds. These procyanidins are condensed tannins, found mostly in dietary substances and possess several pharmaceutical properties like antioxidant (Grace et al. 2019), antibacterial (Nawrot-Hadzik et al. 2021), anti-inflammatory (Tian et al. 2019), antineoplastic (Choy et al. 2016), anti-allergic (Nur Sazwi et al. 2013), lipid-lowering, and anti-obesity properties (Wang et al. 2020). Procyanidins exhibit potent antibacterial activity, by breaking the bacterial membrane leading to the leakage of intracellular substances (Schmuch et al. 2015). Incorporating procyanidins into natural products can effectively treat dental caries by weakening the mechanical strength of *S. mutans* biofilm, remineralizing the hydroxyapatite (Yoo et al. 2011), and interrupting the synthesis of insoluble exopolysaccharides (Kim et al. 2015), thereby offering a comprehensive approach to combating dental caries.

Previous studies have investigated the antibiofilm of certain compounds against *S. mutans* and other pathogenic microbes. Likely, quercetin and kaempferol significantly reduced *S. mutans* biofilm formation by decreasing dry weight, total protein, and insoluble/soluble glucans formation (Zeng et al. 2019). In addition, ursolic acid inhibited GTF synthesis and prevented the biofilm formation of *S. mutans* (Liu et al. 2021). Ursolic and asiatic acids exhibited promising antibiofilm effects against pathogenic microbes (Sycz et al. 2022).

4.5.5 Compounds Target Pathway Analysis

To elucidate the interactions between the bioactive compounds of PHDF and dental caries targets, a network consisting of antimicrobial agents, compound target protein interaction, and KEGG pathways was constructed using Cytoscape. This compound-target-pathway network shown in **Figure 4.37**, demonstrated the complex relationship in multiple pathways including transit interaction and cross-talk pathway. From the results, it was observed that the network comprised 98 nodes (78 herb-compound nodes, 9 disease-related target nodes, 5 pathway nodes, and, 6 disease nodes), and 596 edges. **Figure 4.38** illustrated the interactions within the signalling pathway where the key targets of PHDF involved. Therefore, this analysis revealed that the therapeutic efficacy of PHDF against dental caries involved a multi-component, multi-target, multi-pathway

approach, which collectively regulates the prevention of dental caries. Similarly, Zhang et al. (2020) constructed a network comprising 224 nodes and 550 edges using 47 compounds from *R. coptidis* and *E. rutaecarpa* present in the Chinese traditional medicine Zuojinwan and 188 target proteins, related to gastric cancer. They reported that nodes' interaction with more edges showed significant interactions, highlighting the intricate relationship among the target proteins and compounds.

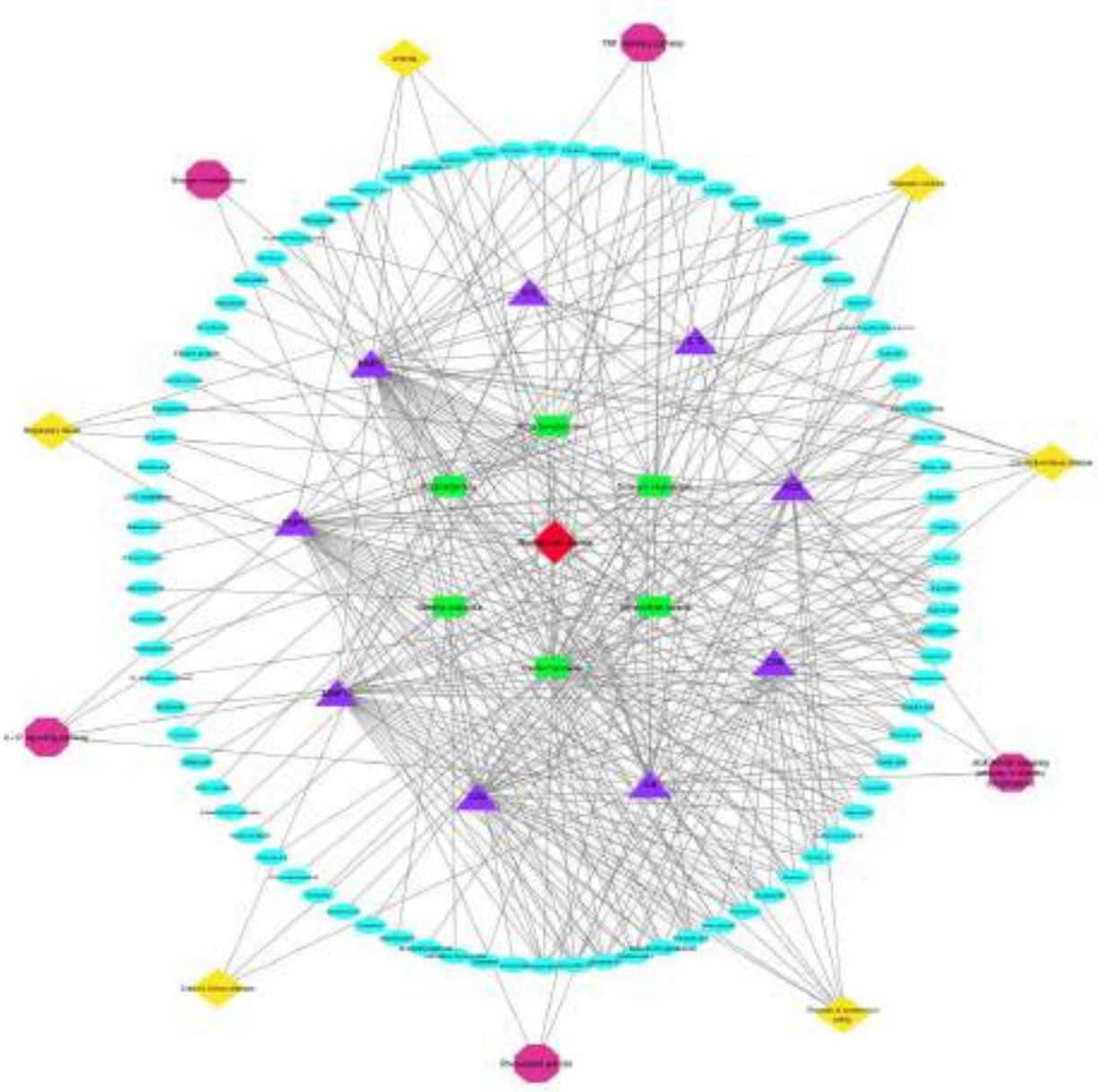

Green color indicates herbs; purple color indicates potential targets of dental caries; Blue color indicates potential compounds of PHDF; yellow color indicates signaling pathway; pink color indicates disease.

Figure 4.37 Compound target pathway disease network

Our findings are supported by the study of Guzmán-Flores et al. (2024) which elucidated the molecular mechanism of curcumin in preventing dental caries and the identification of MAPK1, BCL2, KRAS, CXCL8, TGFB1, MMP9, and IL1B as the key targets. The participation of these key targets in the specified pathways significantly eliminated caries formation and related diseases like anatomical disorders, connective tissue disease, diabetes mellitus, arthritis, respiratory failure, and chronic kidney disease. By targeting these genes and pathways, a promising therapeutic strategy may emerge for preventing dental caries and its associated diseases (Ev et al. 2023).

Table 4.22. Targets involved in signalling pathways

Entry	KEGG Pathway	Genes
hsa04657	IL-17 signalling pathway	MMP13, IL1B, MMP3, IL6
hsa05323	Rheumatoid arthritis	IL1B, MMP3, IL6
hsa04933	AGE-RAGE signalling pathway in diabetic complications	MMP2, IL1B, IL6
hsa04668	TNF signalling pathway	IL1B, MMP3, IL6
hsa00910	Nitrogen metabolism	CA4, CA6

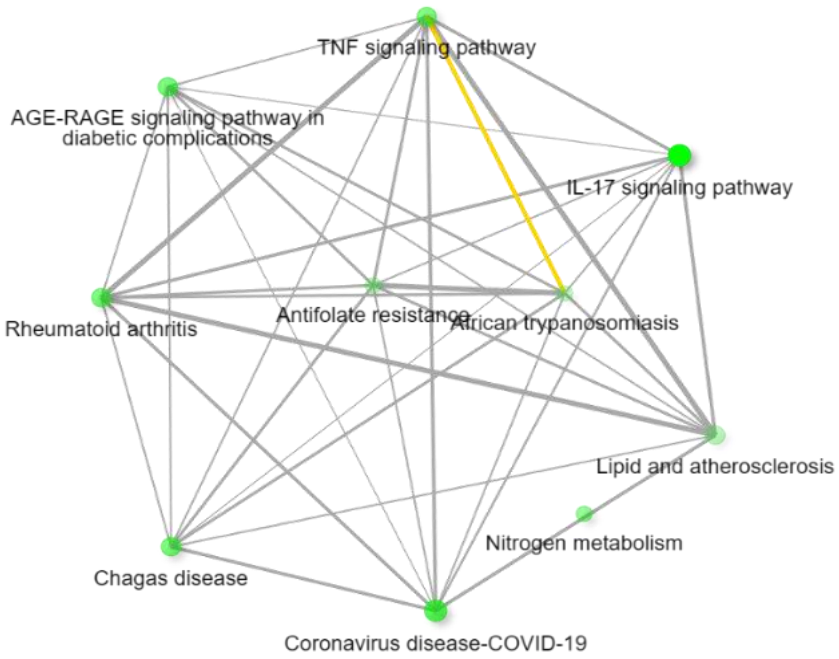

Figure 4.38. Signalling pathway interaction network of PHDF for dental caries

Table 4.23. Targets involved in associated diseases

Term ID	Disease	Targets	Gene count
DOID:7	Disease of anatomical entity	MMP2, MMP13, IL1B, ACE, ALB, MMP3, CA4, IL6	**8**
DOID:65	Connective tissue disease	MMP2, MMP13, IL1B, ALB, MMP3, IL6	**6**
DOID:9351	Diabetes mellitus	IL1B, ACE, ALB, IL6	**4**
DOID:848	Arthritis	MMP13, IL1B, MMP3, IL6	**4**
DOID:11162	Respiratory failure	IL1B, ACE, ALB, IL6	**4**
DOID:784	Chronic kidney disease	ACE, ALB, IL6	**3**

The continual rise in untreated dental caries affects the quality of life and increases the risk of developing various ailments (Marcenes et al. 2013; Vos et al. 2012; Chapple et al. 2017). Research has extensively explored the connections between periodontitis and systemic disease conditions such as atherosclerosis, diabetes mellitus, pneumonia, chronic obstructive pulmonary disease (COPD), rheumatoid arthritis, and Alzheimer's disease (Henderson et al. 2009). Similarly, the enriched metabolic pathways and the key targets in our study were predominantly associated with diseases including anatomical disorders, (DOID:7), connective tissue disease (DOID:65), diabetes mellitus (DOID:9351), arthritis (DOID:848), respiratory failure (DOID:11162), and chronic kidney disease (DOID:784). A strong association between dental caries and metabolic syndromes has been scientifically evidenced from *in vivo* experiments (Sabharwal et al. 2021). From this, it is evident that targeting the hub genes associated with dental caries can help prevent these related illnesses and contribute to a healthier lifestyle.

4.5.6 Gene Ontology (GO) Functional Enrichment Analysis Biological Process, Cellular Components, and Molecular Functions

GO enrichment analysis was carried out to understand the biological, cellular, and metabolic processes in which the 9 genes were involved, which will help to identify the disease-related targets, and the results are presented in **Figure 4.39**. The potential targets of PHDF were enriched in the biological process (GO:0008152), response to stimulus (GO:005089), cellular component organization (GO:0016043), multicellular organismal process (GO:0032501), biological regulation (GO:0065007), cell communication (GO:0007154),

developmental process (GO:0032502), cell population proliferation (GO:0008283), localization (GO:0051179), reproduction (GO:0000003), and growth (GO:0040007). This GO enrichment suggests that PHDF may play a potential role in metabolic regulation.

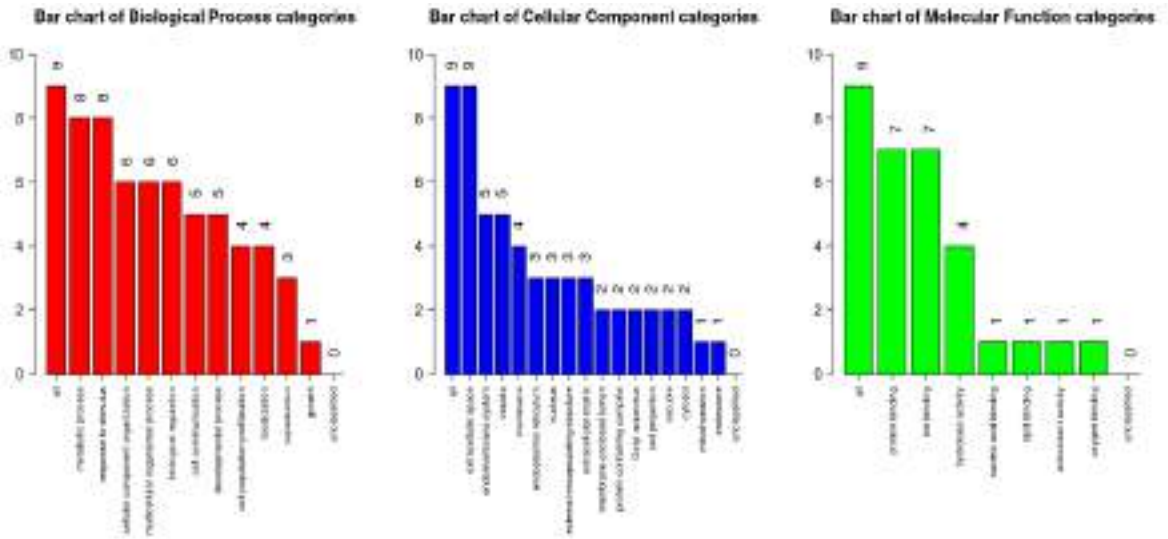

Figure 4.39. Gene Ontology (GO) functional enrichment analysis of biological process, cellular components, and molecular functions

The results of cellular component and molecular function analyses revealed significant enrichment in various cellular components and molecular functions in extracellular space (GO:0005615), endomembrane system (GO:0012505), vesicle (GO:0031982), membrane (GO:0016020), endoplasmic reticulum (GO:0005783), nucleus (GO:0005634), external encapsulating structure (GO:0030312), extracellular matrix (GO:0031012), membrane-enclosed lumen (GO:0031974), protein-containing complex (GO:0032991), golgi apparatus (GO:0005794), cell projection (GO:0042995), vacuole (GO:0005773), cytosol (GO: 0005739), mitochondrion (GO: 0005829), and endosome (GO:0005768). In the process of molecular function, the key targets were highly enriched in protein binding (GO:0005515), ion binding (GO: 0043167), hydrolase activity (GO:0016787), nucleic acid binding (GO:0003676), lipid binding (GO:0008289), antioxidant activity (GO:0016209), and oxygen binding (GO:0019825). These findings suggested the involvement of immune and proliferative pathways in the disease model and highlighted the potential targets for therapeutic intervention.

Similar studies were conducted by Guzmán-Flores et al. (2024) revealed significant insights into the molecular mechanisms of dental caries with curcumin. The enrichment analysis revealed that 134 genes were significantly associated with the biological processes related to programmed cell death and cytokine activity. Furthermore, key targets of curcumin in dental caries were primarily located in the endoplasmic reticulum and cell membrane.

4.5.7 KEGG Pathway Enrichment Analysis

KEGG pathway enrichment analysis identified several significant pathways associated with dental caries. The top pathways, selected based on P value (<0.05), included the IL-17 signaling pathway (hsa04657), Rheumatoid arthritis (hsa05323), AGE-RAGE signaling pathway in diabetic complications (hsa04933), TNF signaling pathway (hsa04668), and Nitrogen metabolism (hsa00910), all of which contributed to the formation and progression of dental caries.

To unveil the molecular mechanism of PHDF in dental caries, the Interleukin-17 pathway was identified as a significant pathway related to cavities identified through the KEGG pathway. In the Interleukin-17 pathway as shown in **Figure 4.40** the putative targets involved are highlighted in a red rectangle. Among these targets, 4 targets, IL-6, MMP3, MMP13, and IL1B were involved in the mechanism of the Interleukin-17 signalling pathway, which is associated with dental caries.

This IL-17 signalling pathway is mainly responsible for the development and progression of dental caries by regulating the immune response in the oral cavity. Th17 cells are a part of pro-inflammatory T-helper cells and stimulate inflammation by producing IL-17 (Abusleme & Moutsopoulos, 2017). In dental caries, the activation of the IL-17 signalling pathway, recruits immune cells to the point of infection, aiding in the defense against cariogenic bacteria. However, excessive activation of this pathway contributes to the severity of dental caries and worsens other oral health issues (Wang et al. 2023). Thus, targeted therapies for the treatment of dental caries can be formulated by balancing and regulating the IL-17 signalling pathway.

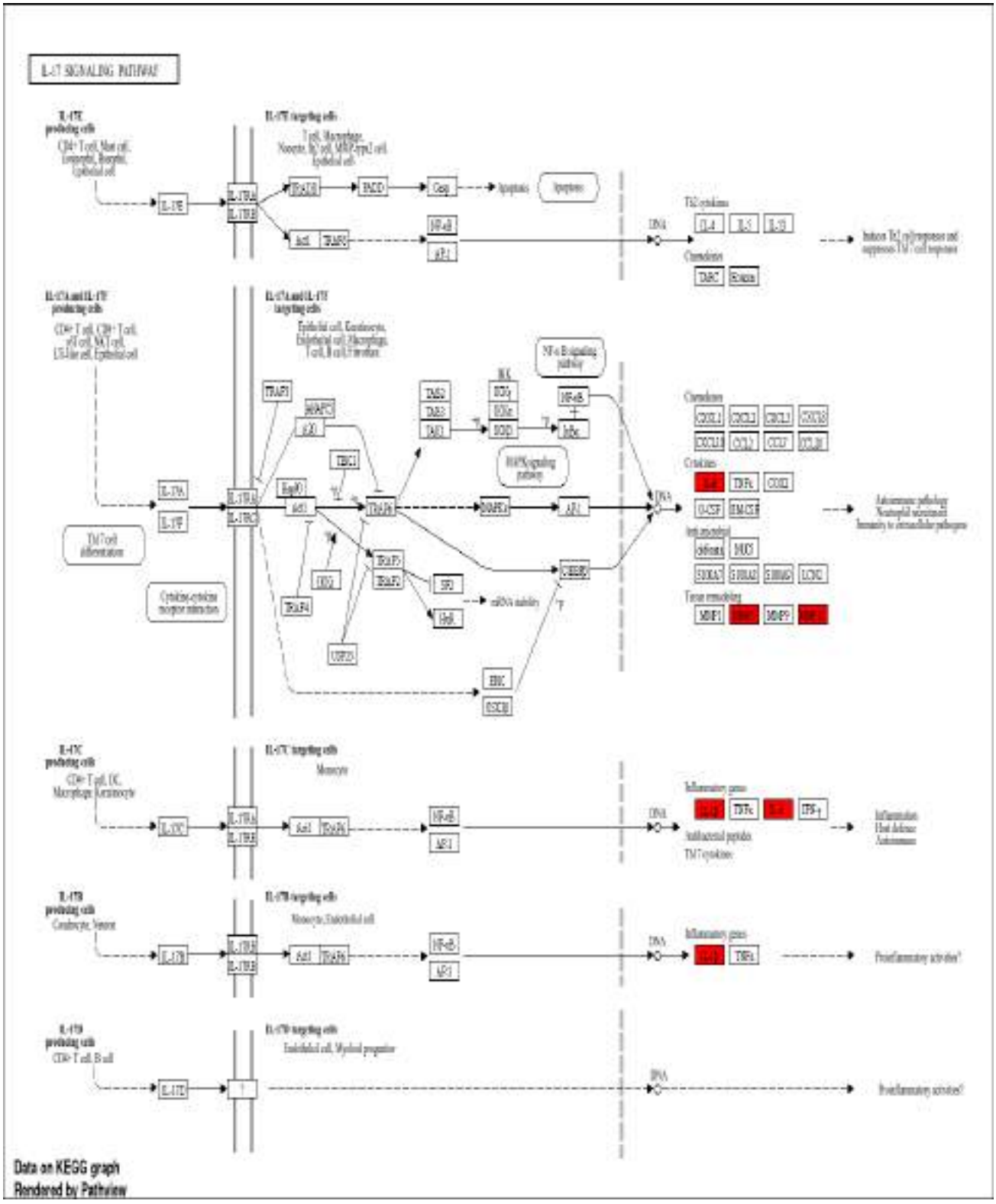

Figure 4. 40. Targets of PHDF involved in the IL-17 signalling pathway

The red rectangles represent identified proteins of PHDF

4.5.8 Validation of Key Targets-Compound Interaction using Molecular Docking

Following the analysis of the Target-Compound-Metabolic Pathways network, molecular docking was performed to inquire about interactions between compounds and key proteins such as Matrix metalloproteinase 2 (MMP2) and Carbonic anhydrase IV (CA4). Sitemap analysis predicted the active site of these enzymes, which were then used for docking studies employing extra precision (XP) glide mode. The results revealed five phytocompounds with a greater binding affinity (≥-7.0Kcal/mol) towards the target protein MMP2. The highly interacting ligands with their 3D and 2D interactions, are depicted in **Figure 4.41.** The data obtained as a result of molecular docking is shown in **Table 4.24**. along with the positive interactions between the target proteins, and the compounds which were sorted by their docking scores. Among the plant extracts, PGL exhibited a strong binding affinity towards the MMP2 protein. The docking interactions of the ligand quercetin-3-O-gentiobioside exhibited the highest inhibition constant values of -9.93Kcal/mol, followed by guaijavarin, procyanidin B1, procyanidin B3, and leucocyanidin of -7.351, -7.076, -8.228, and -7.669 Kcal/mol, respectively. The compounds from PGL namely stachyurin, procyanidin B2, leucocyanidin, procyanidin B3, and strictinin, proanthocyanidin, and cianidanol, represented the highest docking scores of -13.807, -10.731, -9.619, -9.229, -8.634, -7.917 and -7.348Kcal/mol, respectively. Furthermore, proanthocyanidin from AAR exhibited a binding affinity of -7.917Kcal/mol towards CA4 (**Figure 4.42**). The differential interaction of CA4 protein with the bioactive compounds reported can be further studied to elucidate the underlying mechanism behind its regulation at a molecular level.

According to Guzman-Flores et al. (2024), curcumin has been shown to interact with seven major proteins (CXCL8, BCL2, IL1B, TGFB1, MMP9, MAPK1, and KRAS) through strong hydrogen bonds, displaying a high binding affinity ranging from -6.2 to -8.4 Kcal/mol. Furthermore, Salman et al. (2024) demonstrated that among the four cinnamic acids (Cynarin, chlorogenic acid, rosmarinic acid, and cinnamyl caffeate), cynarin emerged as the most potent MMP3 inhibitor with a $\Delta G_{binding}$ score and inhibition constant value of −15.57Kcal/mol and 3.83pM, respectively.

Table 4. 24. Docking score of highly interacted ligands and proteins

Compound name	Docking score (Kcal/mol)	PubChem ID	Interactions	Amino acids Residues
MMP2- Matrix Metalloproteinase 2				
Quercetin-3-O-Gentiobioside	-9.93	5320834	H-bond, Pi-Cation	A: ARG 67, B: HIS 70, ASN 64, GLU 58, GLY 71
Procyanidin B-3	-8.228	146798	H-bond, Pi-Cation	A: ARG 67, ASP 26, B: GLU 58, GLY 71, HIS 70
Leucocyanidin	-7.669	71629	H-bond, Pi-Pi Stacking	A: ASP 101, B: PHE 65, ASN 64, GLY 71, ASP 96, HIE 98
Guaijavarin	-7.351	5481224	H-bond	A: ARG 67, B: GLY 71, GLU 58, ASN 64
Procyanidin-B1	-7.076	11250133	H-bond	A: ARG 67, B: GLU 58, GLY 71, ASN 64
CA4- Carbonic anhydrase IV				
Stachyurin	-13.807	157395	H-bond, Pi-Cation	A: TYR 102, GLY 111, GLN 250, GLN 249, LEU 248, B: GLN 250, GLY 111, LYS 103
Procyanidin B2	-10.731	122738	H-bond, Pi-Pi Stacking	A: SER 105, HIS 113, TYR 102, B: LEU 248, HIS 113, GLY 111
Leucocyanidin	-9.619	71629	H-bond	A: GLY 111, TYR 102, B: ASN 32, GLN 250, GLN 249
Procyanidin-B-3	-9.229	146798	H-bond, Pi-Pi Stacking	A: ASN 32, GLN 250, GLY 111, HIS 113, B: TYR 102, GLY 111, HIS 113
Strictinin	-8.634	73330	H-bond, Pi-Cation	A: LEU 248, ASN 32, B: LYS 103, TYR 102, GLU 112
Proanthocyanidin	-7.917	108065	H-bond, Pi-Pi Stacking	A: GLN 250, HIS 113, B: TYR 102, GLY 111
Cianidanol	-7.348	9064	H-bond	A: GLY 111, HIS 113, B: ASN 32, LEU 248

Ligand	3D-Interaction	2D-Interaction
Quercetin-3-O-Gentiobioside (-9.93 Kcal/mol)		
	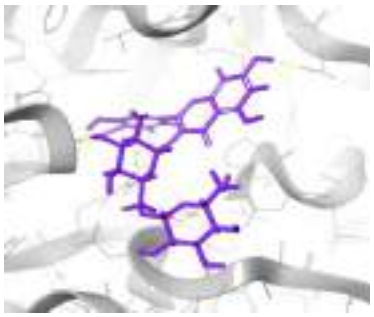	
Procyanidin B-3 (-8.228 Kcal/mol)		
	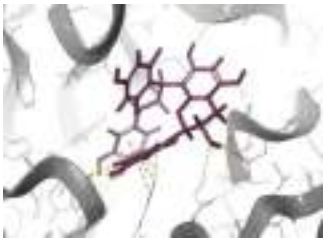	
Leucocyanidin (-7.669 Kcal/mol)		
	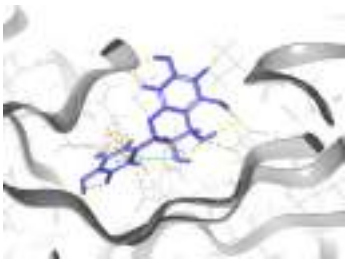	
Guaijavarin (-7.351 Kcal/mol)		
	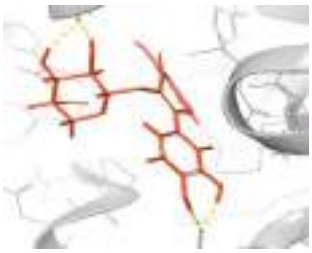	
Procyanidin-B1 (-7.076 Kcal/mol)		
	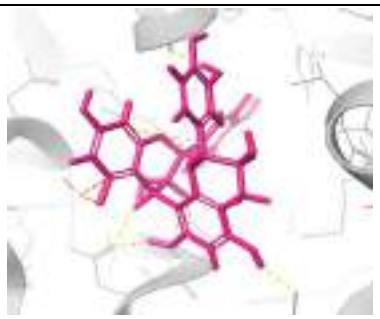	

Figure 4.41. 2D and 3D interaction of top hit ligands with MMP2- Matrix Metalloproteinase 2

Ligand	3D-Interaction	2D-Interaction
Stachyurin (-13.807 Kcal/mol)		
	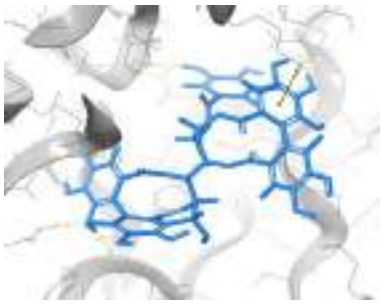	
Procyanidin B2 (-10.731 Kcal/mol)		
	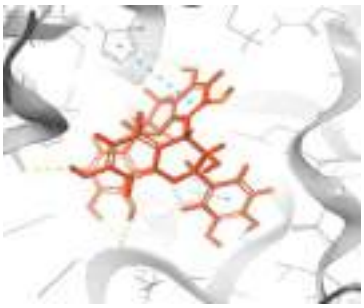	
Leucocyanidin (-9.619 Kcal/mol)		
	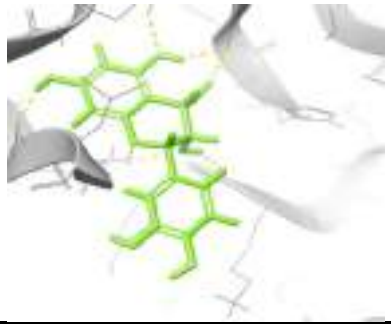	
Procyanidin-B-3 (-9.229 Kcal/mol)		
	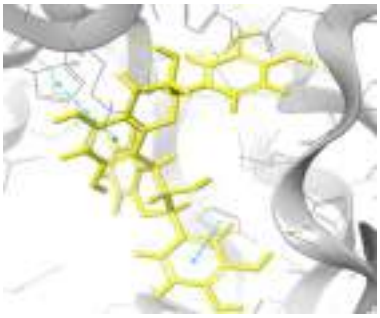	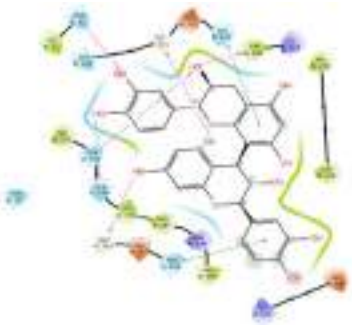

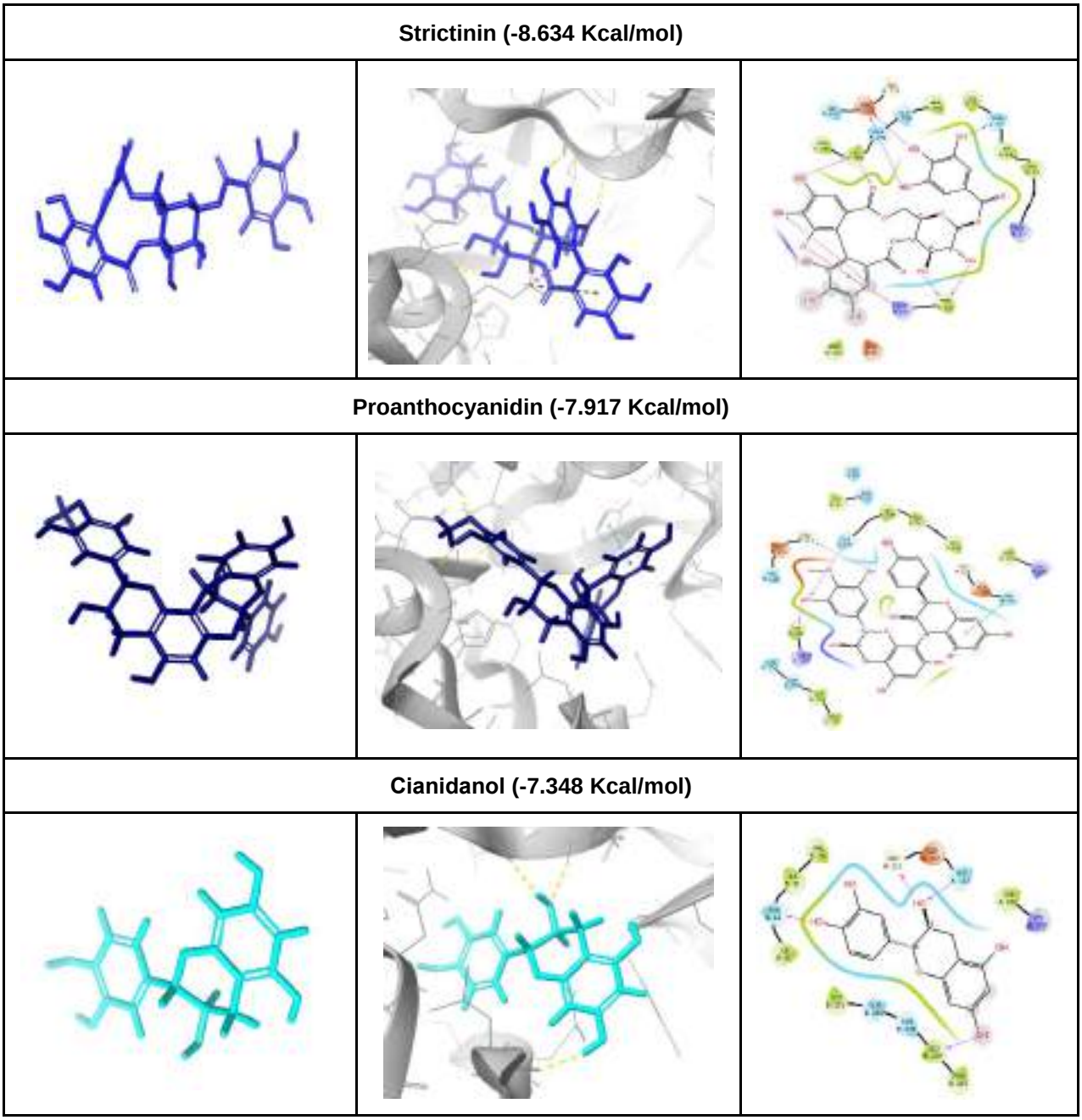

Figure 4. 42. 2D and 3D interaction of top hit ligands with CA4- Carbonic anhydrase IV

4.5.9. Effect of Potential PHDF Compounds on *S. mutans*

Streptococcus mutans, a primary bacterium responsible for dental caries, was subjected to *in-silico* analysis to investigate the inhibitory potential of PHDF compounds. **Figure 4.43** showed the interaction network of PHDF compounds and *S. mutans* self-proteins representing protein-protein, protein-chemical, and chemical-chemical interactions.

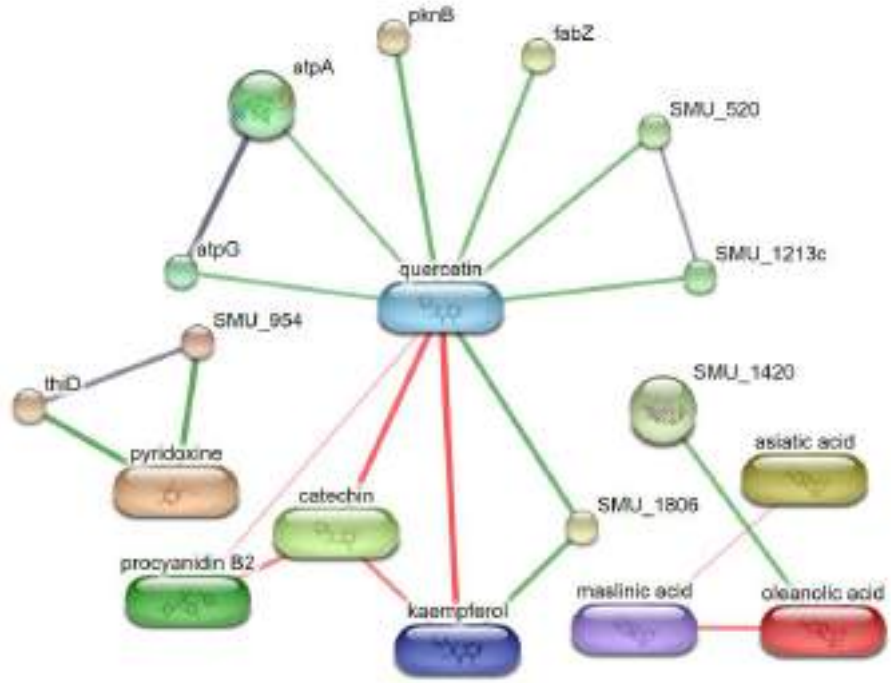

Line thickness represents the stronger interactions. Protein-protein interactions are in the grey line, chemical-chemical in the green line, and protein-chemical in the red line.

Figure 4. 43. Interaction Network View of PHDF Compounds and *S. mutans* Proteins

Oleanolic acid is a pentacyclic triterpenoid that highly interacts with putative enzymes and genes in *S. mutans* including quinone oxidoreductase (SMU_1420), DNA gyrase (gyrB, gyrA), and partitioning system genes parE, and parC. Additionally, oleanolic acid interacted with maslinic acid, asiatic acids exhibiting its synergistic effect on *S. mutans.* The compound pyridoxine from PGL showed strong interaction with thiD, a gene involved in thiamine (vitamin B1) biosynthesis and pyridoxal kinase (SMU_954). Ergosterol acetate interacted with oppC, a putative oligopeptide permease component. Furthermore, the compounds quercetin, procyanidin B2, catechin, and kaempferol displayed their synergistic effects and strongly interacted with various *S. mutans* proteins, including transcriptional regulator (SMU_520), SMU_1213c, glycogen phosphorylases (glgP), glucosyltransferase (SMU_1806), serine/threonine protein kinase (pknB), and enzymes involved in fatty acid biosynthesis (fabZ) and energy metabolism (phsG, atpG, atpD, atpA). Therefore, it can be stated that PHDF compounds exert an effect on *S. mutans* through these metabolic pathways.

In conclusion, our research provided comprehensive insights into the potential therapeutic effects of PHDF compounds against dental caries. By employing network pharmacology and molecular docking approaches, we identified multiple gene targets and metabolic pathways that are modulated by PHDF compounds, both in humans and *S. mutans*. These findings suggest that PHDF compounds may exert their anti-caries effect through a multifaceted approach targeting multiple pathways and biological functions. Overall, our study highlighted the promise of PHDF compounds as a novel therapeutic strategy for the treatment and prevention of dental caries and warrants further investigation into their clinical applications.